RELAY-ASSISTED HYBRID FIBER/MMWAVE-WIRELESS BACKHAUL NETWORK

A Thesis
Presented to
The Academic Faculty

By

Yan Yan

In Partial Fulfillment
of the Requirements for the Degree
Doctor of Philosophy in the
School of Electrical and Computer Engineering

Georgia Institute of Technology

May 2022

RELAY-ASSISTED HYBRID FIBER/MMWAVE-WIRELESS BACKHAUL NETWORK

Approved by:

Dr. Douglas M Blough, Advisor
School of Electrical and Computer Engineering
Georgia Institute of Technology

Dr. Raghupathy Sivakumar
School of Electrical and Computer Engineering
Georgia Institute of Technology

Dr. Yusun Chang
School of Electrical and Computer Engineering
Georgia Institute of Technology

Dr. Henry L Owen
School of Electrical and Computer Engineering
Georgia Institute of Technology

Dr. David Goldsman
School of Industrial and Systems Engineering
Georgia Institute of Technology

Date Approved: January 11, 2022

Believe you can and you’re halfway there.

Theodore Roosevelt

ACKNOWLEDGEMENTS

It has been 4 years since I started my Ph.D. journey and 6 years I came to Atlanta to start my graduate study at Georgia Tech. During this wonderful journey at Georgia Tech, there are many difficulties, but this period of time is when I gain the most. Over the past six years, I have received support and help from a great number of individuals in different forms and I would like to take this opportunity to express my gratitude to those who made this dissertation possible with their help and encouragement.

Foremost, I would to express my sincere gratitude to my advisor Prof. Douglas M. Blough for his continuous support for my Ph.D. study and research, for his patience, motivation and enthusiasm. His immense knowledge and plentiful experience have encouraged me in all the time of my academic research and daily life. His guidance helped me in all the time of research and writing of this thesis. I could not have imagined having a better advisor and mentor for my Ph.D. study.

I would like to thank the rest of my dissertation committee: Prof. Raghupathy Sivakuma, Prof. Yusun Chang, Prof. Henry Owen and Prof. David Goldsman, not only for their time and extreme patience but also for their encouragement, insightful comments and feedback that greatly improved the quality of my work.

I would also like to thank all my lab mates at Georgia Tech, Mengyao Ge, Qiang Hu, Jenny Zhang, Hemin Yang, Yuchen Liu, Huiye Liu, Ang Deng and Jingyuan Zhang, for the discussion, for the support and help and for all the fun we have had in the last four years. Every moment in the lab is an unforgettable memory for me.

Last but not the least, I would like to thank my family and my boyfriend, for their endless love and accompany. I could never successfully complete my Ph.D. program without their trust and encouragement. Thank them for always supporting me.

TABLE OF CONTENTS

LIST OF TABLES

LIST OF FIGURES

SUMMARY

Globally, the demand for higher network capacity is continually increasing. The next generation ultra-high bandwidth communication system, known as 5G, is planned to increase the capacity of existing networks by 1000 fold within the next 20 years. 5G mobile communications will support a wide range of use cases and emerging applications including augmented reality, data sharing, machine-to-machine applications and real-time HD video streaming. With the explosive growth of mobile data demand, capacity of both access and backhaul networks has become a critical issue. For access networks, dense deployment of small cell base stations (SBSs) is a key approach to enhance the system throughput. However, dense SBS deployments require the backhaul to provide flexible and reliable connections between SBSs and the core network.

Fiber connections, where available, are ideal for backhaul traffic. However, connecting large numbers of SBSs via fiber is expensive and time consuming to deploy. This is especially true in areas where fiber is still not widely available, such as much of North America. Millimeter-wave (mmWave) communication, with its spectrum availability and multi-Gigabit-per-second (Gbps) data rates, is an attractive alternative to support the high demand in backhaul networks. However, there are challenges with mmWave, including higher propagation loss, link directivity, and susceptibility to blockage. These factors can limit the communication range of mmWave wireless links to a few hundred meters or less to achieve the promised multi-Gbps data rates, especially in urban dense scenario. With wireless networks becoming more dense and heterogeneous, it is necessary to guarantee connectivity and capacity in a cost-effective and sustainable way for a diverse set of applications. Hybrid backhaul architectures with a combination of fiber and mmWave connections have received considerable attention to address these challenges. In a hybrid backhaul network, only a subset of SBSs in a given region connect directly to the core network via fiber (these are referred to as anchor BSs (ABSs)), while the other SBSs connect wirelessly

to nearby SBSs/ABSs via mmWave links. However, there are still some challenges that need to be overcome for hybrid backhaul network.

The poor propagation characteristics and severe blockage effect of mmWave signals must be considered and overcome within the design and optimization of hybrid backhaul network. To both extend the range of communications and to deal with obstacles, the use of relays for mmWave communications has been proposed in our works. With the deployment of relays in backhaul networks, multi-hop relay paths with multi-Gbps data rates will be selected between SBSs, where the source and destination SBSs cannot communicate with each other directly with Line-of-sight (LoS) path. In hybrid fiber-wireless backhauls, the ABSs relay all traffic to/from their assigned SBSs across the wireless channel, making the ABSs potential bottleneck points that limit backhaul performance. Balancing load across the ABSs is thus another important challenge. We transform the problem into a load-balanced routing problem and develop an efficient algorithm in our work.

The objective of this dissertation is to select and optimize communication links between densely deployed SBSs in the grid-based 3D hybrid fiber-wireless backhaul networks for 5G communication system. At the same time, the load-balanced problem in hybrid backhaul networks is also considered. First of all, in order to select long range ultra-high-speed mmWave backhaul links, relays are selected between a pair of source and destination base stations to achieve the highest signal-to-noise ratio (SNR) at the destination. Different algorithms are proposed to select relays from a set of candidate relay locations and find a single optimal-throughput path using different relay strategies. We also design some algorithms to find the high throughput path with using limited number of mmWave relay nodes and show how these algorithms can be combined to efficiently find different paths. Secondly, instead of the selection of a single path, we explore the possibility of deploying multiple relay paths between a single pair of base stations in mmWave backhaul scenario. Multiple independent and interference-free paths can be used in parallel, potentially doubling or tripling the achievable data rate between a pair of base stations. We first formulate the prob-

lem of feasibility of multi-path selection as a constraint satisfaction problem that includes several different constraints that arise from the problem setting. We then transform the multiple paths selection problem into a Boolean satisfiability problem. Different methods have been used and compared to solve this problem. Lastly, we focus on the load-balanced routing problem in our hybrid backhaul networks with grid topology. In hybrid backhaul architecture where some BSs connect with fiber to the core network and provide mmWave backhaul connections for the rest of the BSs. this architecture brings new challenges, e.g., how to prevent a large amount of traffic from becoming concentrated at certain egress BSs, thereby hurting overall backhaul performance. To address this challenge, we propose an efficient tree-based routing algorithm, which is based on a tree-like topology rooted at a fixed base station (sink node) of the network with a fixed grid topology. Moreover, we also present a variation of the algorithm that permits trade-offs between routing path length and balanced factor.

CHAPTER 1
INTRODUCTION

1.1 Motivations and research objectives

With the implementation of fourth-generation cellular systems, LTE and LTE-A, within the past few years, the fifth-generation and beyond (5G/6G) has already entered our field of vision and begun to be investigated. In view of current trends of mobile device data usage, it indicates that there will be a huge increase in global mobile user traffic. Facing a spectrum deficit at the frequency bands currently in use, the current cellular backhaul network is experiencing difficulty in keeping up with the explosive growth of mobile data demand. As a result, operators and vendors are looking for new approaches to increase network capacity. Among the different considered approaches, network densification is considered as the most promising solution to meet the traffic requirement, since it not only provides greater coverage and capacity but also enables carriers to maximize spectral efficiency. However, because of the limited space and cost, the densification of macro cell base stations is only possible up to a certain extent. Therefore, further network densification requires new BSs with a smaller form factor, the so-called small cell BSs (SBSs) [1], which offer more flexible deployment opportunities. Small cell BSs are low-cost low-power BSs, which have similar functionalities as macro cell BSs but with a much smaller form factor. The use of dense deployment of SBSs enable further improvements in network coverage, allowing additional access points to be placed in more area. With the use of dense SBSs and the increased traffic demands, the question of what type of backhaul network can support this type of deployment is an important one. In this thesis, we focus on the problem of building communication links and routing between the densely deployed SBSs in a hybrid fiber/wireless backhaul network based on a structured grid topology.

In a grid topology, each node of the network is connected with two neighboring nodes along one or more dimensions. We focus on dense urban scenarios in this thesis, where

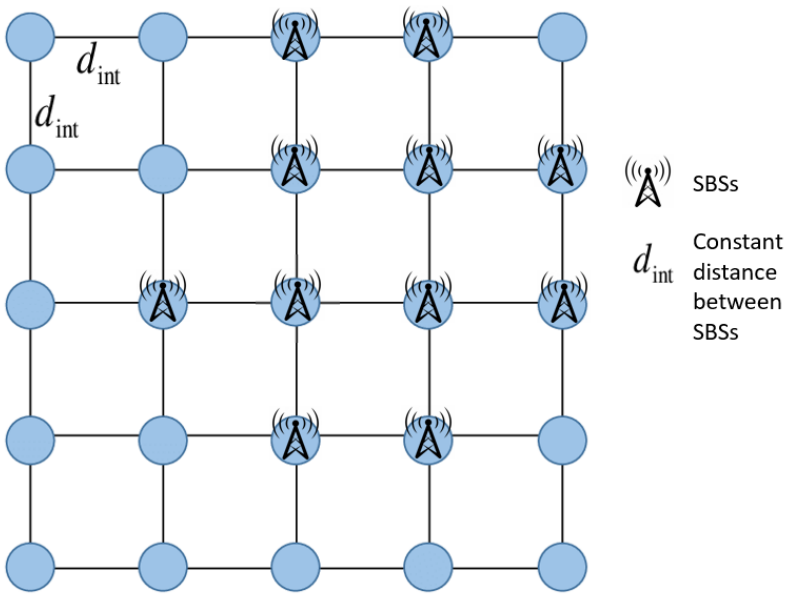

Figure 1.1: Backhaul network with grid topology

cells are typically laid out in grid-like patterns. Thus, we study a grid topology of the SBSs, as shown in Fig 1.1, where the base stations are placed at the intersection points of the grid.

The densification of small cell base stations requires the mobile backhaul to provide flexible and reliable data transmission and connection between base stations and core network. Generally, there are two different backhaul solutions which can largely be categorized into wired or wireless.

Wireless backhaul is considered especially suitable for 5G networks in urban environments due to the large number of SBSs that will be required for coverage. Millimeter wave (mmWave) transmission, in the 30–300 GHz range, has been proposed. MmWave communication can provide higher data rates than is possible at lower frequencies such as the currently used sub 6 Ghz bands. Due to its enormous amount of spectrum and multi-Gigabit-per-second (Gbps) data rates, mmWave is considered a strong candidate for 5G wireless backhaul networks. Moreover, by exploiting the use of high-gain highly-directional antennas, it becomes practical to cope with the explosive growth of mobile data demand and to

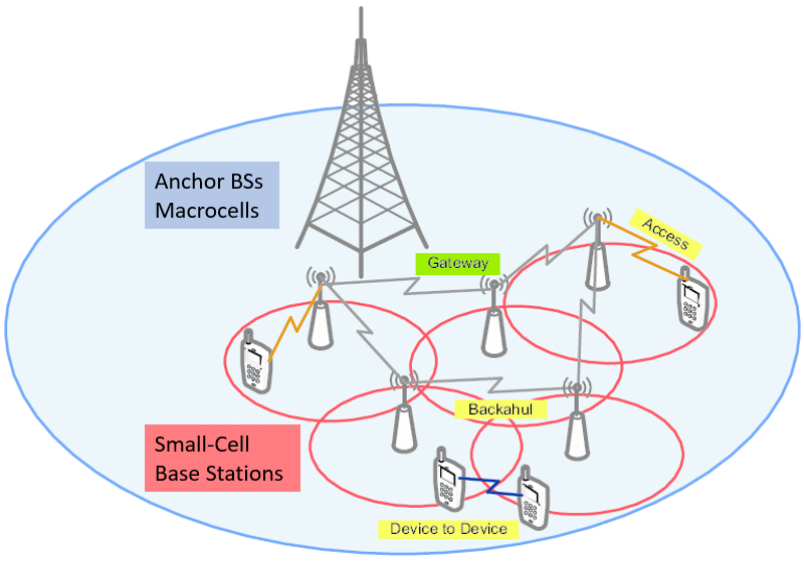

Figure 1.2: Dense deployment of small cells scenario

deal with the interference problems. However, there are a number of differences between mmWave communications and lower-frequency communications, and so there are several challenges that need to be addressed before mmWave communications for 5G become a reality. Among these challenges are a high propagation loss, directivity and sensitivity to blockage of mmWave signals. Due to these issues, for mmWave in very high data rate use cases such as backhaul, the communication range could be limited to a few hundred meters or less.

For wired transmission, the fiber-based connections in backhaul network are considered as ideal media for data transmission due to their efficiency and ultra-low transmission loss. However, dense deployment of small cell base stations makes a fully wired backhaul infeasible owing to the high cost. The prohibitive cost of connecting these massive number of small cell base stations through the fiber is a crucial challenge for wired communication. Therefore, the concept of a hybrid network system, including both fiber and mmWave links, is used in our works, which takes advantages of the strengths of both fiber and mmWave connections [2, 3, 4, 5].

In our hybrid fiber-mmWave networks with grid topology, a small cell network is con-

sidered where a fraction of SBSs in the grid, referred to as anchor base stations (A-BSs), have a fiber-based connection with the core network, and the remaining SBSs in the grid connect wirelessly to other SBSs or A-BSs. Each SBS transfers the backhaul traffic to the adjacent SBSs or one of the A-BSs using wireless transmission. All the traffic then from the A-BSs to the mobile network center is forwarded by using fiber connections. However, this small cell deployment trend brings the backhaul challenge of transmitting a massive amount of traffic between different SBSs and A-BSs. The non line-of-sight (NLoS) mmWave links cannot support the ultra-high data rate required in backhaul due to the severe reflection attenuation. Thus, to support multi-Gbps wireless links between SBSs and A-BSs, line-of-sight (LoS) mmWave communication is utilized in the wireless part of our network. LoS propagation refers to the path that an electromagnetic wave must travel on its way from a transmitting antenna to a receiving antenna. However, the LoS mmWave path suffer from several drawbacks. Due to its high path loss and sensitivity to blockage, the communication range for high data rate LoS mmWave links can be limited to few hundred meters or less, and even shorter especially in dense urban canyons. In order to address this problem, relay-assisted backhaul paths are investigated to maintain high-throughput connections between neighboring SBSs in the grid topology.

A relay-assisted network is commonly used in mmWave communication networks, where the source and destination are interconnected through some nodes. In such network, the source and destination cannot communicate with each other directly because the distance between them is longer than the transmission range or there are some blockages between them, and it may not be possible to find LoS paths between them. Therefore, the relay nodes help to divide the long link into some short but very high rate LoS links which can overcome high propagation loss and sensitivity to blockage of mmWave. In relay-assisted mmWave backhaul network, the relay selection between different BSs and the selection of relay paths is decisive to form high-throughput multi-hop relay paths in backhaul network. This is one of the core problems that is investigated in the thesis.

Routing is another important problem in our hybrid fiber/mmWave backhaul network with grid topology. In our hybrid backhaul network, the A-BSs node may become easily overloaded by the large traffic from the connected SBSs in the grid. Therefore, we propose and study a load balancing problem in our hybrid networks. We develop and evaluate routing algorithms that can balance the load for different ABSs with our fixed grid topology while achieving good throughput performance.

1.2 Research contributions

The primary contributions of this thesis are:

- The first contribution (Chapter 3) focuses on the problem of path selection with amplify-and-forward (AF) relays for long range ultra-high-speed mmWave backhaul networks in urban environments with grid topology. Relays are selected between a pair of source and destination BSs to achieve the highest signal-to-noise ratio (SNR) at the destination. We first derive an equation for the end-to-end SNR of a relay path in a setting that approximates the urban mmWave backhaul environment with grid topology. Based on the derived equation, we transform the maximum throughput relay selection problem to the shortest path problem in graphs. Dijkstra's algorithm can then be used to find maximum throughput relay paths, which however are shown to require a large number of relays. To address this, we propose a dynamic programming algorithm to find a highest throughput path with a given number of hops.

- The second contribution (Chapter 4) considers the problem of selecting paths using decode and forward (DF) relays for mmWave backhaul communications in urban environments with grid topology. We present algorithms, based on a novel widest-path formulation of the problem, for selecting decode and forward relay node locations in multi-hop paths. Our main algorithm is the first polynomial-time algorithm that selects a relay path with a throughput that is proven to be the maximum possible. We also present variations of this algorithm for constrained problems in which: 1) each

possible relay location can host only one relay node, and 2) minimizing the number of hops in the relay path is also an objective. The simulation results show that, over a large number of random cases, our algorithms can always find paths with very high throughput and a small number of relays.

- The third contribution (Chapter 5) focuses on the problem of finding multiple paths with relay nodes to maximize throughput for ultra-high rate millimeter wave backhaul networks in urban environments with grid topology. Relays are selected between a pair of source and destination base stations to form multiple interference-free paths. We investigate the feasibility of multiple inference-free path selection between a pair of BSs. We first formulate this problem as a constraint satisfaction problem that includes different constraints based on the problem setting. From the derivation of constraint equations, we transform the paths selection problem into a Boolean satisfiability problem and use a SAT Solver based on the Davis-Putnam-Logemann-Loveland (DPLL) algorithm to solve it. However, the results show a very high running time for realistic problem sizes. Therefore, we also propose a heuristic algorithm that have much less running time compared with the SAT solver method.

- The fourth contribution (Chapter 6) is that routing algorithms are proposed for hybrid fiber/mmWave backhaul networks with grid topology. For the hybrid backhaul architecture, as aforementioned, a large amount of traffic can cause congestion at a certain egress BSs and thereby hurting the overall backhaul performance. Therefore, a load-balanced routing algorithm is proposed to address this challenge and construct a efficient topology. We define the concept of load balance factor (LBF) and address this challenge through a hill climbing procedure that attempts to minimize LBF. Results show that the proposed algorithm can distribute the dynamic traffic loads from different BSs nearly optimally among fiber-connected BSs for the simulated settings. We also present a variation of the algorithm that permits trade-offs between routing

path length and load balance factor.

1.3 Thesis organization

The rest of the thesis is organized as follows. In Chapter 2, we review the related literature review in the domain of densely deployment of small cell BSs in hybrid fiber/mmWave relay-assisted backhaul networks with grid topology. In Chapter 3 and 4, we present our contribution to single path selection with different relay strategies in mmWave backhaul networks, where different algorithms are designed to optimize different problems and constraints. In Chapter 5, we will investigate the multi-path selection problem instead of the single path between BSs to improve the throughput performance. In Chapter 6, load-balanced routing topologies are analyzed and designed in our hybrid fiber-wireless backhaul network with grid topology to achieve the high data rate requirement for each small cell base stations with different data traffic load. Finally, in Chapter 7, we discuss some of the existing challenges for the proposed work and present suggestions for future works.

CHAPTER 2
LITERATURE SURVEY

Mobile technology plays an important role that is constantly developing to provide better connectivity, higher data rate and large user experience. Future networks will be richer and more complex with new applications and services, which will require more processing power, transmission time and bandwidth. 5G networks are expected to provide high data rates and area capacity, reduced end-to-end latency, seamless mobility, and lower energy consumption compared to current 4G LTE networks [6]. In order to improve the spectral efficiency and increase the bandwidth, network densification is receiving a great deal of attention to realize 5G data traffic requirements. The major concern in network density deployment is the backhaul network, which should be flexible, cost-effective and have the ability to support large traffic demand of small cells. Wired and wireless are two major transmission method in backhaul communication system, both of them have their advantages and drawbacks.

In this chapter, we present the research works on 5G backhaul networking. We first discuss the improvements and requirements of 5G, and provide some recent developmental endeavors toward 5G. Next, we provide some surveys related to network densification and small cell backhauling networks. Then, fiber-based wired transmission system will be compared with the wireless transmission system which is using mmWave technologies. After that, we briefly summarize the research works in blockage handling and relay-assisted networks. Finally, research works related to hybrid backhaul networks will be introduced.

2.1 5G use cases and key performance Indicators

5G Technology stands for 5th Generation Mobile technology. The rapid growth of mobile traffic has raised concerns regarding the capacity of traditional cellular networks in 4G LTE. The emergence of smart-phones, tablets, laptops, as well as new applications like

UHD video streaming, video conference, augmented reality, virtual gaming, intelligent farming, and connected vehicles motivates the continue increase of mobile data in 5G networks [7, 8]. It is predicted by CISCO that globally, between 2017 and 2022, the mobile data traffic will rise at a compound annual growth rate (CAGR) of 46%, which will reach 77 exabytes per month by 2022 [9]. Additionally, according to the report in [10], the total number of connected devices in future communication system will reach 100 billion and the industry is getting ready for an astonishing 1000-fold of data traffic growth by 2020 and beyond [11]. Based on these requirements of the ever growing number of mobile devices and new applications, the international telecommunication union(ITU) have identified a set of standard requirements for 5G networks, devices and services, which is the International Mobile Telecommunications-2020 (IMT-2020 Standard). Fig. 2.1 illustrates potential usage scenarios and capabilities of IMT-2020. Note that 5G is not only expected to support a

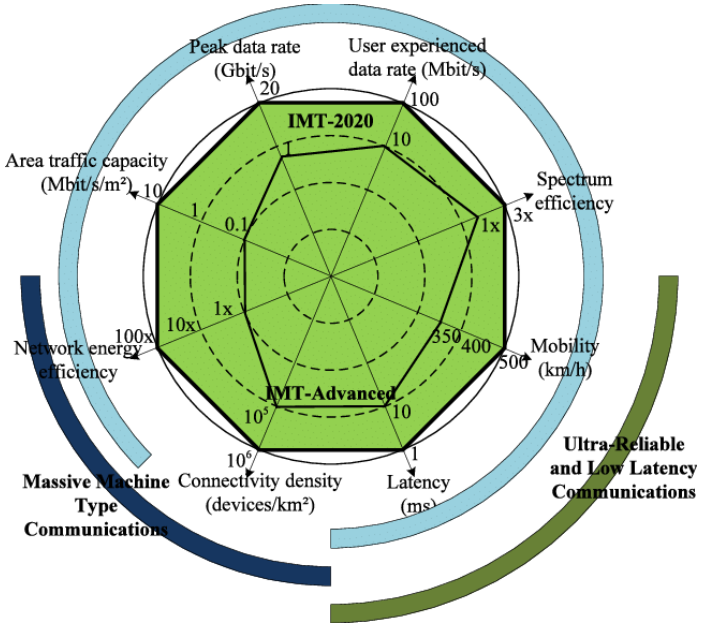

Figure 2.1: Enhancement of key parameters in 5G [6]

variety of diverse usage scenarios and applications of current cellar networks, but also need to expand and support a broad range of new applications scenarios, including:

1. Enhanced Mobile BroadBand (eMBB);

2. Massive Machine Type Communications (mMTC);

3. Ultra Reliable Low Latency Communication (URLLC).

IMT-2020 suggested eight different expected enhancement of key performance indicators (KPIs). Some of the KPIs relevant to this thesis are listed and described in the following:

- Requirement for bandwidth to be at least 100 MHz.
- Peak data rate is the maximum achievable data rate under ideal conditions in bit/s, which is the received data bits assuming error-free conditions assignable to a single mobile station. The minimum requirements for downlink peak data rate is 20 Gbit/s and uplink peak data rate is 10 Gbit/s.
- Area traffic capacity is the total amount of traffic capacity of a network in a given area and is measured in Mbps/km2.
- Minimum requirement for connection density is 1 million devices per square kilometer.

These different KPIs emerge a new bottleneck for 5G networks: the backhaul. The responsibility of a backhaul network is to connect access networks to their core networks via a wired (e.g. fiber and copper) or wireless medium (e.g. microwave and mm-wave). To achieve these KIP requirements will require huge changes in how mobile networks and their underlying infrastructures are built—especially for the wireless backhaul. Different heavy traffic cells connect to the core network through the backhaul, often with extreme requirements in terms of capacity, availability, energy, and cost efficiency [12]. In the backhaul, where latency requirements are less stringent compared to fronthaul and midhaul networks, capacity will be a key performance to improve. Network densification will be one of the key enablers to boost the capacity and coverage of future networks especially in city centres and other high traffic areas.

2.2 Small cell backhauling

For 5G mobile and wireless networks, one of the challenges is how to satisfy the requirement of high data rates and capacity. One of the solutions to solve the data rate requirement is to allow network densification by deploying small cells [13]. Densification of small cell base stations can provide high spectral efficiency, reduce mobile device power consumption and fill in areas that cannot be covered by the macro cells. It can also improve network performance and service quality by offloading from the macro cell base stations. The integration of small cells into the traditional macro cells results in heterogeneous networks (HetNets). HetNet is a mixture of various types of cells and various access technologies. The basic idea of HetNets is to bring the access nodes (ANs)/access points (APs) very close to the end users and provide a near-field network which can improve the signal-to-noise ratio and provide additional capacity. However, conventional HetNet is not capable of addressing the exponential growth of traffic in the coming years. By contrast, ultra dense HetNet (UDN) is one of the important method in 5G network to address capacity crunch and realize the high capacity requirement [14]. In UDN, small cells are deployed more dense and the links distance are shorter, small cells are uniformly distributed around a macro cell BS and forward massive amount of traffic to core network through a backhaul connection with macro cell BS like shown in Fig. 2.2. In [15], all of the works are based on this UDN scenario. However, we proposed a new scenario in our work, where we have multiple anchor base stations instead of one macro cell base station connect to the core network. With the dense deployment of small cell base stations, the capacity of backhaul links is seen as the biggest challenge for deployments. While wired and wireless are two major communication methods in 5G networks, fiber and mmWave communications will be compared and evaluated.

With dense deployment of small cell BSs, different network architectures has been investigated in backhaul scenario. Typically, there are two options for network architectures in 5G. One is the centralized backhaul solution and the other one is the distributed backhaul

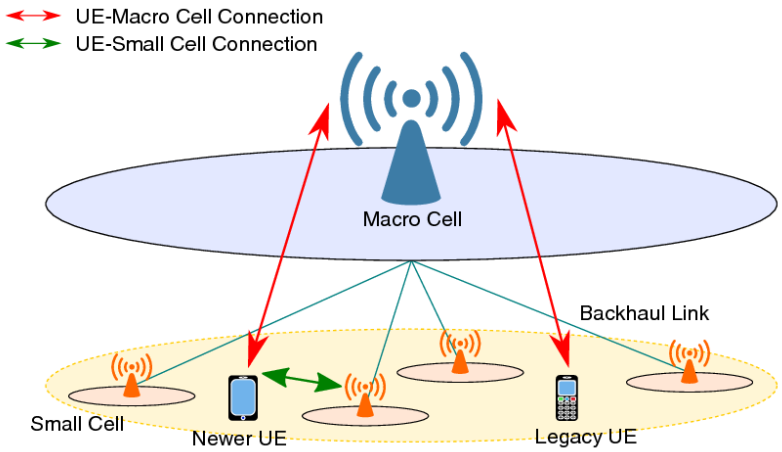

Figure 2.2: An example of UDNs consisting of a macro cell and several small cells [16]

solution [17]. In centralized network architectures, a MBS is located in the centre with small cell BSs are located around MBS. Direct links between SBSs are not allowed. In distributed network architectures, backhaul data are allowed to transmit between adjacent SBSs through mmWave links and finally are collected by the designated wired BS to the core network through fiber links. This designated wired BS serves as the gateway node for a number of small cell BSs. In [17], system-level simulations have shown that the distributed network architectures achieve higher throughput gain and more flexible than the centralized network architectures due to sharing different traffic to with multiple SBSs. Therefore, in our scenario, the distributed network architectures is adopted.

To providing low latency and cost effective backhauling mechanisms, point-to-multipoint (PMP) connection is considered as a better choice compared with PTP (point-to-point) [18], which 5G networks can be enabled by deploying small cell BSs over conventional macro cell BSs. In [18], they proposed a PMP in-band mmWave backhaul for 5G networks and they presented scheduling for realizing inter-BS communication, where backhaul links and access links are multiplexed on the same frequency band. After a short time, [19] discusses a wireless backhaul based on mmWave massive MIMO for future 5G UDN. This work proposed a scheme which can guarantee that the MBSs simultaneously support multiple SBSs with multiple streams for each small cell BSs. In [20], they proposed a millimeter wave

gigabit broadband (MGB) system to provides Gbps links to small cell BSs and fixed broadband access points. For the aforementioned related works, they consider the star-topology as the network configuration in their work, however, in [21, 22], they used the mesh and tree typologies with PMP connections as their backhaul network configurations. For all these related works, they are different from our research works. They are all "self-backhaul" solutions while dedicated relay nodes are deployed in our scenario. Moreover, most of the relate works consider in-band while we primarily focus on out-of-band backhaul where the backhaul tier operate at different frequency with the access tier.

To support a dense deployment small cell mobile backhaul with large capacity, a more cost-effective and easy to install backhaul solutions are needed. In next two sections, different backhaul technologies are presented.

2.3 Optical fiber transmission

The optical fiber communication system is an essential component of the broadband networks. It provides high-quality transmission with low latency and it is the most common transmission method for long-distance transmission [23]. Optical fiber can provide unprecedented bandwidth potential compared to any other known transmission medium. A single strand of optical fiber can provide a total bandwidth of 25,000 GHz [24]. Moreover, optical networks lend themselves well to offloading electronic equipment by means of optical bypassing as well as reducing their complexity, footprint, and power consumption significantly while providing optical transparency against modulation format, bit rate, and protocol [24]. In 5G backhaul network transmission, the useful advantages of optical fiber communication can be listed as below [25]:

- Huge possible bandwidth: In wired transmission method, the metallic cables of have less potential transmission bandwidth compared to the optical carrier frequency.
- Isolation of electrical: The material optical fiber is made of either glass or plastic polymer, these are electrical insulators. Moreover, it does not have interface prob-

lems.

- Longer distance: In fiber optic transmission, optical cables are capable of providing low power loss, which enables signals can be transmitted to a longer distance than copper cables and wireless transmission methods [23].
- The transmission loss is low.
- The security of signal: The optical fibers have high degree of protection of the signals, because their light does not radiate significantly.

The above are significant advantages of fiber communication compared to other wired or wireless communication methods. However, there also exist some drawbacks need to be overcame by fiber optical fiber communication:

- The high installation cost: The cost of the physical fiber can vary from $1 (24 count) to $6 (288 count) per foot. Even though it's easy to calculate the fiber value, to calculate the cost of internet connection can be more challenging and the cost can be more expensive [26].
- To repair and maintenance the fiber optic communication takes more effort and costs. It is done by sophisticated and specialized tools [25].
- High leasing fees.

Even though fiber is widely used for macro cell backhaul, the high installation and reparation cost make the fiber connection is not a desired solution for 5G operators, especially in urban dense area and areas where fiber is still not widely available. Deploying fibers in these areas would be a large expense for operators. Therefore, instead of fiber transmission method, mmWave becomes an attractive choice, furthermore, some operators estimated that most of the small cells will be connected with wireless backhaul instead of wired [27, 28].

2.4 Millimeter wave technology: state-of-the-art and trends

The study of mmWave can trace back to more than 100 years, for instance, Bose and Lebedew explored the experiments at wavelengths as short as 5 and 6 mm in the 1890s [29]. As for its application in radio communications, the mmWave mobile communications were invented in the 1990s and early 2000s, including system design and channel measurements [30]. Today, communication systems generally use sub-3 GHz and sub-6 GHz spectrum [14, 31]. However, due to the fact that the spectral resource below 6 GHz is becoming scaring, as the traffic demands grow, whereas a substantial amount of spectrum in the range of 3-300 GHz remains unutilized. Large efforts have been devoted to mmWave communications research and mmWave communication operates within the range of 30-300GHz is becoming a promising technique for 5G cellular system. With high available bandwidth, the tens of gigabits data rate requirement is achievable due to the high capacity.

The research on mmWave wireless communications has attracted a lot attention from both academia and industry. Numerous research literature works have investigated the characteristic of mmWave transmission, as well as sought for ways to utilize theses characteristic for achieving high data rate transmission. The standardization group spend great efforts to establish the criterion for mmWave communication and IEEE 802.11ad is the most frequently used one [32]. Mmwave bands gives where the available bandwidths are much wider than today's cellular network [33]. However, although the available bandwidth of mmWave frequencies is very large, the propagation characteristics of mmWave are significantly different from that of the microwave frequency bands, which are briefly summarized as follows:

- High path loss: In terms of conventional microwave communication, the wavelength of mmWave signals is shorter than that of microwave signals, operating at carrier frequency below 6 GHz. Hence, the path loss of mmWave signals is much higher than that of microwave signals. Although the path loss of mmWave is quite high, it is

feasible to communicate over distances that are common in urban mobile networks [30, 34], such as a few hundreds of meters [35] or even a few kilometers [36]. Even more, by using directive antennas, it has been demonstrated that it can support 10km communication ranges under clean air conditions[36]. If the air is not clean, the rain attenuation and atmospheric/molecular absorption can limit the range of mmWave communications due to the high path loss [30].

- Rain attenuation and atmospheric/molecular absorption: Field measurement results have shown that, the losses due to a rain attenuation at mmWave frequency bands are much larger than those of microwave bands and mmWave signals are more susceptible to oxygen absorption than that of microwave signals [37]. These different factors varies with the carrier frequency; Fig. 2 shows the atmospheric and molecular absorption and Fig. 3 shows the rain attenuation.

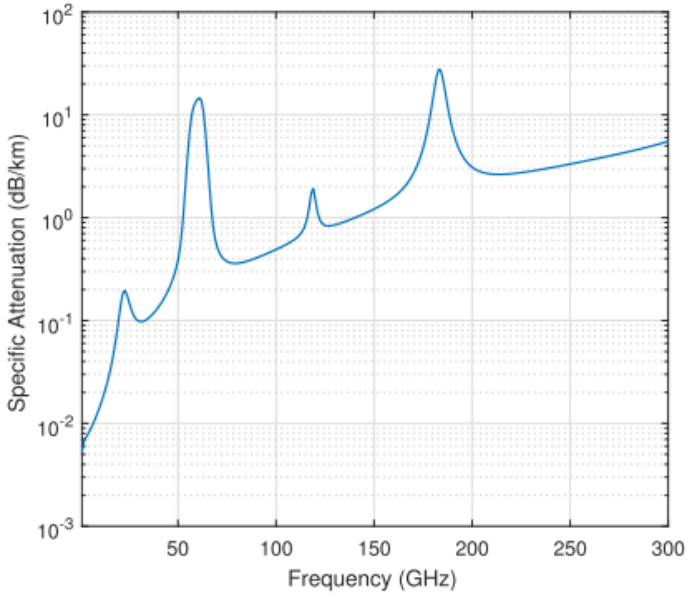

Figure 2.3: Atmospheric and molecular absorption in different frequency bands [30]

- Diffraction and blockage: Signals at microwave bands can penetrate more easily through solid materials and buildings than mmWave bands. Due to these reasons, mmWave signals are influenced by the effect of shadowing and diffraction to a much

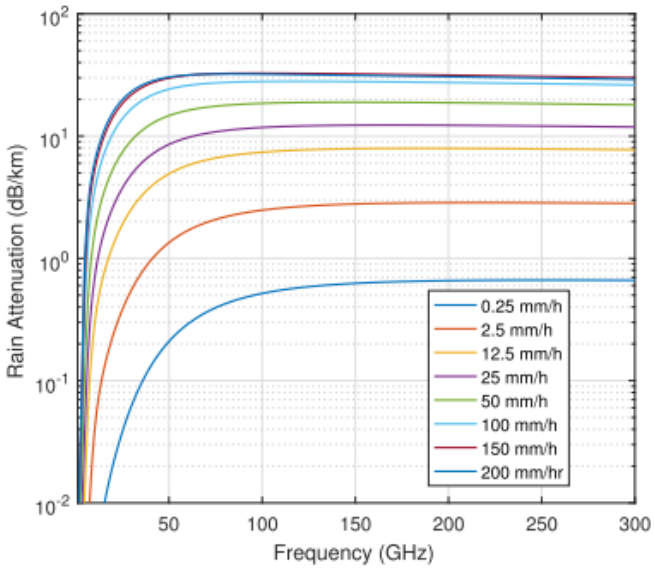

Figure 2.4: Rain attenuation in different frequency bands [30]

greater extent than microwave signals [37]. This work analyzes the severeness of blockage effect in mmWave networks [38].

All these evidences validate that the overall losses of mmWave systems are larger than those of microwave systems, therefore, despite the theoretical potentials for extremely high data rates, these several difficulties make the use of mmWave have been unattractive in outdoor scenario for a long time. Recently, a growing number of works have proposed that mmWave can be used in outdoor environment. The research works of New York University [39] show the feasibility of mmWave transmission at 28GHz, 38GHz and 73GHz bands in the small cell of 4G communication under different urban environment. Similarity, the work [40] discuss several myths on the 60GHz, and it shows the feasibility of mmWave transmission in a range of a few hundred meters, which is an acceptable coverage in mmWave small cell backhaul. However, both of these works consider the utilization of NLoS in mmWave transmission without the requirement of large data rate. In our work, we require the LoS transmission in network backhaul to guarantee the high data rate transmission. In mmWave networks, the highly directional links are modeled as pseudowired in outdoor wireless mesh networks due to the narrow beamwidth of antennas [41]. With

the highly directional antenna, it can greatly reduce the interference and path loss. For the research works in recent time, mmWave technologies have also been proposed to provide high data rate in outdoor urban dense small cell backhaul network [18]. However, several works point out the small cell base stations are not likely to have LoS to other base stations because of the blockage effect and the small cell BSs are often deployed at lower elevations than macro base station [42, 43, 44, 45]. This blockage effect is a big challenge to implement mmWave small cell BSs in backhaul networks. It is the work we discuss in the next several sections.

2.5 Blockage handling

As mentioned before, several works point out it is hard to have LoS connection between different BSs, especially in urban dense scenario. There are many works focus on the blockage handling of mmWave transmission. In works [46, 47, 48, 49], they proposed introducing infrastructure mobility to APs/BSs to improve LoS coverage and in work [50], it proposed deploying multiple APs/BSs to resist blockage effects. However, all of these works focuses on the indoor WLAN scenario instead of outdoor urban dense scenario. In works [42, 43], they considered the use of NLoS paths for small cell backhaul network. In these works, they proposed that mmWave NLoS backhaul can outperform sub-6 GHz solutions. However, in their 28 GHz backhaul network, the maximum data rate can only achieve 400 Mbps due to the high path loss. Due to the very high path loss coefficients for mmWave signals on NLoS paths, NLoS is not feasible to maintain very high data rates in the presence of blockages in outdoor environments for backhaul network. This result supports the adoption of relay nodes in our network architecture.

To quantify the obstacle problem in LoS transmission, a research work [51] shows that mmWave signals reflected off common construction materials such as concrete and brick at distances of 50-75 meters show 10-15 dB of signal strength loss. This amount of loss is large enough to influence the data rate in backhaul transmission. Therefore, we introduce

the relay nodes in our network to address the obstacle sensitivity in our LoS transmission.

2.6 Relay-assisted hybrid networks

The relay node has simple structure and is easy to be deployed. It has lower cost and is more flexible compared with base stations. Furthermore, using relay can reduce the traffic load of BS and the complexity of scheduling [52]. For the relay system, it has been developed to improve the cell-edge performance on a macro cell [53]. Various kinds of relay systems have been introduced in the third-generation partnership project (3GPP), they are used to improve the signal quality and the overall performance of the network. [53]. In such relay system, the relay nodes not only can repeat the signal but also can increase the signal quality, because the relay node can recover or amplify the received poor signal and retransmit the strengthened signal to the user end (UE). In such cases, the relay systems are used to connect the UEs located at the cell-edge to the adjacent relay node, and therefore, improve the cell-edge performance by improving the received SINR of cell-edge UEs.[54, 55, 56]. However, compared with our works, these works use relay systems to improve the cell-edge coverage and performance. In our works, we use relay nodes to extend the transmission range of mmWave communication for backhaul network and overcome the blockage effect of mmWave. There also have some other works using relay nodes. The use of single relay for WLANs/WPANs has been considered in [57, 58, 59, 60]. However, our work is significantly different with these works since we consider the outdoor long-range ultra-dense mmWave communications with multi-hop relay paths. In [32], they find multi-hop relay paths across a set of devices connecting to an AP or BS within a single mmWave BSs or cell. Due to the highly dynamic nature of the devices, in particular their locations, the primary concern is finding a relay path with the highest probability of reaching the AP or BS, rather than the aspects of design, optimization, and characterization of relay paths, which are the subject of our research, where relays are static.

In addition to the use of relay nodes, hybrid backhaul networks that utilise both fiber

and mmWave communication links is another way to overcome the shortcomings of fiber and mmWave communication. As aforementioned in previous sections, in network densification, one of the major drawbacks of the optical fibers is the high capital/operational cost of deployment. An attractive implementation solution for network densification is using wireless backhaul instead of conventional wired-optical-fiber backhaul [61]. Wireless backhaul can not only provide almost the same transmission rate as optical fiber backhaul, but also bring considerable cost decline and more flexible/timely deployment [61]. However, like aforementioned, mmWave with high frequency cannot travel long distances and are more susceptible to physical obstructions, this drawback serious impact the transmission range of mmWave especially in urban dense area. Therefore, hybrid fiber/mmWave backhaul network is an attractive transmission candidate which merges different technologies and is being considered possible supplementary for above-mentioned limitations and challenges. In 5G backhaul design, the first challenge is the need for reliable and cost-effective networks that can handle the increasing number of cells, while ensuring sufficient capacity and quality of service. The second challenge is to guarantee the user experience with varying weather conditions. Finally, it is an energy efficiency backhaul networks [62]. To meet these challenges, hybrid backhaul networks with both wireless and optical fiber links is therefore a cost-effective and energy-efficient solution to support the massive backhaul traffic [62].

There are also many related works of hybrid backhaul networks. In [63], this paper details the various technologies that are being considered to enable the integration of wireless backhaul and optical fiber networks. It also outlines the key roles that optical technologies can play and identifies the various challenges that optical networks need to overcome in order to support the next-generation of wireless networks. Additionally, [64] experimentally demonstrate how to seamlessly combine a radio-over-fiber and millimeter wave system at 90 GHz for high-speed wireless signal transmission. However, in both of these two works, optical fiber is still the main transmission medium and the wireless backhaul network is

confined to the fixed fiber-based architecture [62]. Such fiber-based architecture is still cost-prohibitive and hard to implement in dense deployment urban areas. In work [65], they evaluate various radio access technologies used in small and macro base stations, and propose algorithm splits and routs the traffic for different topologies and traffic profile Their results demonstrate the feasibility of a hybrid wireless and wired technologies. However, in their works, they assume the hybrid network topology contains a macro cell BS and a set of small cell BSs, which is different with us. In our hybrid backhaul networks, we assume that we have several fiber-connected small cell BSs connect to core network, and a set of wireless-connected small cell BSs connect to other BSs, like shown in Fig. 2.5.

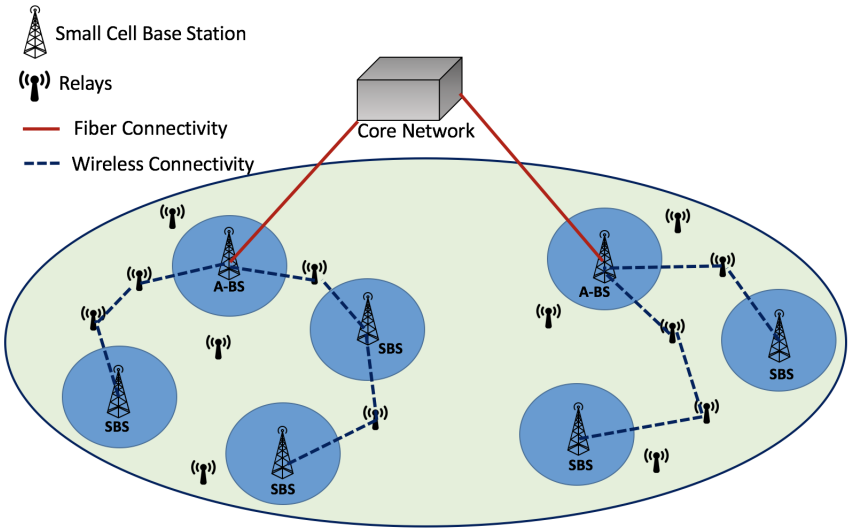

Figure 2.5: Hybrid Fiber/mmWave backhaul for 5G network

CHAPTER 3

PATH SELECTION WITH AMPLIFY AND FORWARD RELAYS IN MMWAVE BACKHAUL NETWORKS

3.1 Introduction

With the explosive growth of mobile data demand, fifth generation (5G) mobile networks with carrier frequencies in the mmWave bands are undergoing initial pilot studies. As aforementioned, mmWave communication links have enormous amount of spectrum and it can achieve individual link rates in the tens of gigabits per second. However, due to the limited communication range of very high data rate mmWave links, relay-assisted communication is required to achieve the promised ultra-high mmWave data rates. In relay-assisted communication networks, instead of a single direct long transmission from a transmitter to a receiver, intermediate (relay) nodes can be used to enhance the diversity and reduce individual transmission length by relaying the source signal to the destination. In such a situation, the source and destination cannot communicate with each other directly because the distance between them is too long to achieve the data rate requirement and/or there are some obstacles between them preventing direct communication. The relay nodes divide the long link into some short but very high rate links which can overcome high propagation loss and sensitivity to blockage of mmWave.

The most common relay strategies are decode-and-forward (DF) and amplify-and-forward (AF). While a DF relay decodes the received signal, re-encodes it, and forwards packets toward the destination, an AF relay just amplifies its received signal and forwards it on. A DF relay's complexity is significantly higher than an AF relay and it also requires greater computing power to perform decoding and re-encoding.

In this work, we consider the use of AF relays in mmWave backhaul networks. Several prior works have suggested using DF relay nodes to achieve backhaul data rates [66, 67] but, to our knowledge, this is the first work to consider improving data rates by path selec-

tion with AF relays for mmWave backhaul. Some prior works have analyzed and optimized the performance of AF relay networks [68], [69], [70], [71], [72], [73],[74]. However, these works only considered two-hop relay networks instead of the arbitrary-hop situations that are investigated herein. In [75], the authors investigated the performance of AF relays in mmWave backhaul, but the work focuses on two-hop relay networks, whereas we consider an arbitrary number of relays herein. Other work has studied the performance of N-hop AF relaying systems under different situations, e.g., with or without interference, and full or half duplex communication [76], [77]. These works focus on analysis of a given N-hop path but do not consider how to efficiently find a *best* arbitrary-hop path with a given set of candidate relays, which is one of the problems we solve herein for the mmWave backhaul problem setting. We also efficiently solve the hop-constrained optimal relay path selection problem, which has not been considered in any of the prior work.

To summarize, end to end performance and relay path selection form the basis for our study in this chapter. The precise problem we study is how to select the best amplify-and-forward relay locations to support long-range ultra-high-data-rate mmWave communication links between a given pair of source-destination BSs. Multiple relays are selected from a set of relay candidates to form a path with maximum throughput value. We first present an SNR analysis for an AF relay path with mmWave signals. We then use this analysis to transform the relay selection problem into a graph-based shortest path problem. We then apply existing graph algorithms to derive the first known efficient solutions to the optimal throughput path selection problem and the hop-constrained maximum throughput path selection problem, in a realistic wireless network setting with grid topology. We also show how these algorithms can be combined to efficiently find high-throughput paths using a small number of mmWave relays. Simulation results based on 3-D models of a section of downtown Atlanta show that these algorithms work efficiently and can find relay paths with limited number of hops and high throughput.

3.2 AF protocol

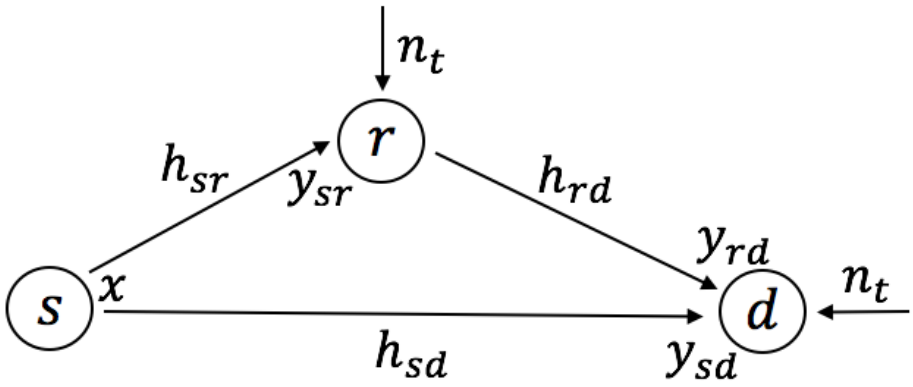

Figure 3.1: AF relay network

The AF relay function is an amplification of the received signal. Consider the relay fading channel from a source (s) to a destination (d) via a relay node (r), as shown in Fig. 3.1. It assumes that each station and relay node cannot transmit and receive simultaneously. The signals received by the relay node is

$$y_{sr} = h_{sr}x + n_t \tag{3.1}$$

where x is the transmitted signal with power constraint on average transmit power $E\{x\} \leq P_t$, h_{sr} is the amplitude of the channel gain or the channel fading coefficients from source to relay node, and n_t is complex additive white Gaussian noise (AWGN) with power σ_n^2. The relay node amplifies the received signal y_{sr} and retransmits it to the destination which receives

$$\begin{aligned} y_{rd} &= \beta h_{rd} y_{sr} + n_t \\ &= \beta h_{rd} h_{sr} x + \beta h_{rd} n_t + n_t \\ &= \beta h x + \beta h_{rd} n_t + n_t \ , \end{aligned} \tag{3.2}$$

where h_{rd} is the channel fading coefficients from relay node to the destination, $h = \beta h_{sr} h_{rd}$ is the overall channel gain from the source to the destination. For noise, which will be discussed in detail in the next section, we assume that all the channel chains have identical

noise properties, and hence, the same AWGN power. β is the relay transmit average power constraint coefficient or amplification factor scaling the power transmitted by the relay. It ensures that the average transmit power at the relay (P_r) is constant. Therefore, β can be derived as

$$E[|\beta y_{sr}|^2] \leq P_r \tag{3.3}$$

$$\beta \leq \sqrt{\frac{P_r}{h_{sr}^2 E[|x|^2] + E[|n_t|^2]}} \tag{3.4}$$

in the signal level, and β can also be derived as

$$\beta \leq \frac{P_R}{h_{SR}^2 E[|x|^2] + E[|n_{SR}|^2]} \tag{3.5}$$

in the energy level.

3.3 Network model and environment

In this work, we consider the mmWave wireless backhaul links between different dense deployed small cell BSs in urban areas with grid topology and focus on how to use relays to support the high data rate mmWave communication links. In order to achieve the high data rate requirement of mmWave links (around 10 Gbps) in backhaul networks, LoS paths have to be utilized. However, in urban areas, the LoS path between two BSs is often blocked due to the existence of buildings, walls, trees, and other obstacles. Therefore, we use a 3D model of the environment like our earlier work [67] instead of 2D here, as it gives us a more practical view of the transmission environment and more realistic measurement of the existence of LoS. Furthermore, mmWave signals in 5G scenarios are highly directional and nodes can be placed at different heights in urban settings, therefore we consider the 3D effects in our system model here. We build a 3D topology of buildings in downtown Atlanta, Georgia, and use it in the simulations presented later.

We set the maximum physical link distance in the simulations to be no more than 300 meters since longer LoS paths rarely exist in a dense urban environment. Similarly, con-

sidering the abundance of trees, moving vehicles and other obstacles located at relatively low heights, it is a wise choice to deploy outdoor mmWave BSs and relays at a height higher than 5m. The topology gives an area 1200 m $\times$ 1600 m, which includes 227 buildings higher than 5 meters. All of these buildings are modeled as cuboids for simplicity like shown in Fig. 3.2. For better cellular coverage, for each building with a height between 20 and 200 meters, one of its rooftop corners is randomly picked as a candidate location for deploying a BS position (183 positions in total). Considering the high path loss of mmWave signals, if a building is higher than h_t (e.g., $h_t = 50$ m), its candidate BS location will be set at the height of h_t. Since 183 small cell BSs are too many and BSs will be too close to each other, we partition the area into square grids with length l_g (e.g., $l_g = 200$ m), and each grid has only one BS selected randomly. Therefore, the BSs connection is based on the basic 3D grid-topology. BSs are expected to be deployed at positions with a good coverage of other relays mounted on the surfaces of surrounding buildings. A large number of candidate relay locations are uniformly distributed on the surfaces of each building, their locations are placed randomly on every building surface and an additional $0.002/m^2$ candidate relay locations are uniformly distributed over all surfaces. In simulation sections, BS pairs are randomly chosen with separations in the range of $[20, 200)$, $[200, 400)$, $[400, 600)$, $[600, 800)$, and $[800, 1000)$.

Fig. 3.2 shows a top and 3D view of the building topology in downtown Atlanta, the blank areas are ground parking lots and parks and Fig. 3.3 shows an example of BS placements and relay nodes deployed to implement communication paths between BSs in 3D topology.

3.4 Interference consideration

MmWave signals are generally less prone to mutual interference due to the directional nature of their transmissions, which limits interference between links. The highly directional links are modeled as pseudowired in outdoor wireless mesh networks due to the

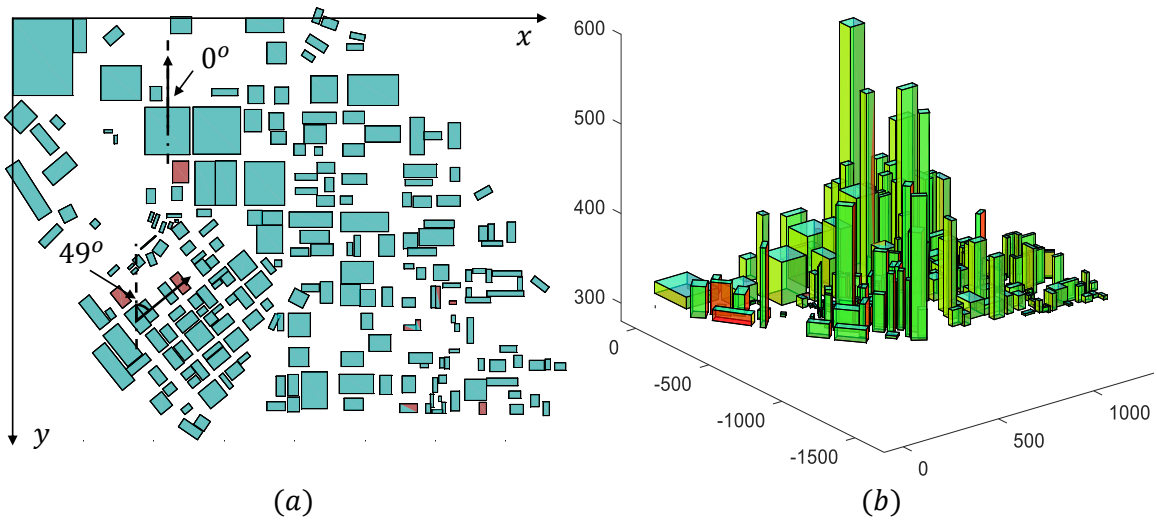

Figure 3.2: Building topology in downtown Atlanta. (a) Top view. (b) 3D view.

narrow beamwidth of antennas [41]. The urban environment considered herein makes interference even less impactful. The relays are placed on the surfaces of different buildings with different heights. These 3-dimensional differences in relays' positions and the narrow-beamwidth antennas reduce the likelihood that different links will align sufficiently to produce interference. Furthermore, many potentially interfering links will be blocked by large obstacles, i.e., the tall buildings present in urban settings. For these reasons and as in prior work on outdoor mmWave, we ignore interference in our initial analyses and designs. On the other hand, because relays are simple devices without advanced capabilities such as multiple radio chains, we assume that they are subject to the primary interference constraint meaning that no relay can transmit and receive simultaneously. This simplifies mutual interference avoidance as consecutive physical links are guaranteed not to interfere with each other. This also increases the distance separation between two physical links that could be active at the same time, thereby also lessening interference effects. However, in our simulation results, we evaluate how often this lack of interference assumption is violated to understand the potential impacts of the assumption and a corresponding method is proposed.

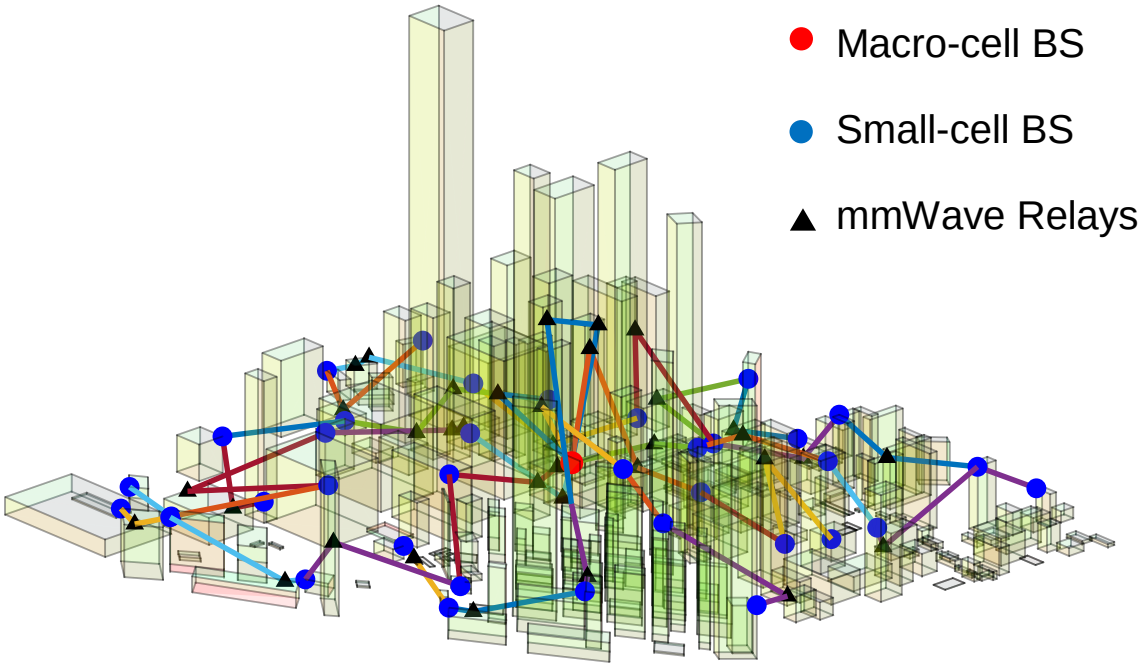

Figure 3.3: Building topology in downtown Atlanta.

Note that in our work, we only consider LoS interference but not potential interference from reflected signals. Reflected signals experience extra attenuation from obstacle surfaces and larger path loss due to longer transmission distances. Moreover, 3-dimensional differences in relay positions mean that the transmission links are generally not in a horizontal plane. Therefore, the reflected signals typically point to the ground or to the sky and will not affect the unreflected signals.

3.5 Channel model

Our channel model follows our earlier work on DF relays [67], which will facilitate future comparisons of AF and DF relay solutions. We use the standard assumption of additive white Gaussian noise. Link capacities are assumed to follow Shannon's Theorem, i.e.

$$C = B\log_2(1+\min\{\text{SINR}, \text{SINR}_{\max}\}) \ , \tag{3.6}$$

where B is the channel bandwidth in hertz and SINR is the signal to interference plus noise ratio at the receiver. In real networks, the data rate is determined by the coding and modulation schemes and has a maximum achievable value based on the technology deployed. The inclusion of SINR_{max} reflects this reality (without it, the capacity can become infinitely high, which is clearly unrealistic). We also note that our approach ensures that there is no interference along the relay paths that are selected. This, combined with the very short LoS links, will produce very stable SINR values (and therefore very stable data rates also), which can be used for path selection at network deployment time.[1]

The SINR can be stated as the following relationship:

$$\begin{aligned} \text{SINR} &= \frac{P_r}{N_T + I} \\ &= \frac{P_r}{KTB + I} \\ &\approx \frac{P_r}{KTB} \\ &= \text{SNR} \ , \end{aligned} \tag{3.7}$$

where P_r is the power of the intended transmitter's signal when the signal reaches the receiver, N_T is the power of thermal noise, I is the power of signals from any interfering transmitters. For the thermal noise, K is Boltzmann's constant and T is the temperature. SNR is the signal to noise ratio without considering interference.

Without considering interference, the path loss and attenuation loss are still taken into account when calculating P_r at the receiving antenna. The Friis transmission equation is used to calculate the transmit power P_r:

$$P_r(d) = P_t \times G_t \times G_r \times \left(\frac{\lambda}{4\pi d}\right)^{\eta} \times e^{-\alpha d} \ , fei \tag{3.8}$$

where P_t is the transmit power of transmitting antenna, G_t and G_r are antenna gains of the transmitting and receiving antenna respectively, λ is the wavelength of the signal, d is the distance between the transmitting and receiving antenna, η is the path loss exponent, and

[1] We do not consider temporary physical link blockages in this work, since we assume that base stations and relays are deployed on tops of buildings and temporary blockages will therefore be rare.

α is the attenuation factor due to atmospheric absorption.

The fixed values mentioned in previous equations are shown in Table 3.1. Due to the short LoS link used in the backhaul and the high SNR at the receiver, the relatively small random attenuation due to the shadowing effect is ignored in our analysis without influencing the effectiveness. However, the implementation loss (5dB), noise figure (5dB), and heavy rain attenuation (10dB/km) need to be considered in analysis. So, we include an additional link margin $L_m = 10\text{dB} + 10\text{dB/km} \times d$ when calculating the received power. As mentioned earlier, these values are the same as those used in our earlier work [67], in order to facilitate the comparison of these works in the future research. For these values, only the beamwidth of the antenna is different from that of the earlier work. The chosen beam width of 5^o is more in line with typical values of mmWave devices and allows for a more realistic evaluation of interference in later sections.

Table 3.1: Parameters of simulation environment

B	2.16 GHz	P_t	1 W	$G_{tx,rx}$	21.87 dBi
f_c	60 GHz	ϕ	5^o	η	2.0
L_m	10 dB	α	16 dB/km	$SINR_{max}$	50 dB

3.6 Maximum throughput relay path selection

The above formulas allow us to express our problem quantitatively. There are many possible relay paths connecting the same source and destination nodes. In order to find a path with large enough capacity, from Eqs. 3.6 and 3.7, it is obvious that a large value of transmitting power P_r will give a large capacity. Then from Eq. 3.8, we can see that the magnitude is only related to the distance as the other parameters are fixed. Therefore, an intuitive conclusion would be that the shortest overall distance path will have the largest capacity. However, the analyses we perform later prove that this is not the case.

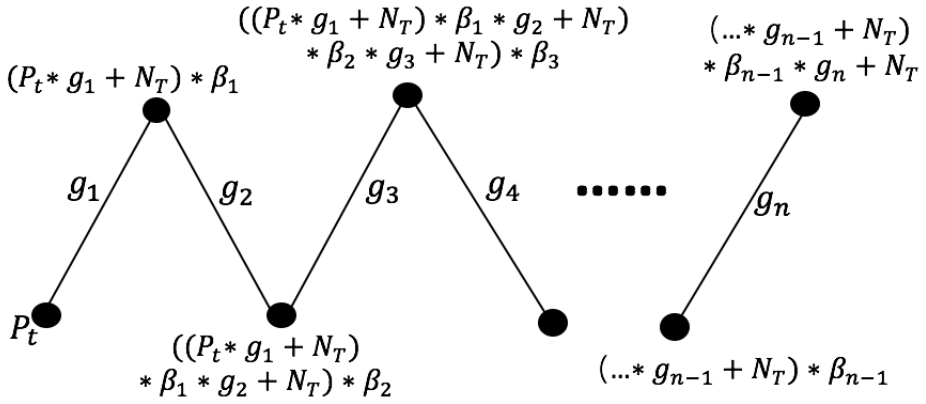

Figure 3.4: The whole path in a relay network and transmit powers of different relay nodes

3.6.1 Algorithm for finding maximum throughput relay paths

Fig. 3.4 shows an AF transmission model for a whole relay path in a network. In Fig. 3.4, g_i is obtained from Eq. 3.8 as

$$g_i = G_t \times G_r \times (\frac{\lambda}{4\pi d_i})^{\eta} \times e^{-\alpha d_i} \ , \tag{3.9}$$

where $i = 1,2,\ldots n$ and $n-2$ is the total number of relay nodes. β_i is the power amplification factor of each relay node, the transmission power P_t of each sender and each relay node is assumed to be the same value and N_T is the thermal noise power, which is the same on every link, from Eq. 3.5, β_i can be derived as:

$$\beta_i = \frac{P_t}{P_t \times g_i + n_t} \tag{3.10}$$

Hence, the intended transmitter's signal power P_r at the receiver n in Fig. 3.4 can be derived as:

$$P_r = P_t g_1 g_2 \ldots g_n \beta_1 \beta_2 \ldots \beta_{n-1} \tag{3.11}$$

The total thermal noise which is transmitted to the receiver, $N_{Total}l$ can be derived from Fig. 3.4,

$$N_{Total} = N_T(1 + \beta_{n-1} g_n + \beta_{n-2}\beta_{n-1} g_{n-1} g_n \ldots) \tag{3.12}$$

Substituting Eqs. 3.11 and 3.12 into Eq. 3.7, the SNR of the whole path can be found to be:

$$\begin{aligned} \text{SNR} &= \frac{P_r}{N_{Total}} \\ &= \frac{P_t g_1 g_2 \dots g_n \beta_1 \beta_2 \dots \beta_{n-1}}{N_T(1+\beta_{n-1}g_n+\beta_{n-2}\beta_{n-1}g_{n-1}g_n\dots)} \end{aligned} \tag{3.13}$$

Then, from substitute Eq. 3.10 into the Eq. 3.13, the SNR equation can be simplified into

$$\begin{aligned} \text{SNR} &= \frac{P_t^n g_1 g_2 \dots g_n}{\frac{N_T}{P_t^{n-1}}(G_{n-1})+\frac{N_T^2}{P_t^{n-2}}(G_{n-2})+\dots} \\ &= \frac{g_1 g_2 \dots g_n}{\frac{N_T}{P_t}(G_{n-1})+\frac{N_T^2}{P_t^2}(G_{n-2})+\dots} \end{aligned} \tag{3.14}$$

Where G_{n-m} means the random combinations of n-m numbers of g_i added together. For example, if $n = 4$:

$$G_{n-1} = G_3 = g_1 g_2 g_3 + g_1 g_2 g_4 + g_2 g_3 g_4 + g_1 g_3 g_4 \tag{3.15}$$

The value of the thermal noise power, $N_T = KTB$, is approximately 10^{-12}, where K is the Boltzmann's constant, T is temperature and B is bandwidth. The typical value of P_t is about 1W. In comparison with the value of $\frac{N_T}{P_t}$, the values of $\frac{N_T^2}{P_t^2}$, $\frac{N_T^3}{P_t^3}$ ... can be ignored. Therefore, Eq. 3.14 can be simplified to:

$$\text{SNR} \approx \frac{1}{\frac{N_T}{P_t}(\frac{1}{g_1}+\frac{1}{g_2}+\dots+\frac{1}{g_n})} \tag{3.16}$$

Consider the following term in the denominator of Eq. 3.16:

$$\sum \frac{1}{g_i} = \frac{1}{g_1}+\frac{1}{g_2}+\dots+\frac{1}{g_n} \tag{3.17}$$

The values of N_T and P_t are constant in this equation. Thus, the minimum value of Eq. 3.17 will give the maximum value of SNR. This means that in order to find a relay path with maximum throughput, we need to find a relay path that minimizes Eq. 3.17[2].

[2]Note that this analysis matches that in [76], where the authors analyzed a more general case but also discussed the high SNR case, which roughly corresponds to the network setting we consider herein.

We can now use Dijkstra's shortest-path algorithm to find a maximum-throughput path. First, we build a graph with an edge for every pair of possible relay node locations that are connected with a LoS path (and also all possible source-relay and relay-destination pairs). We can then compute the weight of every edge in the graph as the corresponding $\frac{1}{g_i}$ value. Using Dijkstra's algorithm to find a path with the minimum sum of edge weights will then also produce a path that minimizes Eq. 3.17, which is a maximum-throughput path.

3.6.2 Numerical results and simulations

We compare the results for three different cases. All three cases use Dijkstra's algorithm, but each case has different edge weight values. The first case uses $\frac{1}{g_i}$ as the edge weight and will produce a maximum-throughput relay path. The second case uses the distance between two nodes as the edge weight. This case will produce a path with the shortest total distance. In the third case, we set all edge weights to be 1, which will produce a path with the minimum number of hops.

Fig. 3.5 compares the average throughput and the average number of hops that are produced for these three different cases. It can be seen that, using $\frac{1}{g_i}$ as the weighted value in Dijkstra's algorithm, the highest throughput is achieved, as expected. The throughput difference can be quite substantial for larger values of BS separation. When the BS separation is 800–1000m, the average throughput of the maximum-throughput paths is about 9 Gbps, which is quite good. However, in this case, the maximum-throughput path uses about 28 hops on average. From the other two cases, we can see that paths with fewer than 5 hops on average exist in this situation.

The results of Fig. 3.5 show that, while our analysis allows us to use Dijkstra's algorithm to find maximum-throughput paths, these paths can have a very high cost in terms of the number of relays needed. With a large number of relays, the network stability, connectivity, reliability and delay will all be negatively affected. In many situations, achieving close to maximum throughput while using a much smaller number of relays would be a preferable solution. This is the problem we consider in the next step.

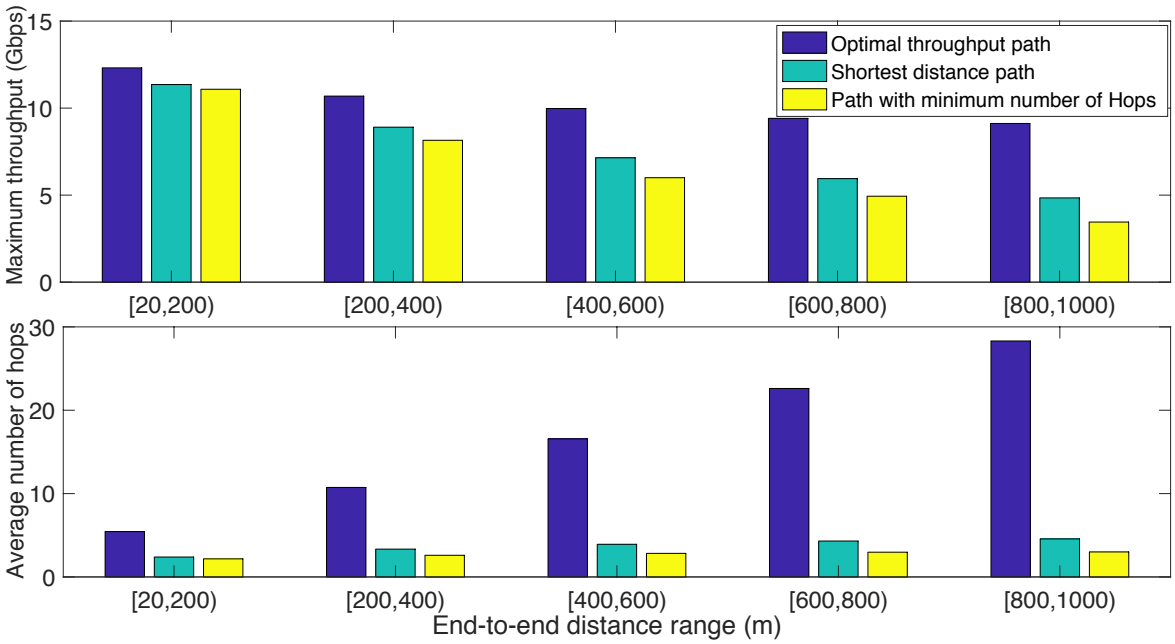

Figure 3.5: Average maximum throughput and number of hops among all available paths under three different cases

3.7 Relay path selection with maximum hop constraint

3.7.1 Hop-Constrained relay path selection algorithm

To control the number of hops in a searched path, we adopt the idea of dynamic programming (DP). We can easily find the optimal throughput path from s to d with at most h hops, if we know the optimal throughput paths from s to all neighboring nodes of d and d itself with a maximum $(h-1)$ hop constraint.

Algorithm 1 shows the pseudo-code for our improved path selection algorithm, which does a search of possible maximum throughput paths with a limited number of hops. The pseudocode uses a dynamic programming approach with recursion. Since best paths found with shorter hop counts are recorded as the algorithm executes and these values can be looked up later in constant time without additional recursion, the time complexity of the algorithm is $O(hN^2)$, where h is the maximum hop count and N is the number of nodes in the graph.

Algorithm 1 Finding the path with maximum throughput using a limited number of hops

Input: s (source), d (destination), V (nodes), N (neighbor map), h (max hop), W (weight matrix)
Output: $path$

Initialize $|V| \times (h+1)$ matrix $dist$ to Inf;
$dist[s][0] = 0$; // distance from s to s at 0 hop is 0.
Initialize $|V| \times (h+1)$ matrix pre to -1;
$pre[s][0] = s$; // pre node from s to s at 0 hop is s.
$minDist = \text{findPath}(d, h, dist, pre)$;
if $minDist == \text{Inf}$ **then**
    return NULL; // no path found
else
    return $\text{pathRecovery}(d, h, pre)$;
Function $\text{findPath}(d', h', dist, pre)$
if $h' == 0$ **then**
    return $dist[d'][0]$;
if $dist[d'][h'] < \text{Inf}$ **then**
    return $dist[d'][h']$;
$N_{d'} = N.get(d')$; // store neighbors of d' in $N_{d'}$
for n in $N_{d'}$ **do**
    $temp = \text{findPath}(n, h'-1, dist, pre) + W[n][d']$;
    if $temp < dist[d'][h']$ **then**
        $dist[d'][h'] = temp$;
        $pre[d'][h'] = n$;
$\text{findPath}(d', h'-1, dist, pre)$;
if $dist[d'][h'-1] < dist[d'][h']$ **then**
    $dist[d'][h'] = dist[d'][h'-1]$;
    $pre[d'][h'] = pre[d'][h'-1]$;
return $dist[d'][h']$;
Function $\text{pathRecovery}(d', h', pre)$
$cur = d'$
while $cur \neq s$ **do**
    $path.add(cur)$;
    $cur = pre[cur][h'--]$;
$path.add(cur)$;
return $path$;
=0

We can combine Algorithm 1 with Dijkstra's Algorithm to find a good relay path. We first use Dijkstra's algorithm to find both the maximum throughput and the minimum number of hops. For a given throughput goal, e.g., 90% of maximum, we can then repeat Algorithm 1 starting from the minimum hop count + 1 and increasing the hop count until the target throughput is reached. This ensures that a target throughput is achieved using the

minimum number of hops.

3.7.2 Numerical results and simulations

We first discuss one representative example to illustrate how throughput varies with hop count. Fig. 3.6 shows the results for this example, which is a pair of base stations in the separation range of $[600, 800)$ meters. Note that throughput increases rapidly as hop count is increased beyond the minimum value and then increases only gradually up to the maximum throughput of 9.501 Gbps, which occurs at a hop count of 24. With a hop count of only 8, a throughput of 8.673 Gbps is achieved, which is already more than 90% of the maximum.

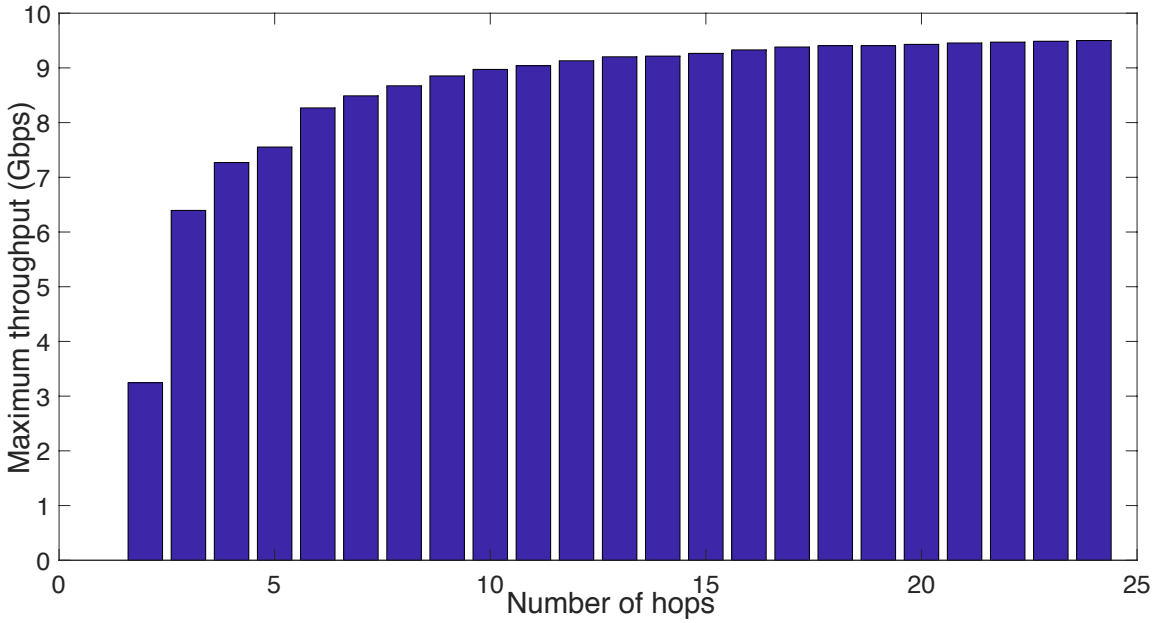

Figure 3.6: Throughput vs. hop count for one example BS pair

We also evaluate the combination algorithm in aggregate using the same 100 pairs of BSs in the five different ranges of distances as described in Section 3.6.1. Here, we set the throughput target to be 90% of the maximum throughput. Fig. 3.7 shows that the number of hops is significantly reduced with only a 10% reduction in throughput. For example, in the 800m to 1000m BS separation case, the average number of hops is reduced from about 28

to about 8, which represents a substantial savings in the number of relays, a corresponding reduction in delay, and other aforementioned benefits.

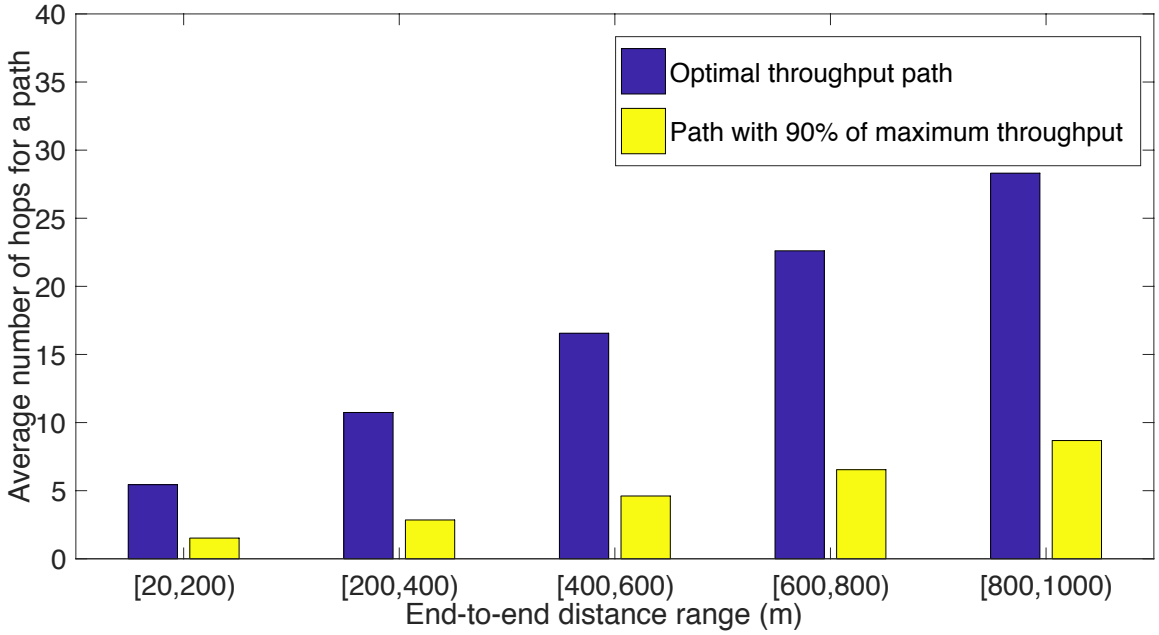

Figure 3.7: Number of hops required for a maximum-throughput path and a 90% of maximum throughput path

3.8 Interference considerations

The results presented in the previous sections assume that self-interference does not occur along paths. If this assumption is violated, the actual throughput will be lower than our analyses predict. For the same data sets used in previous sections (100 BS pairs for each BS separation range), Table 3.2 shows the frequency of interference occurring on the minimum hop, maximum throughput, and 90% of maximum throughput paths. The table shows that interference is rare. For example, on the 90% of maximum throughput paths, there are only 10 paths out of 500 total that experience interference.

We also investigate the cases where interference occurred. In 96.5% cases, the interference occurs between two links, i.e., one physical link of the transmission path has

Table 3.2: Percentage of paths with interference

BS distance (m)	Optimal path	Path with 90% throughput	Path with min. hops
$[20, 200)$	0%	0%	0%
$[200, 400)$	3%	0%	0%
$[400, 600)$	2%	1%	0%
$[600, 800)$	1%	3%	0%
$[800, 1000)$	5%	6%	0%

interference with the other physical link, no more interference happens between other pair of links. In a small number of cases, one of the physical links has interference with more than one link. There is no case that have interference between more than three links. The percentages of these different cases are shown in Table 3.3.

Table 3.3: Probability of different situations of interference occurring

Interference between 1-to-1 physical link	96.5%
Interference between 1-to-more than 2 physical links	3.5%
Interference between 3 physical links	0%

While the interference probability is small, our approach does occasionally choose a path with interference. In this situation, we want to be able to find a different non-interfering path with close to the same performance (throughput and hop count) as the interfering path. We therefore investigated a simple method to guarantee interference-free paths. In this method, if a path is chosen that has interference between links, we pick any one of the links experiencing interference and give it a very high weight value. We then re-run the algorithm to find a new path, which will not contain that link. We repeat this procedure as many times as necessary until an interference-free path is found.

We compared the newly found interference-free paths using this method with the previous paths, using 90% of maximum throughput paths as examples. From Table 3.2, the previous paths with 90% of maximum throughput in $[400, 600)$ distance range, interference occurred in one pair of BSs out of 100 total pairs. Comparing this one path with the interference-free path we found using our method, the hop count of the interference-free

path increased from 3 to 6. In this case, the average number of hops for these 100 pairs of BSs (compare to Fig. 3.7) only increased from 4.61 to 4.63. For the distance ranges of $[600, 800)$ and $[800, 1000)$, there are three pairs and six pairs of BSs that have interference in the paths, respectively. For the interference-free paths found by our method, two of the three pairs hop counts increased by 1 and two of the six pairs hop counts increased by 1, while the other paths' hop counts did not increase at all. The average number of hops for the $[600, 800)$ case increased from 6.54 to 6.56 and for the $[800, 1000)$ case, it increased from 8.68 to 8.70.

In summary, our approach can easily be modified to only produce interference-free paths, with minimal impact on the average throughput and hop count.

3.9 Antenna beamwidth investigation

As aforementioned, the value of antenna beamwidth is different from the earlier work. We choose 5^o as the beamwidth value, since it is more in line with typical values of mmWave devices and allow for a more realistic evaluation of interference. However, in order to be more comparable with other works, we also evaluate the interference occurrence with different values of antenna beamwidth, the values include 5^o, 8^o and 11^o. Table 3.4 shows the frequency of interference occurring on the optimal throughput paths with different values of antenna beamwidth.

Table 3.4: Percentage of optimal paths with interference

BS distance (m)	5^o beamwidth	8^o beamwidth	11^o beamwidth
$[20, 200)$	0%	1%	3%
$[200, 400)$	3%	3%	5%
$[400, 600)$	2%	4%	6%
$[600, 800)$	1%	2%	5%
$[800, 1000)$	5%	5%	7%

The results show that with the increase value of beamwidth, the occurrence frequency increases, however, the interference is still not a lot in large value of beamwidth. This

benefit from the blockage effect and the many obstacles in the urban environment, the 3D model for buildings reduces the overall impact of interference. We also compare the optimal throughput difference between different beamwidth value. Fig. 3.8 shows the results.

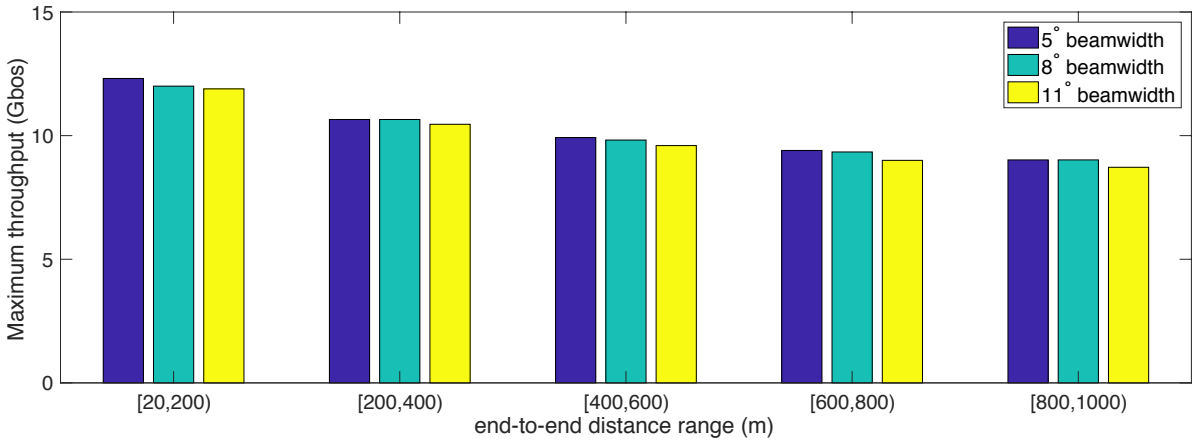

Figure 3.8: Optimal Throughput value of AF interference-free paths with different beamwidth values

Fig. 3.8 shows that with the increments of beamwidth, our algorithms are still able to find high enough throughput paths with AF relays. The maximum throughput values are virtually the same as the paths with different beamwidth value.

3.10 Chapter summary

In this chapter, we have presented path selection algorithms to find high-throughput paths using amplify-and-forward relays to support mmWave backhaul networks. While we can very efficiently find maximum-throughput paths, they often require a very large number of relays. With a slightly less efficient algorithm, however, we were able to find high-throughput paths that use far fewer relays. We also verified that the paths produced by our algorithms have a very high likelihood of being interference free and we presented an extended approach that handles the rare interference cases. Finally, we also find the frequency of interference occurring in different beamwidth degree values. We find that due

to the blockage effect in 3D urban dense environment, interference rarely exist even if we increase the beamwidth value. The interference free paths find by our algorithm are all have the high throughput values with different beamwidth value.

CHAPTER 4

PATH SELECTION WITH DECODE AND FORWARD RELAYS IN MMWAVE BACKHAUL NETWORKS

4.1 Introduction

In chapter 3, we have explored the maximum-throughput paths selection with AF relays for mmWave backhaul communications in urban environments with grid topology. As mentioned in Chapter 3, the primary relaying strategies are AF and DF. In AF relaying, each relay node simply amplifies and forward the received signal. In DF relaying, each relay node decodes, re-modulates and re-transmits the received signal. Because AF relaying amplifies noise along with intended signal at each hop, while DF relaying eliminates the noise at each hop, the end-to-end performance of DF should be superior to that of AF [55]. Hence, after the AF strategy has been investigated in chapter 3, in this chapter, we focus primarily on the DF relay case. Moreover, at the end of the chapter, we also do compare the DF relay results with existing work that studied AF relays.

The average error performance analysis of the multihop-based DF protocol is analyzed in [78][79][80][81][82]; however, these works only considered the performance of the protocol but didn't consider the path selection problem. A few works have considered the relay path selection problem with DF relays [67][83][84] previously. However, in [83][84], the possible paths are given and the methods simply choose the best one, whereas in our work, possible relay locations are given and the goal is to *select* an optimal path that goes through a subset of the given locations. The closest prior work to the work in this paper is our previous work in [67]. However, the algorithm of [67] focuses on very short relay paths with minimum or near-minimum number of relays. While the algorithm of [67] could be extended to find the overall maximum-throughput path, its time complexity grows exponentially with the length of the path and so it is impractical as a general solution to the optimal-throughput path selection problem. Thus, our algorithm presented herein is the

first polynomial-time algorithm with provably optimal throughput performance for the DF relay selection problem in mmWave backhaul.

We propose three different algorithms in this chapter, based on a novel weighted directed graph model, where nodes in the graph represent possible pairs of consecutive links in a relay path. We transform the maximum-throughput relay path selection problem into a widest path problem in this graph. Our first algorithm selects a provably optimal path, in terms of throughput, with no limitation on length and under the assumption that multiple relay nodes can be placed at the same location. In the second algorithm, we are able to constrain the graph formulation to prevent multiple relays at the same location. While our solution to this constrained problem does not guarantee the optimal throughput under this constraint, we demonstrate through simulation that the throughput is extremely close to an upper bound, making the algorithm near-optimal. Finally, to account for latency considerations, we modify the algorithm to find high-throughput paths with a small number of relays. As validated by a large number of random cases in a realistic wireless network setting, this final algorithm finds paths with very high throughput and a small number of relays. We also compare the performance of Amplify and Forward protocol in our earlier work [85] with Decode and Forward protocol in the same scenario, the algorithms they used to find the best path are both adapted from the Dijkstra algorithm, making them more comparable. The results show that compared with AF, DF protocol has better throughput performance and use fewer relays for the optimal path in a same scenario.

4.2 Network model

In order to compare the AF and DF protocols in the later section, the channel model and network environment in this chapter follow our previous AF relay works in chapter 3, we use an actual 3D based grid topology of a section of downtown Atlanta to drive the simulations. Similar to chapter 3, we focus on finding multi-Gbps backhaul logical link between a given pair of BSs. However, due to the well-known *blockage effect* on mmWave

signals, LoS links will often be unavailable in obstacle-rich urban environments. To find high throughput backhaul links, we use dedicated relays to form a multi-hop path between a given pair of BSs with each hop being a LoS link. We assume a set of candidate locations for deploying relays is given.

However, the candidate relay locations are different with our setting in chapter 3. In our DF algorithms which will be introduced in section 4.6 and 4.7, since each two consecutive links in the original graph will compose a new vertex, a bunch of new nodes will be generated in the new graph. Therefore, the new graph is larger and contains more information compared with the original graph. In order to reduce the amount of data set, we reduce the number of our relay node locations in DF simulations. Instead of randomly placed on every building surface, we pick the diagonal corners of the BSs rooftop locations as possible relay locations (183 in total). In the following comparison section, AF will use the same data set with DF.

The highly directional signals from the narrow beamwidth mmWave antennas, together with the blockage effect in mmWave, the many obstacles in the urban environment, and the 3D nature of the network topologies, make interference a fairly rare occurrence in our mmWave backhaul setting. For these reasons, we ignore interference in our initial analyses and designs like chapter 3. However, interference must be handled carefully; otherwise, the throughput performance could degrade a lot. Therefore, like the work in chapter 3, we can check the final selected paths for interference and iterate the selection process, if necessary, to find interference-free paths in the small number of cases where the original path contains interference. The last set of results we present in section 4.9 demonstrate that this process finds interference-free paths with virtually no reduction in performance compared to the paths generated without considering interference.

4.3 Channel model and propagation assumptions

The channel estimation penalty is negligible when the signal to noise ratio is high and the small scale fading is mild. In this situation, the maximum achievable rate is closely approximated by the capacity of a continuous time additive white Gaussian noise (AWGN) channel with the same SNR [66]. Our approach, presented in subsequent sections, produces very short LoS physical links, which will operate in the high SNR region and, therefore, the AWGN assumption is reasonable and link capacities can be estimated by Shannon's equation, which is Eq. 3.6 we also used in chapter 3. Note that our approach assumes that there is no interference along the relay paths that are selected. This, combined with the very short LoS links, will produce very stable SINR values (and therefore very stable data rates also), which can be used for path selection at network deployment time.[1] SINR is defined by Eq. 3.7 and the Friis transmission equation Eq. 3.8 is used to calculate the receive power.

4.4 DF protocol

Consider the simplest relay path consisting of a source station (s), a single relay station (r), and a destination station (d), as shown in Fig. 4.1. Let h_{sr} be the channel gain from s to r and h_{rd} be the channel gain from r to d.

For the data transmission along this two-hop path, r decodes the received signal y_{sr} to obtain a signal $\widehat{x}$, which it then forwards to d, LoS link from s to d is assumed to be unavailable in our obstacle-rich environments. The received signal y_{rd} at d is:

$$y_{rd} = h_{rd}\widehat{x} + n_t \tag{4.1}$$

It is observed that in case the interference is eliminated, the added noise in the received signal is removed by the decoding at a DF relay node, which then regenerates and re-encodes the signal to be forwarded to the next hop and eventually to the destination. Therefore, un-

[1] We do not consider temporary physical link blockages in this work, since we assume that base stations and relays are deployed on tops of buildings and temporary blockages will therefore be rare.

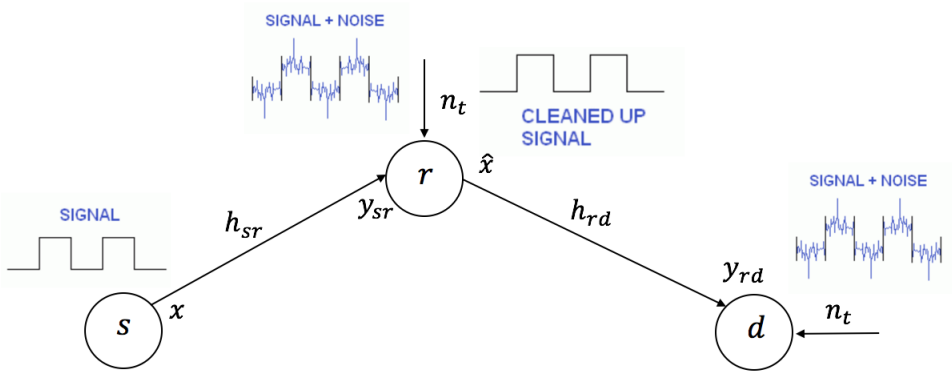

Figure 4.1: Simplest DF relay path

like the case in AF relay paths, where the maximum end-to-end throughput is determined by the end-to-end SNR [85], our previous work[67] shows that the maximum end-to-end throughput of a DF relay path is determined not only by the capacity of each individual link but also by the link schedule.

4.5 Problem formulation

Assume the same traffic demand on each individual physical link along a path is D bits. The time demand f_i of link i can be obtained as,

$$f_i = D/C_i \tag{4.2}$$

From Theorem 1 in [67]: the minimum schedule length t in a multi-hop interference-free relay path is equal to the maximum demand sum of two consecutive links, i.e.,

$$\begin{aligned} t &= \max_{1\le i\le |V|-1} f_i + f_{i+1} \\ &= \max_{1\le i\le |V|-1} D(1/C_i + 1/C_{i+1}) \ , \end{aligned} \tag{4.3}$$

where $|V_l|$ is the number of nodes in a relay path l. Thus, to obtain the maximum throughput T among all possible DF relay paths $\mathcal{L}$ between a pair of BSs, we have to find a path $l \in \mathcal{L}$

with the minimum schedule length $\min_{l\in\mathcal{L}}\{t_l\}$.

$$\begin{aligned} T &= \max_{l\in\mathcal{L}}\{D/t_l\} \\ &= \max_{l\in\mathcal{L}}\{\min_{1\le i\le |V|-1}\{\frac{C_iC_{i+1}}{C_i+C_{i+1}}\}\} \end{aligned} \tag{4.4}$$

The problem of finding a maximum-throughput DF relay path is mathematically equivalent to solving Eq. 4.4. In [67], the authors present a heuristic algorithm that finds a maximum throughput DF relay path with a very limited number of hops; however, due to its high computation complexity, it cannot be used to find a path with globally optimal throughput over paths with an arbitrary number of hops. In the next section, we propose a novel graph model that can be used to transform this problem into a well-known widest path problem in graph theory, such that a DF relay path with globally optimal throughput can be found in polynomial time.

4.6 Novel weighted directed graph model

In the widest path problem in graphs, the objective is to find a path between two designated vertices such that the weight of the minimum-weight edge in the path is maximum among all paths between the two vertices [86]. We note that this problem is similar in form to Eq. 4.4 that it maximizes some minimum quantity over the paths between two vertices. However, there is a clear gap between these two problems, because in the widest path problem, the weights are defined on the edges of the graph, while in Eq. 4.4, the weights are defined on pairs of links. To bridge this gap, we propose to transform the original graph, which consists of BSs, candidate relay locations, and possible physical links, into a novel weighted directed graph model where:

- the vertices represent 3-tuples of nodes that form a pair of links from the original graph,
- the edges connect each two vertices where the second link in the link pair of one vertex is the same as the first link in the link pair of the other vertex,

- the weight of each edge is defined as $\frac{C_i C_{i+1}}{C_i + C_{i+1}}$, where link i and link $i+1$ are the consecutive link pair specified by the edge's starting vertex.

An example of an original network graph is shown in Fig. 4.2 and its corresponding new weighted graph is shown in Fig. 4.3. In the original network graph, A represents the source BS, F represents the destination BS, B, C, D, and E represent possible relay locations, an edge between two nodes indicates that there is a LoS link between them, and the edge weights represent the capacities of the associated links. Next, we describe how the new weighted graph of Fig. 4.3 is constructed from the original graph of Fig. 4.2.

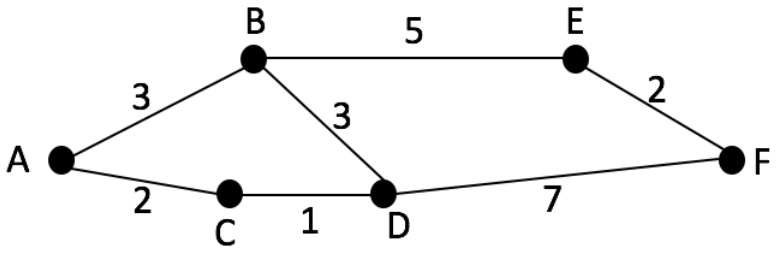

Figure 4.2: Original Weighted Graph

As mentioned, the vertices of the new graph are 3-tuples representing a pair of consecutive links in the original graph. For example, the vertex ABE represents the link (A, B) followed by the link (B, E) in the original graph. The first two columns of Table 4.1 list the nodes and their neighbors from the original graph. From the nodes and their neighbors, we generate combinations of the form neighbor, node, neighbor to form the set of vertices of the new graph. The last column of Table 4.1 shows the vertices in the new graph generated in this way. Note that not all possible combinations become new vertices. This is because the paths that we consider start from the source BS (A) and end at the destination BS (F). Thus, no path links should end at the source or start from the destination. In the table, this means that A can only appear in combinations as the first element of the tuple and F can only appear as the last element. Also, in the new graph, A is the source node and F is the sink node. For consistency in labeling, we denote those vertices by 00A and F00,

respectively. Note that the generated vertices in the new graph are directional and different notations with the same 3 nodes of the original graph have different meaning, e.g., BDC and CDB both use edges (B, D) and (D, C) but in opposite order.

Table 4.1: Create New Vertices for Weighted graph

Nodes	Neighbors	New Vertices
B	A, D, E	ABD, ABE, DBE, EBD
C	A, D	ACD
D	B, C, F	BDC, BDF, CDB, CDF
E	B,F	BEF
A	B, C	00A
F	D,F	F00

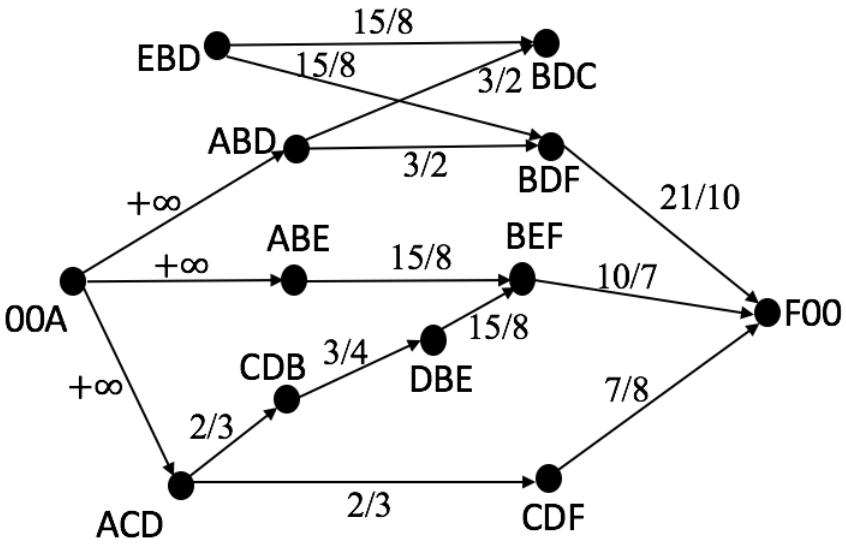

Figure 4.3: New Weighted Directed Graph

As mentioned earlier, an edge exists between two vertices in the new graph if the second edge of the first vertex's 3-tuple is the same as the first edge of the second vertex's 3-tuple. As for the source and destination vertices, since they are in the special form of 00S and D00, we define that all vertices of the form SYZ are neighbors of 00S and, similarly, all vertices of the form WXD are neighbors of D00. Based on the above methods, after identifying the neighbors of each vertex in the example, as shown in Table 4.2, we can generate different edges that point from a vertex to its neighbors like shown in Fig. 4.3.

Table 4.2: Neighbors for New Vertices

New Vertices	Neighbors	New Vertices	Neighbors
ABD	BDC, BDF	BDF	F00
ABE	BEF	CDB	DBE
DBE	BEF	CDF	F00
EBD	BDC, BDF	BEF	F00
ACD	CDB, CDF	00A	ABD, ABE, ACD
BDC	NULL	F00	NULL

The last elements of the new weighted graph are its edge weights. Referring to Eq. 4.4, we set the weight of each edge in the new graph as the weight value of the edge's starting vertex, i.e. $\frac{C_i C_{i+1}}{C_i + C_{i+1}}$, where link i and link $i+1$ are the consecutive link pair specified by the edge's starting vertex. For example, the weight of the edge (EBD, BDC) is the weight of EBD, which (referring to the capacities in Fig. 4.2) is $\frac{5\times 3}{5+3} = 15/8$. We set the weight of any edge emanating from the source vertex to infinity, which allows those edges to be used in any path without constraining the path's throughput.

Once we have generated a new weighted directed graph from an original graph, we find the widest path in the new graph, which represents the maximum throughput path in the original graph, as shown by Eq. 4.4. The path in the new graph can be easily converted to the corresponding path in the original graph. For example, the widest path in the graph of Fig. 4.3 is 00A $\rightarrow$ ABD $\rightarrow$ BDF $\rightarrow$ F00 and this corresponds to the path A $\rightarrow$ B $\rightarrow$ D $\rightarrow$ F in the original graph.

4.7 Basic DF relay path selection algorithms

4.7.1 High throughput path selection algorithm

Algorithm 2 shows the pseudo-code of our algorithm based on the widest path problem, which finds the maximum minimum weighted path in the new weighted graph and then converts the widest path to an optimal-throughput path in the original graph. The following theorem states the optimality of Algorithm 2 and gives its time complexity:

Theorem 1. *For a given source, destination base station pair and a given set of pos-*

Algorithm 2 Finding the DF relay path with maximum throughput using the method of widest path search

Input: $srcId$ (original source station), $dstId$ (original destination station), src (new source vertex), dst (new destination vertex), V_o (original vertices), V_n (new vertices), N_o (original neighbor map), N_n (new neighbor map)

Output: $OriginalPath$

Function NewGraphPath($Graph, Source, Destination$)
$width[src] = +Inf$
for each new vertex V in Graph **do**
    $width[V] = -Inf$; $prevIndex[V] = undefined$
Q = unvisited set in new Graph
while Q is not empty **do**
    u: a vertex in Q with largest $width[]$; remove from Q
    if $width[u] = -Inf$ **then**
        break;
    for each new neighbor n of u **do**
        $alt = max(width[n], min(width[u], width[n,u]))$
        if $alt > width[n]$ **then**
            $width[n] = alt$; $previous[n] = u$;
return $width; prevIndex$
Function newpathRecov($src, dst, prevIndex$)
$cur = dst$
while $cur \neq src$ **do**
    $newnodespath.add(cur)$; $cur = preIndex[cur]$;
$path.add(cur)$;
return $newpath$;
Function pathRecov($srcId, dstId, prevIndex, newpath$)
$path.add(dstId)$
for $0 < i < newnpath.size - 1$ **do**
    $path.add(newnpath[i][1])$;
$path.add(srcId)$;
return $path$; =0

sible relay locations, Algorithm 2 produces a decode-and-forward relay path with highest throughput in time $O(|E|^4)$, where $|E|$ is the number of line-of-sight links between different possible relay locations.

Proof. The optimality of the selected relay path follows directly from the graph construction of the previous section.

The time complexity of the widest-path algorithm is $O(|V|^2)$, where $|V|$ is the number of vertices of the modified graph. There is at most one vertex in the modified graph for each pair of edges in the original graph. Since $|E|$ is the number of edges in the original graph, $|V| \in O(|E|^2)$ and the overall complexity is then $O(|E|^4)$. □

In addition to producing a relay path with maximum throughput, Algorithm 2 also provides an upper bound throughput value against which the results of other non-optimal algorithms can be compared.

4.7.2 Path selection algorithm without repeat nodes

As we evaluated Algorithm 2 on different data sets, we discovered that it can produce relay paths in which the same relay location occurs multiple times. For example, if S is the source base station and D is the destination base station, then the path 00S → SIJ → IJK → JKL → KLI → LID → D00 in the modified graph is converted to path S → I → J → K → L → I → D in the original graph and this path passes through relay location I twice. This situation arises because the optimal algorithm selects widest paths on *link pairs*, rather than simply on *links*. So, in the given example, link (S, I) pairs better with link (I, J) than it does with link (I, D), while link (L, I) pairs well with link (I, D). Because of these link pairings, relay location I appears twice in the path.

In some scenarios, it might be possible to deploy two relay nodes at the same location by physically separating their antennas and this situation would not cause any major problem. However, other scenarios might have physical constraints that prevent multiple relay nodes

from being deployed at the same location. To handle scenarios in which each possible relay location can host at most one relay, we modify Algorithm 2 by not searching links in the modified graph that would produce a repeat node in the original graph. It turns out that this modification some times causes optimal paths to be missed in these new scenarios.

For example in Fig. 4.4, from source vertex 00A, the algorithm will choose path $00A \rightarrow ABC \rightarrow BCD \rightarrow CDE \rightarrow DEG$ until vertex DEG, as this path has better weighted value 4 than the other choice 3. After vertex DEG, EGB is the next choice with weight value 5 which is larger than another option 2. However, EGB reuses vertex B, therefore, EGB will be ignored and EGH will become as the next vertex. After these steps, vertex DEG determines its next vertex and will be removed from Q (unvisited set) like shown in algorithm 1. After these steps, the minimum weight value of path changes to 2 which is less than 3. Then the algorithm will consider the path $00A \rightarrow AML \rightarrow MLD \rightarrow LDE \rightarrow DEG$ in the next step. For vertex DEG, it already determined its next vertex EGH and be removed from the unvisited list, therefore, the path will choose vertex EGH after vertex DEG. However, EGB does not have repeat vertex with path at this time and it has better performance, but it is ignored in our algorithm. Therefore, our second algorithm does not consider all the paths in the graph, it only can find a near-optimal path instead of an exact optimal path. However, in the next subsection, we demonstrate that this modified algorithm still produces paths that have very close to optimal throughput.

4.7.3 Simulation results

We compare three different cases. First, we use Algorithm 2 to find an optimal-throughput relay path that might contain multiple relays of the same location. Second, we use Dijkstra's algorithm to find a path with the minimum *number* of hops. Third, we use the modified algorithm to find a relay path where each possible relay location occurs at most once.

Fig. 4.5 compares the average throughput and the average number of hops that are produced for these three cases. Note that the optimal throughput is 2–3 times higher than that

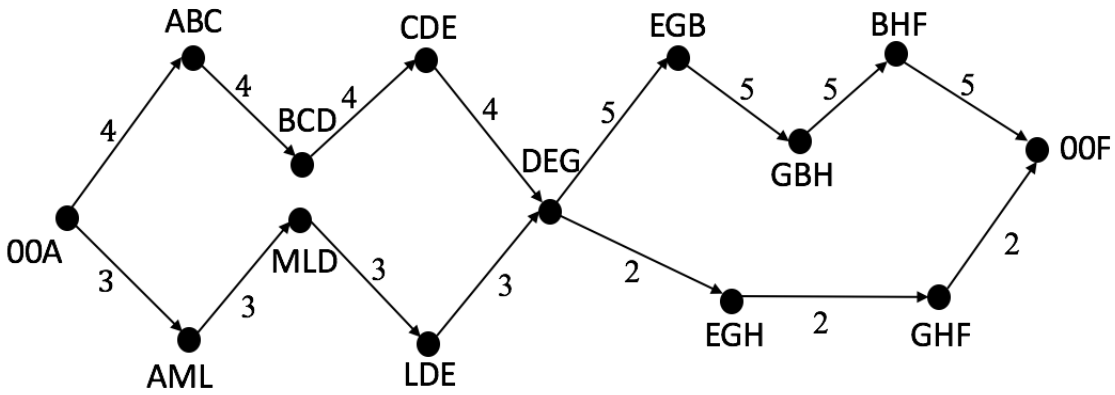

Figure 4.4: Algorithm 2 Example

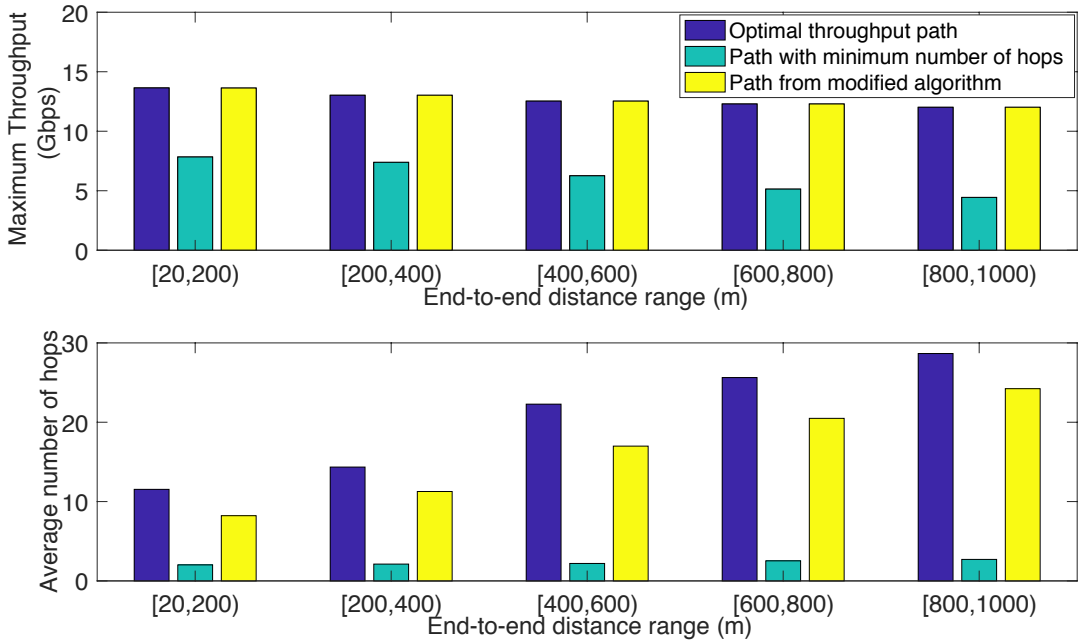

Figure 4.5: Average throughput and number of hops among selected paths with and without repeated nodes

achieved by minimum-hop paths. However, optimal-throughput path has a large number of hops in the paths. For example, in the most extreme case (maximum BS separation), the average number of hops needed for the optimal-throughput path is about 29, while minimum-hop paths use an average of only around 4 hops.

It is interesting to note that the modified algorithm that does not allow repeat nodes produces an average throughput that is very close to that of the optimal algorithm. Thus,

while the modified algorithm is sub-optimal in some cases, in practice it is very close to optimal. Eliminating repeat nodes reduces the lengths of the paths somewhat, but the number of hops is still quite high, e.g., around 24 for the maximum separation case.

The above results show that our algorithms are able to find paths with very high throughput. However, these paths can have a high cost in terms of the number of relays deployed. In the next step, we consider the path selection problem where a throughput requirement is given and the goal is to minimize the number of relays while achieving the required throughput.

4.8 Minimum hop relay path selection with throughput constraint

Given a target percentage of maximum throughput, e.g., 90%, our throughput-constrained path selection algorithm consists of the following steps:

1. Use Algorithm 2 to find the maximum throughput value, and set the throughput threshold to be the specified percentage of the obtained value.

2. Prune all edges whose weights are smaller than the threshold value from the modified weighted graph.

3. Use Dijkstra's algorithm to find a minimum-hop path in the pruned graph.

Any path in the modified graph that contains an edge with weight below the target throughput threshold will not meet the target. Furthermore, once all such edges are pruned from the modified graph, *all* remaining paths meet the throughput target. Therefore, we select a minimum-hop path from the pruned graph as the best path to satisfy the minimum throughput requirement.

As an example, we set 90% of the maximum throughput as the threshold value and compared the throughput-constrained algorithm to the algorithm from the previous section that maximizes throughput while selecting paths without repeat nodes. Fig. 4.6 shows that,

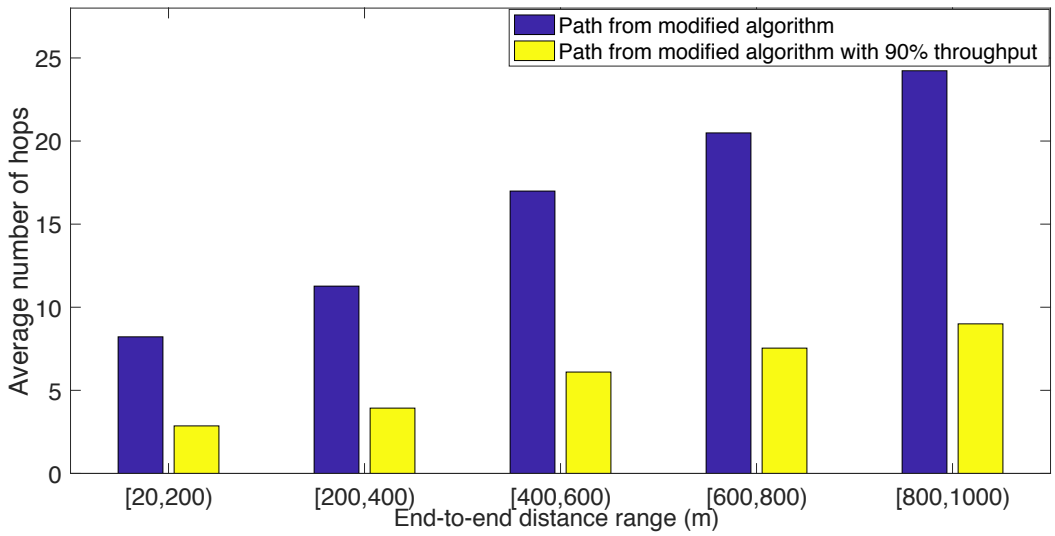

Figure 4.6: Number of hops required for best paths without repeated nodes and 90% of maximum throughput paths

for all base station separation ranges, the number of hops is reduced significantly with the throughput-constrained algorithm while only sacrificing 10% of the throughput.

4.9 Interference considerations

The results presented in the previous sections do not consider the interference issue which we mentioned before. As we assume all wireless nodes are at the top vertices of buildings in our model, the mutual interference has many chances to appear since these nodes have larger LoS view compared with the deployment in other scenarios such as on the walls of buildings. If this assumption is violated, the actual throughput will be lower than we obtained before. For the same data sets used in previous section, we find out the frequency of interference occurring on the maximum-throughput no repeat node path to verify the assumption. Table 4.3 shows the interference happens a lot as we expected before, especially when the distance between the two BSs is long.

While the interference probability is large, we want to be able to find a non-interference path. In the results presented in this section, we first ran the algorithm of Section 4.7.2 with at most one node per relay location and we then checked the resulting paths for interfer-

Table 4.3: frequency of interference occurring

BS Distance (m)	Interference on maximum throughput path
[20,200)	24%
[200,400)	25%
[400,600)	56%
[600,800)	58%
[800,1000)	70%

ence, assuming an antenna beamwidth of 11^o. If interference was found, we iterated the algorithm by removing an interfering link and re-running it. In this way, we were able to find interference-free paths in all cases. Note that in this chapter, the antenna beamwidth is 11^o, and as aforementioned, the relay locations are different with chapter 3. Therefore, the optimal throughput values of AF are different with chapter 3.

Fig. 4.7 compares the interference-free paths with the paths generated under the assumption of no interference. The results show that interference-free paths can be found with virtually the same performance (throughput and number of hops) as the paths in which interference is ignored.

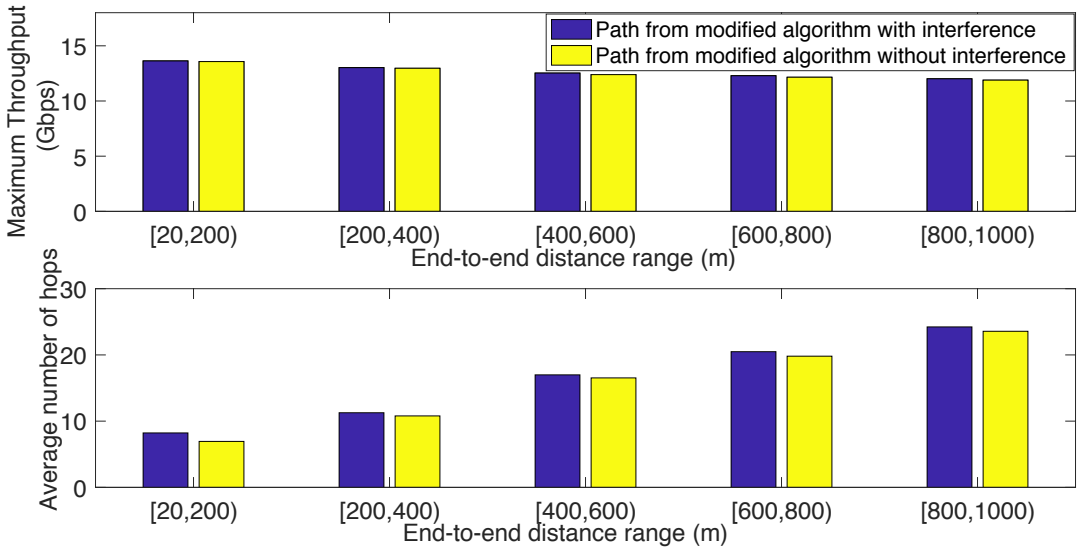

Figure 4.7: Comparison between maximum throughput path (assuming no interference) and maximum throughput interference-free path

4.10 Comparison between DF and AF

In this section, we compare two different kinds of fixed relaying protocols that are defined for wireless cooperative communications in mmWave backhaul situation. In fixed relaying protocols, we allow the relay either to amplify its received signal, maintaining a fixed average transmit power, or to decode and re-encode the received signal and then forward it to the destination. These two relaying strategies are known as amplify-and-forward and decode-and-forward, respectively. The main advantage of the DF strategy is that it eliminates the noise at relay nodes. However, the DF strategy has higher complexity and delay at each node due to modulation, demodulation, encoding, and decoding. The AF strategy is simpler and can, therefore, be implemented with lower cost. However, the AF strategy is prone to noise propagation effects because the relay node also amplifies the noise when the retransmitted signals are amplified. The noise amplification problem can degrade the signal quality.

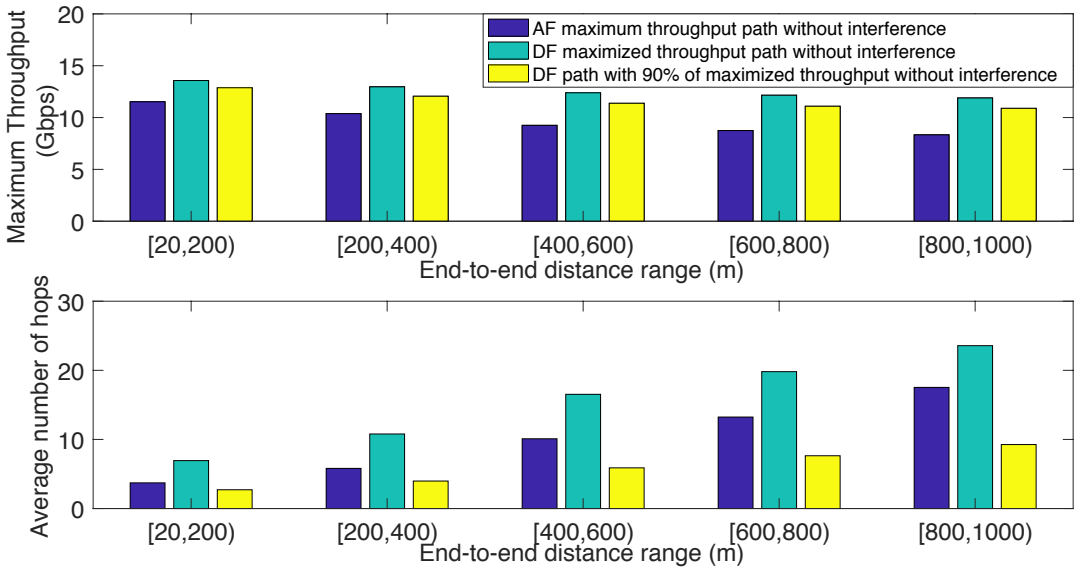

Figure 4.8: Average maximum throughput and number of hops among all available paths for DF and AF protocol

Our prior work solved the problems considered herein for AF relay paths [85] using a simpler modification of Dijkstra's algorithm that worked for the AF setting. Fig. 4.8

compares the paths selected by that algorithm for the AF case with the DF algorithm for maximized throughput without repeat nodes.[2] In both cases, we added the interference checking step at the end and found new paths without interference for the small number of interference cases that occurred. The maximized throughput DF algorithm has 10–30% higher throughput than the AF algorithm but it also requires significantly more hops. However, if we compare the DF paths with 90% of maximized throughput to the AF paths, we find that the DF paths still have larger throughput than the AF paths and they are also shorter. This indicates that to find a relay path in the same environment, DF has better performance than AF both in terms of throughput and number of hops. Of course, as mentioned earlier, DF relays are more complex and, therefore, have higher cost than AF relays. Nevertheless, the performance gains of DF relays are quite significant.

4.11 Chapter summary

In this chapter, we have developed a novel widest-path formulation of the problem of finding high-throughput paths using decode-and-forward relays to support mmWave backhaul links. This novel formulation allowed us to develop a series of algorithms, the first of which has provably optimal throughput, that solve several variations of the problem. This represents the first polynomial-time algorithm for this problem with probably optimal throughput. Simulation results verified that all of our algorithms achieve very high throughput and our final algorithm does so while using a small number of relays. We also demonstrated that relay paths using DF relays significantly outperform those with AF relays, both in terms of throughput and number of hops.

[2]For the AF algorithm, there is no benefit to having multiple relays in the same location, so we used the DF algorithm without repeat nodes for a fair comparison.

CHAPTER 5

FEASIBILITY OF MULTIPATH SELECTION IN MMWAVE BACKHAUL NETWORKS

5.1 Introduction

In chapter 3 and 4, we explored the single path selection problems for long-range ultra-high-speed relay-assisted millimeter wave backhaul networks in grid topology. To meet the increasing traffic demand and quench the ever-ending thirst of data rates in 5G mobile networks, in addition to millimeter wave communication links, using multiple paths through a network is another intuitive method to increase the bandwidth in network. Due to the dense small cell deployment and heavy traffic demands, 5G backhaul networks will need to support hundreds of gigabits per second of traffic from the core network. Even with the high data rates achievable with mmWave communication, conventional single path transmissions might not be able to meet these demands. Therefore, selecting multiple multi-hop mmWave paths in backhaul networks is a promising technique with the capability of providing a multi-gigabit transmission rate in backhaul networks. In this chapter, we focus on the problem of feasibility of multiple path selection with relays for long-range ultra-high-speed millimeter wave backhaul networks in 3D urban environments with grid topology. Multiple interference-free paths will be selected through relay selections between a pair of base stations. Due to the mmWave transmission issues mentioned in the previous chapters, relay nodes are used in this work to support the sequence of shorter communication links. Moreover, in order to achieve the ultra high rates necessary for mmWave backhaul networks, line-of-sight communication links are still utilized on each hop and the scenario considered herein is still based on the 3D outdoor grid topology of Atlanta downtown area.

Fig. 5.1 illustrates a localized piece of the reference scenario considered in this chapter with multi-path selection. SBSs are densely deployed in an urban area. Only some BSs have fiber connections to the broader network and, therefore, other BSs need to communi-

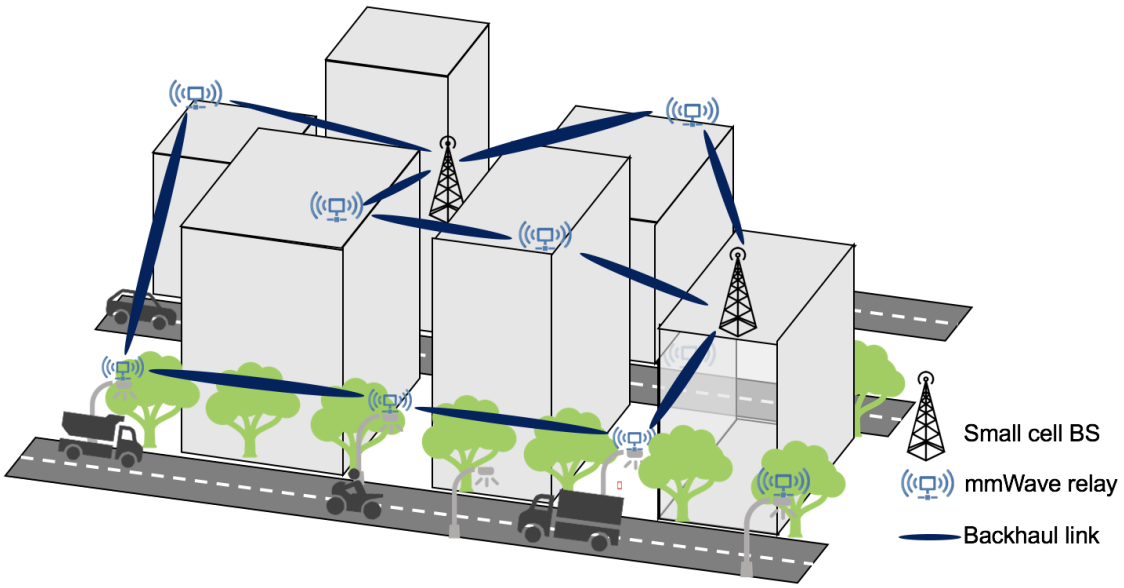

Figure 5.1: Multipath Selection in Relay Assisted mmWave Backhaul Network

cate wirelessly to send traffic to/from the wired connectivity points. Such an architecture is referred to as a self-backhaul network [87]. To facilitate line-of-sight communications between BSs in this dense urban environment, relay nodes are deployed at strategic points. As mentioned, prior works have considered how to select the best relay locations to support a *single* high-data-rate path between a pair of SBSs using line-of-sight communication at each hop. However, such a solution might still not be able to support the ultra-high data rates necessary for backhaul traffic, particularly for the links close to the wired connectivity points, where traffic is typically aggregated from a fairly high number of SBSs.

In this chapter, we explore the possibility of deploying *multiple* relay paths between a single pair of SBSs in this wireless backhaul scenario. Multiple independent and interference-free paths can be used in parallel, potentially doubling or tripling the achievable data rate between a pair of BSs. Fig. 5.1 depicts an example, where 3 independent relay paths are deployed between two SBSs. Subsequent sections present the formulation of the multi-path problem as a Boolean satisfiability problem, a heuristic algorithm for finding multiple constraint-satisfying paths, and extensive simulation results based on a realistic 3-D urban

topology. The specific contributions of this chapter include:

- the first exact formulation of the multi-path selection problem in mmWave backhaul networks with constraints,
- a reformulation of the multi-path problem as a Boolean satisfiability problem, which allows satisfiability (SAT) solvers to check for existence of multiple paths that satisfy the constraints,
- design of a heuristic algorithm to efficiently find constraint-satisfying multiple paths in many cases, and
- extensive simulation results, which demonstrate that:
  - the SAT solver can judge the existence of multiple paths precisely, but it can take more than one hour to produce a result for some of the cases we evaluated,
  - the heuristic multi-path selection algorithm produces substantial throughput improvements for mmWave backhaul connections, and
  - the heuristic algorithm is able to find multiple paths satisfying the given constraints in almost all cases where they exist and it produces its result within a few seconds for all evaluated cases.

5.2 Preliminaries

5.2.1 Network model and Channel model

We consider the same scenario with previous works in chapter 3 and 4, in order to promote the result comparison in later section. The network model based on our 3D-based grid topology of buildings in downtown Atlanta, Georgia with 227 buildings higher than 5 meters. The candidate locations for BSs and relays are similar to chapter 4, where one of the building rooftop corners is randomly picked as a candidate location for deploying a BS and the diagonal corners of these rooftops are picked as possible relay locations (183

positions in total). To avoid too many BSs in the same area, we correspondingly partition the area into square grids and each grid has only one BS selected randomly. Therefore, a grid topology with given BSs locations is used in our simulation.

Our channel model also follows earlier work in chapter 3 and 4, which facilitates comparisons of single path and multiple path solutions. We use the standard assumption of additive white Gaussian noise. Link capacities are assumed to follow Shannon's Theorem like Eq. 3.6. The SINR can be calculated as Eq. 3.7 and the Friis transmission equation Eq. 3.8 is used to calculate the transmit power P_r.

5.2.2 Interference analysis

As aforementioned, mmWave signals are generally less prone to mutual interference due to the directional nature of their transmissions resulting from the use of narrow beamwidth antennas. The highly directional signals, together with the blockage effect and the many obstacles in the urban environment, reduce the overall impact of interference. However, the interference impact of multi-path selection could be worse than the single path cases, especially the secondary mutual interference could exist when multiple physical links transmit and receive simultaneously in close proximity. For urban wireless backhaul networks, nodes are likely to be relatively high up on the sides or tops of buildings. In this situation, mutual interference has more chance to appear since the wireless nodes have wider LoS view compared with other scenarios such as the street canyon model [88]. Mutual interference must be handled carefully; otherwise, the throughput performance of a multi-hop relaying path could be significantly degraded. *Secondary mutual* interference is applied on each wireless node (i.e., BS and relay), due to the concurrent transmissions of different wireless links in the network. Mutual interference could exist between any pair of physical links in the network, including BS-to-BS, BS-to-relay, and relay-to-relay physical links. ‘

Fig. 5.2 shows different interference cases between two disjoint physical links: a) shows the highest interference case, where the interference signal is amplified by a gain of G_{high} at both ends; in this case, the angle between the useful link direction and the interference

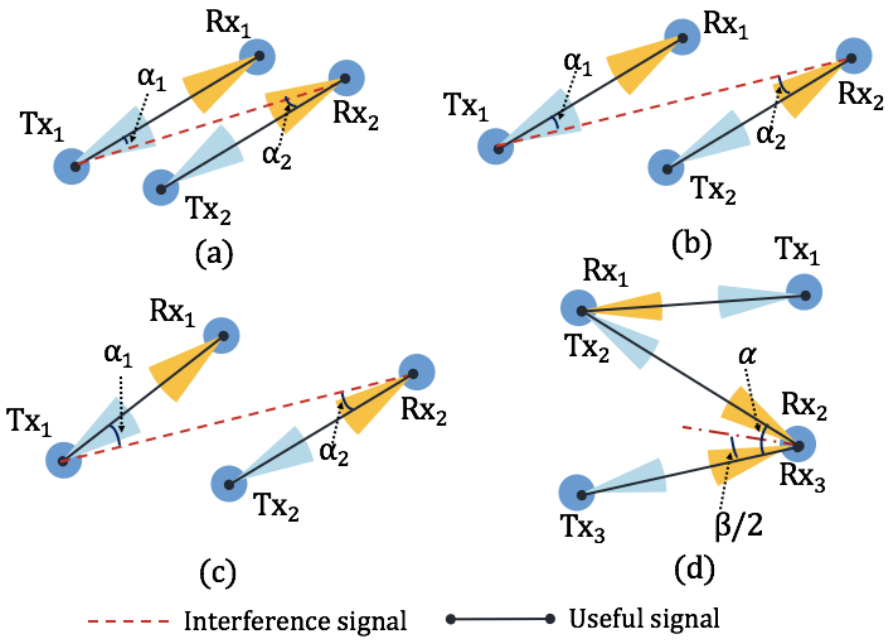

Figure 5.2: Interference conditions

signal direction (i.e., α_1 and α_2 in the figure) is smaller than the half beam width $\frac{B}{2}$, b) shows the medium interference case, where the interference signal is only amplified by G_{high} at one end, and c) shows the lowest interference case, where the interference signal experiences a gain of G_{low} at both ends; in this case, the interference strength becomes extremely low due to the rapid attenuation of mmWave signals, and we consider this case to be mutual *interference-free*.

However, in the multi-path selection problem, where a pair of physical links can transmit simultaneously to the same BS,[1] the analysis of mutual interference changes. As shown in Fig. 5.2d, when two antennas at the sharing node are receiving at the same time, it is the medium interference case, similar to case Fig. 5.2b. However, when the angle α between the two physical links becomes larger than a threshold value $\beta/2$ (see Fig. 5.2d), the antenna gain of the side lobe which receives the interference signal becomes extremely small, and this case can also be considered to be interference-free.

[1] We assume that BSs are not subject to the primary interference constraint imposed on relays, because they are complex enough to support multiple antennas.

5.3 Problem formulation

In this section, we formulate the problem of multiple path selection for mmWave backhaul relay-assisted networks using 0-1 integer programming. Specifically, we want to select relay locations from a set of candidate locations to construct multiple paths between a pair of BSs, such that the paths do not interfere with each other and where a relay can be used in only one path.

Given is a network that consists of a set of BSs $\mathcal{B}$, a set of logical links $\mathcal{L}$ and a set of candidate relay locations $\mathcal{R}$. Logical links $\mathcal{L}$ constitute the mmWave backhaul topology, which we assume is given. Each logical link $l \in \mathcal{L}$ is defined by two elements (s_l, d_l), where $s_l, d_l \in \mathcal{B}$ denote the two endpoint BSs of logical link l. In this chapter, we consider only the problem of selecting relay locations to implement one logical link of the overall mmWave backhaul. Due to the ultra high data rate requirement for backhaul links, we want to deploy multiple parallel paths for a single logical link to achieve the highest possible data rate.

Though the idea of selecting relays might seem simple, selecting physical links to select the paths is actually more straightforward. Physical links have directions, therefore, it is easier to select a path from source to destination by selecting physical links. Furthermore, each physical link is unique in our graph model, it is strictly constrained by the starting and ending nodes, however, relays are hard to constrain, they can be used in multiple different physical links. Therefore, we formalize the problem from the perspective of selecting physical links instead of selecting relays.

Using the 3D model of our urban environment and with BSs and candidate relay locations given, we can pre-evaluate the LoS connectivity between each pair of nodes (BS and relays) and obtain a set of possible LoS directional *physical links I* in the model. Note that if there exists a LoS link between a pair of BSs, this means there is a path between the BSs without the use of relays. This is a special case and we use I_{BS} to denote the set of physical links (LoS links) that connect two BSs. The set of physical links that include at

least one relay node are denoted by I_n. Then, we have that $I = I_{BS} \cup I_n$. For each pair of nodes that have a LoS link between them, a pair of directional physical links i and $-i$ are included in I ($i = 1, 2, 3, ..., \frac{|I|}{2}$). Physical links i and $-i$ share the same end nodes but have different directions. To track the selection status of these directional physical links, we use a set of binary variables $\mathcal{X} = \{x_{l,i}\}$, where l and i represent logic link l and physical link i, respectively. Therefore, if physical link i is selected by the logical link l, we set $x_{l,i} = 1$; otherwise, $x_{l,i} = 0$. The problem to be solved is to determine values of $\mathcal{X}$ that satisfy the constraints detailed in the rest of this section.

Single-source single-destination constraint: To select physical links instead of relays in the network, the "starting" and "ending" physical links in a logical link play the equivalent roles as source and destination BSs do in verifying the boundary of the logical link. Therefore, for each logical link l, we collect all physical links whose starting node is BS s_l into the first hop candidate set ($\mathcal{U}_l$), similarly, for all physical links whose ending node is BS d_l, we collect them into the last hop candidate set ($\mathcal{V}_l$). We use binary matrices $U = \{u_{l,i}\}$ and $V = \{v_{l,i}\}$ to record whether physical link i is in set $\mathcal{U}_l$ and/or in set $\mathcal{V}_l$. If $i \in \mathcal{U}_l$, then $u_{l,i} = 1$; otherwise, $u_{l,i} = 0$. Similarly, if $i \in \mathcal{V}_l$, then $v_{l,i} = 1$; otherwise, $v_{l,i} = 0$.

For each logical link l, it must contain the "starting" and "ending" physical links, therefore, each logical link has one physical link from $\mathcal{U}_l$ and one physical link from $\mathcal{V}_l$, which can be formulated as follows[2]:

$$\sum_{i \in I} u_{l,i} x_{l,i} = 1, \sum_{i \in I} v_{l,i} x_{l,i} = 1, \ \forall \ l \in \mathcal{L}. \tag{5.1}$$

If a logical link l contains only one hop, it means there exists a LoS physical link between this pair of BSs and this LoS link is selected. However, as mentioned before, due to the blockage effect, LoS links will often be unavailable between the BSs in obstacle-rich urban environments. Therefore, the logical links often contain several hops instead of one, and the formulation becomes more complicated when logic links have more than one hops.

[2] Additions in this section are decimal, not binary, calculations, i.e. $1 + 1 = 2$, $1 + 1 \neq 1$

Consecutive link constraint: To select multiple paths, it must have paths with more than one hops, the "consecutive" relationship between different physical links is helpful. A pair of physical links $i, j \in I_n$ is "consecutive" if i's ending node is the same as the the starting node of j. We use a binary indicator matrix $C = \{c_{i,j}\}$ to record the "consecutive" relationship between any pair of physical links in I_n. If i and j are consecutive physical links, $c_{i,j} = 1$; otherwise, $c_{i,j} = 0$. Obviously, if $c_{i,j} = 1$, then $c_{-j,-i} = 1$. To prevent multiple relays at the same location and account for latency considerations, we constrain that each relay node can only be selected once. Therefore, we need to avoid loops when selecting physical links, thus, we set $c_{i,-i} = 0,\ \forall i \in I_n$.

It is also obviously that the number of consecutive link pairs contained in a logical link is one less than the number of physical links in the logical link.

Note that for the physical links in the first hop candidate set, there is no physical links followed by them, and for the physical links in the last hop candidate set, there is no physical links follow them. This is because the paths that we consider start from the source BS and end at the destination BS. Therefore, there is no physical link "before" the source BS and there is no physical link "after" the destination BS. Hence, we have,

$$u_{l,i}c_{j,i}x_{l,j}x_{l,i} = 0,\ \forall\ i, j \in I_n,\ \forall\ l \in \mathcal{L}. \tag{5.2}$$

$$v_{l,i}c_{i,j}x_{l,i}x_{l,j} = 0,\ \forall\ i, j \in I_n,\ \forall\ l \in \mathcal{L}. \tag{5.3}$$

Furthermore, to ensure all the selected links construct a well connected path, we need to make sure that :1) all the selected source links which are in the first hop candidate set need to have consecutive link after it, 2) all the selected destination links which are in the last hop candidate set need to have consecutive link before it 3) for all the other physical links, they need to have consecutive links before and after it. Therefore, we can formulate this constraint as

$$u_{l,i}c_{i,j}x_{l,i}x_{l,j} = 1,\ \forall\ i, j \in I_n,\ \forall\ l \in \mathcal{L}. \tag{5.4}$$

$$v_{l,i}c_{j,i}x_{l,i}x_{l,j} = 1,\ \forall\, i,j \in I_n,\ \forall\, l \in \mathcal{L}. \tag{5.5}$$

$$c_{i,j}c_{k,i}x_{l,i}x_{l,j}x_{l,k} = 1,\ \forall\, i,j,k \in I_n,\ \forall\, l \in \mathcal{L}. \tag{5.6}$$

Dedicated relay constraint: As each relay node can only be selected once, and each physical link (except LoS links) contains at least one relay node. Therefore, we constrain that each physical link can only be selected at most once, which can be formulated as

$$\sum_{l\in\mathcal{L}} x_{l,i} \leq 1,\ \forall\, i \in I. \tag{5.7}$$

As logical links are directional, if physical link i is selected by a logical link l, to avoid using repeated relay nodes, physical link $-i$ can not be selected by any logical link in the network. Therefore, we have

$$\sum_{l\in\mathcal{L}} x_{l,i} + x_{l,(-i)} \leq 1,\ \forall\, i \in I. \tag{5.8}$$

Similarity, to avoid using repeated relay nodes, if two physical links belong to a same consecutive link pair, they cannot be selected by different logical links. Thus,

$$c_{i,j}x_{k,i}x_{l,j} = 0,\ \forall\, i,j \in I_n, k \neq l \in \mathcal{L}. \tag{5.9}$$

In-and-out-once constraint: To avoid generating loops when relays are selected to construct a logical link, we restrict that each relay must have exactly one inward physical link and one outward physical link, which is defined as the "in-and-out-once" constraint. However, from the perspective of selecting physical links, it is hard to describe this constraint with relay nodes. The concept of "consecutive" link pairs can be utilized to describe this constraint, instead. We define the "front link" is followed by the "back link" in the consecutive link pair. The following theorem describes a limitation on links designated as front and back links in order to prevent loops in the logical paths.

Theorem 2. *To prevent the generation of loops when selecting logical link l, the physical link i which is selected by logical link l (i.e., $x_{l,i} = 1$) can only be used once as a front*

link and once as a back link among all consecutive link pairs in l.

Proof. If a logical link l contains a loop, there must exist a node connects with at least three physical links (i.e., a branch-like structure), which means there exists at least two consecutive link pairs at this node, and these consecutive link pairs share either the same front link or the same back link, which is denoted as physical link i. Therefore, we constrain that each selected physical link can only be used once as front link and once as the back link among all consecutive link pairs in l. □

From the above theorem, we can formulate this constraint as

$$\sum_{j \in I_n} (1 - u_{l,i}) c_{j,i} x_{l,j} x_{l,i} \leq 1, \ \forall \ i \in I_n, \ \forall \ l \in \mathcal{L}. \tag{5.10}$$

$$\sum_{j \in I_n} (1 - v_{l,i}) c_{i,j} x_{l,i} x_{l,j} \leq 1, \ \forall \ i \in I_n, \ \forall \ l \in \mathcal{L}. \tag{5.11}$$

Mutual interference constraint: The mutual interference relationship between each pair of physical links in the network can be pre-computed based on the interference analysis in Section 5.2. We use a binary matrix $\mathcal{M} = \{m_{i,j}\}$, $i, j \in I$ to record the interference relationship between different pairs of physical links. If physical link i and j interfere with each other, we set $m_{i,j} = 1$; otherwise, $m_{i,j} = 0$.

1. Intra-flow interference constraint: For a logical link l, the intra-flow mutual interference may exist between any pair of physical links i and j, unless they belong to a same consecutive link pair. As we mentioned before, we assume relays are subject to the primary interference constraint which means no relay can transmit and receive simultaneously. Therefore, for the consecutive physical links belong to the same logical link, they cannot be activated simultaneously, thus no intra-flow mutual interference exists between consecutive link pairs. In order to formulate this constraint, we need to guarantee interference link pairs will never be selected by a same logical link simultaneously, unless they belong to the same consecutive link pair. Thus, this

constraint can be formulated as

$$(1 - c_{i,j}) m_{i,j} x_{l,i} x_{l,j} = 0, \ \forall \ i, j \in I_n, \ l \in \mathcal{L}. \tag{5.12}$$

2. Inter-flow interference constraint: In addition to considering the intra-flow interference from the "self-traffic", inter-flow interference from multiple difference logical links also needs to be considered. The concurrent transmissions between different physical links in different logical links may generate the so called inter-flow mutual interference. To formulate this inter-flow interference constraint, we need to specify the fact that if two physical links i, j belong to different logical links, then i and j do not interfere, i.e., $m_{i,j} = 0$. This leads to the following additional constraint:

$$m_{i,j} x_{k,i} x_{l,j} = 0, \ \forall \ i, j \in I, \ \forall \ l, k \in L, \ l \neq k. \tag{5.13}$$

Our final problem formulation is to determine values of X that satisfy the five sets of constraints given above.

5.4 Boolean Satisfiability

Boolean satisfiability (Bool-SAT) problems are well-known constraint satisfaction problems that appear in many areas of computer science and engineering. The significant improvement in Bool-SAT solving methods leads to the development of many successful SAT solver programs. However, even though there are many successful applications of these techniques to assist in finding solutions to various complex engineering problems, to the best of our knowledge, very few researchers have applied SAT-based methods in mobile wireless communication.

A Bool-SAT problem consists of a set of Boolean variables and a set of constraints expressed in a Boolean formula. The objective is to determine an assignment of 0-1 values to a set of Boolean variables so that the Boolean formula evaluates to TRUE and the formula is called satisfiable. Otherwise, if an assignment does not exist, we called the formula

unsatisfiable.

The Boolean formula is built from variables operators AND (conjunction, deoted by $\wedge$), OR (disjunction, $\vee$), NOT (negation,$\neg$) and parentheses. It is typically expressed in conjunctive normal form (CNF), which is also called product-of-sums form. Each conjunction term or each sum term in the CNF is called clause, and each clause is a disjunction of literals, where literal is either a variable or the negation of a variable. In order for the entire formula to evaluate to 1, each clause must be satisfied, i.e., evaluate to 1. For example, the CNF form

$$f = a \wedge (\neg a \vee b \vee c) \wedge (\neg b \vee c) \tag{5.14}$$

consists of 3 variables and 3 clauses. The formula is satisfiable by choosing the assignment of $\{a = 1, b = 0, c = 1\}$, whereas the assignment $\{a = 1, b = 1, c = 1\}$ unsatisfies the formula f. Note that a SAT problem with n different variables will have 2^n different possible assignments. In the above example with 3 variables, it will have 8 possible assignments.

5.4.1 Encoding to CNF format

Now, we study how to construct a formula which is true if and only if there exist multiple paths in a given area. To construct multiple paths by selecting relays in a relay set, all the constraints, as mentioned earlier, need to be satisfied. To present this problem into the CNF format, we can say that this problem is satisfiable if and only if each constraint is satisfied individually. Then we can encode each of the constraints to CNF format.

1. Single-source single-destination constraint: For a given pair of BSs, the binary matrices U and V are given values, thus, the first hop candidate set $\mathcal{U}_l$ and last hop candidate set $\mathcal{V}_l$ are given information. Assuming that there are 3 physical links $x_{l,a}$, $x_{l,b}$ and $x_{l,b}$ in set $\mathcal{U}_l$. Then, the first equation in Eq. 5.1 can be simplified as

$$\sum_{i \in 3} x_{l,i} = 1, \ \forall \ l \in \mathcal{L}. \tag{5.15}$$

In this equation, the sum of $x_{l,i}$ equals one, which means for all the physical links in

$\mathcal{U}_l$, only one of them is selected. To encode to the CNF format, each physical links $x_{l,i}$ can be defined as variable and Eq. 5.15 can be present in CNF format as

$$\begin{aligned} &\neg x_{l,a} \vee \neg x_{l,b} = 1, \neg x_{l,a} \vee \neg x_{l,c} = 1, \\ &\neg x_{l,b} \vee \neg x_{l,c} = 1, x_{l,a} \vee x_{l,b} \vee x_{l,c} = 1; \; \forall \, l \in \mathcal{L}. \end{aligned} \tag{5.16}$$

Each of these equations can be seen as a clause in our CNF formula. Thus, for different logic link l, with the given set $\mathcal{U}_l$ and $\mathcal{V}_l$, it can follow the steps from Eq. 5.15 to Eq. 5.16, to present this constraint in CNF format.

2. Consecutive link constraint: In a given area, the positions of relays and BSs are pre-determined, therefore, the physical links and the consecutive relationship $c_{i,j}$ are given parameters. Thus, Eq. 5.2 and Eq. 5.3 can be simplified as

$$x_{l,i} x_{l,j} = 0, \forall \, l \in \mathcal{L}. \tag{5.17}$$

where $x_{l,i}$ belongs to set $\mathcal{U}_l$ or set $\mathcal{V}_l$ and physical link i, j belong to a same consecutive link pair. To present in CNF format, Eq. 5.17 can be expressed as

$$\neg x_{l,i} \vee \neg x_{l,j} = 1, \forall \, l \in \mathcal{L}. \tag{5.18}$$

Therefore, each of the equations for different links like Eq. 5.18 can be defined as clause and $x_{l,i}$, $x_{l,j}$ can be defined as variables in CNF formula.

For the constraint expressed in Eq. 5.4, Eq. 5.5 and Eq. 5.6, they can follow the same method as Eq. 5.17. However, there is a special case, assuming in Eq. 5.4, for a source physical link i, if it does not have a following consecutive link, then the equation can be simplified as

$$\neg x_{l,i} = 1, \forall \, l \in \mathcal{L}. \tag{5.19}$$

3. Dedicated relay constraint: To select multiple paths in a given area, the number of multiple paths is a given value. Assuming we need to select two paths in this given

area, Eq. 5.8 can be simplified as

$$x_{l_1,i} + x_{l_1,(-i)} + x_{l_2,i} + x_{l_2,(-i)} \leq 1, \ \forall \ i \in I. \tag{5.20}$$

where l_1 and l_2 means the two paths, separately. Each of the physical link can be seen as a variable in the CNF format, therefore, in Eq. 5.20, it constraints that at most one variable can be evaluated to 1 and all other variables have value 0. To present in CNF format, Eq. 5.20 can be expressed as

$$\begin{aligned} &\neg x_{l_1,i} \vee \neg x_{l_1,(-i)} = 1, \\ &\neg x_{l_2,i} \vee \neg x_{l_2,(-i)} = 1, \\ &\neg x_{l_1,i} \vee \neg x_{l_2,(-i)} = 1, \\ &\neg x_{l_1,(-i)} \vee \neg x_{l_2,i} = 1, \ \forall \ i \in I. \end{aligned} \tag{5.21}$$

Each of equations in Eq. 5.21 can be seen as clauses in CNF format. For Eq. 5.9, it follows the same step with Eq. 5.2 to simplify to the CNF format. Therefore, with given number of multiple paths and physical links, the dedicated relay constraint can be presented in CNF format.

4. In-and-out-once constraint: For each physical link $x_{l,i}$, whether it is selected or not is not given, therefore, in Eq. 5.10 and Eq. 5.11, the equations are less or equal than one. These equations can rewrite as

$$\begin{aligned} &(1 - u_{l,i})\{\neg x_{l,i} + x_{l,i} \sum_{j \in I} c_{j,i} x_{l,j}\} = 1, \\ &(1 - v_{l,i})\{\neg x_{l,i} + x_{l,i} \sum_{j \in I} c_{i,j} x_{l,j}\} = 1, \\ &\forall \ i \in I, \ \forall \ l \in \mathcal{L}. \end{aligned} \tag{5.22}$$

where $\neg x_{l,i}$ represents the physical links which are not selected. As mentioned earlier, $u_{l,i}$, $v_{l,i}$ and $c_{i,j}$ are given parameters. Assuming in a logic link l_1, the physical link i is not a "starting" link, it shares a consecutive link pairs with 2 different physical links p and q, i is the back link in these link pairs. Then the first equation in

Eq. 5.22 can be simplified as

$$\neg x_{l,i} + x_{l,i} \sum_{j \in 2} x_{l,j} = \neg x_{l,i} + \sum_{j \in 2} x_{l,j} = 1, \forall\, l \in \mathcal{L}. \tag{5.23}$$

which forces only one of physical link can be selected from the two available physical links. To present in CNF format, Eq. 5.23 can be rewritten as

$$\begin{aligned} &\neg x_{l_1,i} \vee \neg x_{l_1,p} \vee \neg x_{l_1,q} = 1, \\ &\neg x_{l_1,i} \vee x_{l_1,p} \vee x_{l_1,q} = 1. \end{aligned} \tag{5.24}$$

Each of the equation above can be seen as a clause in the CNF formula. Therefore, follows these transformation steps, this constraint can be presented in CNF format.

5. Mutual interference: As mentioned earlier, with the given physical links, the mutual interference relationship between each pair of physical links can be pre-computed and the consecutive relationship are given parameters. Therefore, the values of $m_{i,j}$ and $c_{i,j}$ for different link pairs are given. Then, Eq. 5.12 and Eq. 5.13 can be simplified as

$$x_{k,i} x_{l,j} = 0,\ \forall\, i, j \in I_n,\ k, l \in \mathcal{L}. \tag{5.25}$$

To present in CNF format, Eq. 5.25 can be expressed as

$$\neg x_{k,i} \vee \neg x_{l,j} = 1,\ \forall\, i, j \in I_n,\ k, l \in \mathcal{L}. \tag{5.26}$$

Therefore, each of the equations for different links like Eq. 5.26 can be defined as clause and $x_{k,i}$, $x_{l,j}$ can be defined as variables in CNF formula.

Once we have converted all of the constraints into CNF formulas, which is the standard input format for conventional SAT solvers, we find that this problem is a Boolean satisfiability problem and we can use a SAT solver to check whether there exist multiple paths in a given area. Our simulation results in later sections use a SAT solver which is based on the Davis-Putnam-Logemann-Loveland (DPLL) algorithm [89]. This is a backtracking-based search algorithm that traverses the variable assignments until a satisfying assignment is

found (the formula is satisfiable), or all combinations have been exhausted (the formula is unsatisfiable).

It turns out that when the network size becomes large, i.e. the number of BSs and relays increases, the number of variables and the number of clauses grow rapidly and, therefore, the number of possible assignments to test also increases rapidly. We can predict that, for a SAT solver with a large number of assignments, even with a powerful method that expedites the backtrack search algorithm, a substantial computation time will be required to produce a solution.[3] Thus, in the next section, we propose a heuristic algorithm that terminates much faster than the SAT solver in larger networks.

5.5 Heuristic algorithm for multipath selection

In this section, we devise a heuristic algorithm to solve the multiple paths selection problem in relay-assisted mmWave backhaul networks. In our earlier work [85] [90], we developed single path selection algorithms that find optimal-throughput paths in mmWave backhaul networks. However, in the upcoming simulation section, we show that multiple (non-optimal) paths easily outperform single optimal-throughput paths. Moreover, our earlier algorithms cannot be applied directly to the multiple path selection problem. This is because, in addition to eliminating intra-flow interference, we also need to consider inter-flow interference between different paths, which is not considered in the earlier work. In addition to the interference consideration, if multiple paths are selected independently, the same relay location could be selected in multiple paths. However, this situation is not allowed in our problem formulation, as mentioned earlier.

To restate the problem, we need to find multiple node-disjoint paths in a given area with interference and re-use constraints, using all of the candidate relay locations as potential nodes in the paths. Some earlier works [91] proposed finding multiple paths based on a maximum flow (max-flow) method. Referring to these earlier works, we can find multiple

[3] Our simulation results in Sec. 5.6 validate this.

vertex-disjoint paths by reducing the problem to a max-flow problem in an appropriately constructed graph. After multiple paths are found, we can check pairs of paths for inter-flow interference. In order to maximize performance, we will choose the pair of paths with highest combined throughput among all pairs of interference-free paths.

To construct an appropriate graph for the max-flow problem, we use the "node splitting" method mentioned in [91] as shown in Fig. 5.3. The objective of node splitting is to transform the maximum flow problem with node-disjoint constraint into the standard maximum flow problem with link capacity constraint. An appropriate graph is constructed as follows:

1. Split each relay v into two virtual nodes v_{in} and v_{out}. Add a link (v_{in}, v_{out}) with link capacity 1.

2. Replace each other edge (u, v) in the graph with an edge from u_{out} to v_{in} of capacity 1.

3. Add in a new dedicated source node s and destination node d. Replace each source edge with (s, v_{in}) and each destination edge with (v_{out}, d), and set all edge capacities to 1.

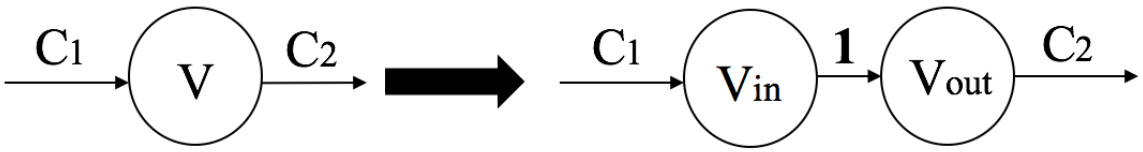

Figure 5.3: "node splitting" method

With these procedures, node v_{in} receives all the input flows of relay v, node v_{out} sends all the output flows of v, and the added link (v_{in}, v_{out}) will constrain relay v to be selected at most once. Since all edges in this graph have a capacity of 1, this means that each physical link can only be used once.

Algorithm 3 Max-IFMP: Finding multiple interference-free paths using a modified max-flow algorithm

Input: original network, transformed network G = (V, E) with all flow capacities equal to 1, a source node s, and a sink node t

Output: A pair of interference-free paths in original graph or empty paths if no solution found

1: Create the residual graph G_f
{ following lines are Ford-Fulkerson Alg. }
2: Initialize flow on all edges to 0
3: **while** path exists from s to t in G_f **do**
4: $c_f(p)$= min $(c_f(u,v) : (u,v) \in p)$
5: add this path to $transform-path$
6: **for** each edge $(u,v) \in p$ **do**
7: **if** (u,v) is forward edge **then**
8: flow(u,v) = flow(u,v)+ $c_f(p)$
9: **else**
10: flow(u,v) = flow(u,v) - $c_f(p)$;
{ now, convert found paths back to paths in original graph }
11: **for** each path in $transform-path$ **do**
12: remove all nodes inserted by the node-splitting method
13: add path to $orig-path$
{ now, find max. throughput pair of interf.-free paths }
14: $P_a = \varepsilon$, $P_b = \varepsilon$
15: **for** each $P_i, P_j \in orig-path$ **do**
16: **if** P_i and P_j are interference-free and combined throughput is higher than previous best pair **then**
17: $P_a = P_i$, $P_b = P_j$
18: **return** P_a, P_b; =0

Once we have generated a new appropriate graph from the original graph, we can transform the multiple paths selection problem into a max-flow problem and find multiple paths in the new graph. We then check the resulting paths for interference. By checking interference only after selecting the multiple paths, some interference-free paths might be missed using this method. However, our results in the later section show that this method finds multiple interference-free paths at a rate very close to the SAT solver meaning that, in practice, potential solutions are not missed frequently. In the case where multiple pairs of interference-free paths are produced by the max-flow method, we simply choose the pair with highest combined throughput. The pseudocode for our heuristic algorithm, referred to as Algorithm Max-IFMP, is shown in Algorithm 3.

5.6 Numerical results and simulations

In this section, we compare Algorithm Max-IFMP against the optimal single path solution and the SAT-solver method.[4] As mentioned earlier, we use an actual 3D topology of a section of downtown Atlanta to drive the simulations. Within this topology, we deployed 42 BSs at select positions and 183 candidate relay locations. We limit the maximum physical link distance to 300 meters and we randomly chose BS pairs separated by a distance in the range of $[20,200)$, $[200,400)$, $[400,600)$, $[600,800)$, and $[800,1000)$. The fixed parameter values mentioned in equations are similar with our previous works in chapter 3 and 4. However, due to the interference issue could be worse in the multi-path cases, we increase the antenna beamwidth in this work to guarantee the accuracy of results. The antenna beamwidth is 30^o in this work.

5.6.1 Comparison of single optimal path vs. multiple paths

In this subsection, we compare the throughput performance of a single optimal relay path against the multiple relay paths produced by Algorithm Max-IFMP. To find the optimal single path, we use our algorithm from [90]. Fig. 5.4 shows the average throughputs that

[4] We used an open-source SAT solver [92] that uses the well-known DPLL method [93].

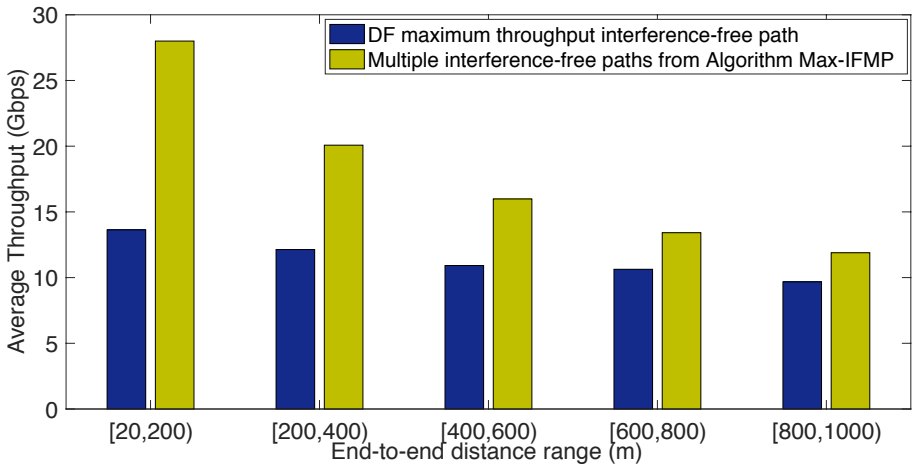

Figure 5.4: Average throughputs for single path and multiple paths

are produced for these two different cases. The figure clearly shows that finding multiple (non-optimal) paths significantly outperforms a single optimal path. For the shorter BS separations, which is the common case for densely-deployed SBSs, the throughput is increased by 60–100% when using multiple paths.

We note that the average throughputs for Algorithm Max-IFMP reported in Fig. 5.4 are calculated only across the cases where a multi-path solution was found. However, there are some cases where the algorithm did not find a solution. To evaluate how frequently this situation occurs and to determine how often Algorithm Max-IFMP fails to find a solution when multiple interference-free paths do exist, we compare it against the SAT solver method in the next subsection.

5.6.2 SAT-Solver vs. Heuristic algorithm

Feasibility of Multiple Paths

Here, we evaluate the feasibility of finding multiple paths for different BS separations in different sized areas with the SAT-solver method and Algorithm Max-IFMP. We considered two BS separations, $[20, 200)$ and $[200, 400)$, and varied the size of the area considered. Within our total area of 1200m $\times$ 1600m, we selected three different subareas of sizes 400m $\times$ 400m, 600m $\times$ 600m and 800m $\times$ 800m, respectively. Fig. 5.5 shows the results for these cases. The satisfaction rate is defined as the fraction of cases for which multiple paths

between BSs that satisfy all the relevant constraints were found. Note that the satisfaction rate increases as the size of the area increases. With an area of size 400m $\times$ 400m and a BS separation in the range $[200, 400)$, the SAT solver is able to find multiple paths about 80% of the time, whereas with an area of size 600m $\times$ 600m and the same BS separation, it finds multiple paths in every case. Note also that Algorithm Max-IFMP produces a satisfaction rate that is very close to that of the SAT-solver method for all area sizes and BS separations in Fig. 5.5. Thus, while Algorithm Max-IFMP does not find multiple paths in all cases where it is possible, in practice it is very close to the perfect solution (in terms of feasibility) given by the SAT solver.

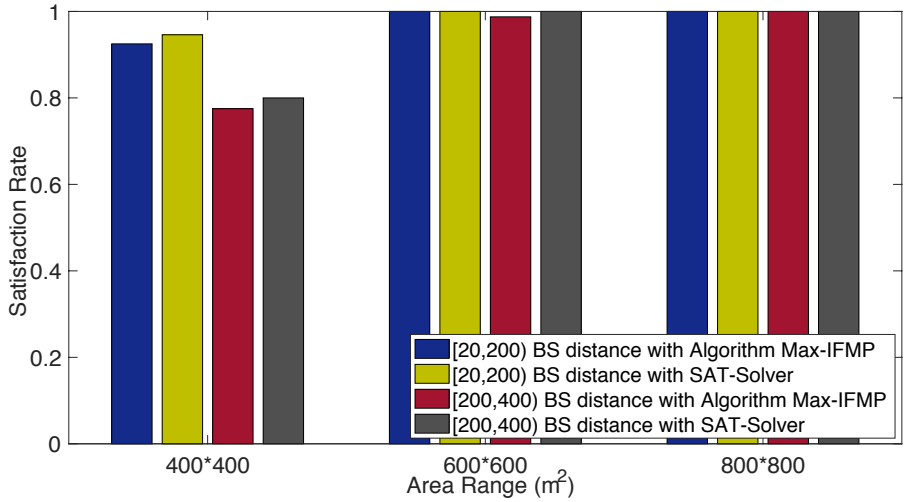

Figure 5.5: Feasibility of multiple paths (SAT-solver) and comparison against Algorithm Max-IFMP

Running Time Comparison

As mentioned earlier, the running time of the SAT solver is likely to increase rapidly as the size of the area grows. This is because a larger area will provide more candidate relay locations, and thus more possible physical links to consider, since the number of possible physical links grows quadratically with the number of candidate relay locations. This will rapidly increase the numbers of variables and clauses, which will greatly impact the running time of the SAT-solver. Fig. 5.6 shows the running times for BS separations in

the ranges of $[20, 200)$ and $[200, 400)$ meters and areas of size 400m $\times$ 400m, 600m $\times$ 600m, and 800m $\times$ 800m. Note that, as expected, the running time for the SAT-solver does increase very rapidly as the area size increases. For example, while both the SAT-solver method and Algorithm Max-IFMP have 100% satisfaction rate in the separation range of $[20, 200)$ meters with 600m $\times$ 600m area, the SAT-solver required more than 2 minutes to find multiple paths for each pair of BSs, whereas Algorithm Max-IFMP only needed 0.255 seconds to obtain the paths. For larger areas, e.g., 800m $\times$ 800m or higher, the running time needed for the SAT-solver is a few hours to tens of hours, whereas Algorithm Max-IFMP handles even very large sizes in a few seconds. Given the small difference in satisfaction ratio, this performance of Algorithm Max-IFMP is quite good.

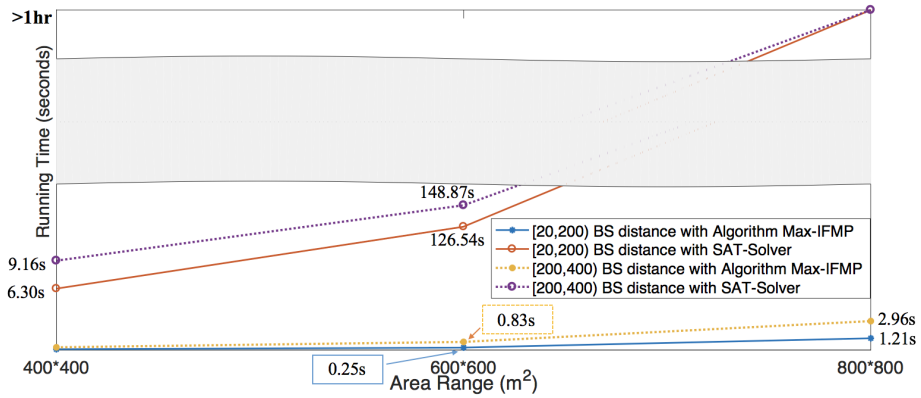

Figure 5.6: Running times for SAT-solver and Alg. Max-IFMP

Throughput Comparison

The SAT-solver only finds a pair of interference-free paths when possible, but it does not factor in the throughput of the paths in its formulation. However, when more than one pair of the paths found by the max-flow algorithm are found to be interference free, Algorithm Max-IFMP chooses the pair with the highest combined throughput. Thus, in many cases, the aggregate throughput of the paths found by Max-IFMP exceeds that of the SAT-solver solution. Fig. 5.7 compares the average aggregate throughput of the solutions found by the

two approaches. The average throughput increase for Max-IFMP is 5–10%.

Combining all the results in this subsection, we see that, for a small sacrifice in satisfaction ratio, Algorithm Max-IFMP finds higher-throughput paths than the SAT solver while taking only a small fraction of the running time. [

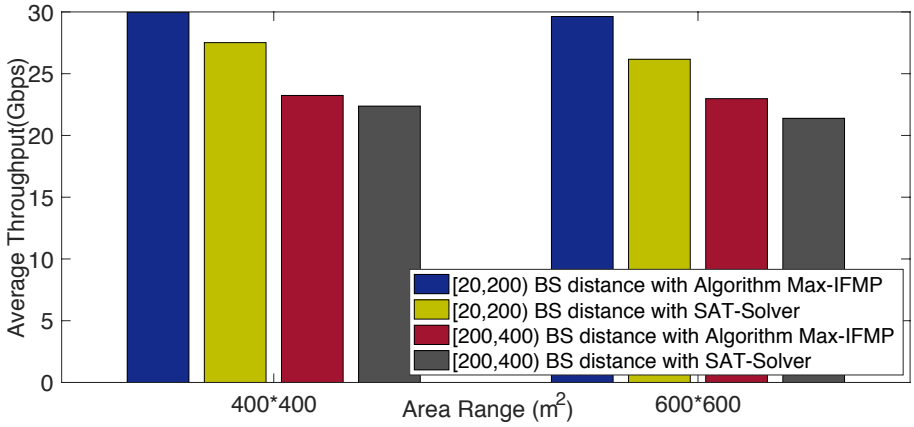

Figure 5.7: Throughput from SAT-solver and Alg. Max-IFMP

The SAT-solver method and the heuristic Algorithm Max-IFMP each have their own merits. The SAT solver can give a precise judgment on whether multiple paths exist, but it can take a very long time to produce a result, especially when the number of candidate relay locations is large. Algorithm Max-IFMP does not guarantee to find multiple interference-free paths when such paths exist, but it finds multiple paths efficiently and factors aggregate throughput into its path selection. In practice, these two methods could work together: first, Algorithm Max-IFMP can be executed and second, only when Max-IFMP fails to find a solution, the SAT-solver method can be used to check if a solution exists. In this way, the long execution time penalty of the SAT solver is only incurred when Max-IFMP fails and we can guarantee to find multiple interference-free paths whenever they exist.

CHAPTER 6

LOAD-BALANCED ROUTING FOR HYBRID FIBER/WIRELESS BACKHAUL NETWORKS

6.1 Introduction

In previous chapters, we considered the single path [85, 90] and multi-path selection [94] problems in mmWave backhaul networks with grid topology, relay nodes are selected between a pair of BSs to form high-throughput paths. In this chapter, instead of investigating problems between single pair of BSs, we consider the routing problem in the whole hybrid backhaul network with grid topology. As mentioned in chapter 1, in hybrid backhaul networks, only a portion of SBSs can connect to the core network through fiber (these are referred to as anchor BSs (ABSs)), while the other SBSs can connect wirelessly to nearby SBSs/ABSs. The ABSs need to deliver all traffic to/from their assigned SBSs across the wireless transmission, which making the ABSs become potential bottleneck nodes in the whole network. Therefore, balancing load across different ABSs is an important topic to be considered.

In hybrid backhaul networks, if multiple ABSs exist in a given region, it is known as a distributed backhaul architecture [95, 96]. In [17], system-level simulations have shown that distributed backhaul achieves higher throughput and is more flexible than a centralized network architecture, where all SBSs connect to a single ABS [97, 87]. In the remainder of this chapter, we focus on a hybrid distributed backhaul architecture.

While we believe the exact problem studied herein is novel, several works are tangentially related [98], [99], [100]. In [98], mmWave backhaul is targeted, but the problem considered is how to allocate resources between access and backhaul tiers in an integrated access backhaul architecture, which is quite different from our problem. In [99], load-balanced tree-based routing is considered for *wireless access networks* with a *single egress node*, whereas balancing load across the *multiple ABS egress nodes* in hybrid fiber/wireless

backhaul networks is a critical aspect of our problem. In [100], multiple egress nodes are considered in MANETs. However, the algorithm in [100] requires exponential time and prioritizes minimizing path length, whereas our algorithm is a hill climbing procedure with polynomial time per step and with load balancing as the primary objective.

The contribution of this chapter begins with a definition of load balance factor (LBF) to describe how balanced (or unbalanced) the load is across ABSs in a given backhaul region. We then use the LBF to transform the problem into a load-balanced routing problem. Next, we develop and evaluate a hill-climbing procedure for selecting routes, which is used to optimize the LBF in the backhaul region. Results show that the proposed algorithm can distribute the dynamic traffic loads from different BSs nearly optimally among fiber-connected BSs for the simulated settings. Finally, we consider a modification to our load-balanced routing procedure, which allows a trade-off between routing path length and load balance factor.

6.2 Network model and problem formulation

In this section, we present the model and assumptions of the network, define the concept of load balancing factor, and formulate the load-balancing problem in our network scenario.

6.2.1 Network model

Backhaul topology: We first define the network model we assume for connections between the core network and the mmWave backhaul network. Fig. 6.1 shows an example of our hybrid distributed network architecture, which includes a fiber connection between the core network and a subset of the base stations that are referred to as ABSs, and a mmWave mesh network connecting the remaining base stations to the ABSs. In the hybrid backhaul network architecture, the traffic of non-fiber-connected SBS is transmitted to/from one of the ABSs via mmWave wireless links. The traffic from ABSs to/from the core network is forwarded through fiber connections. Through the algorithm that we will present in the next section, each SBS is assigned to one ABS and then a virtual tree topology is constructed

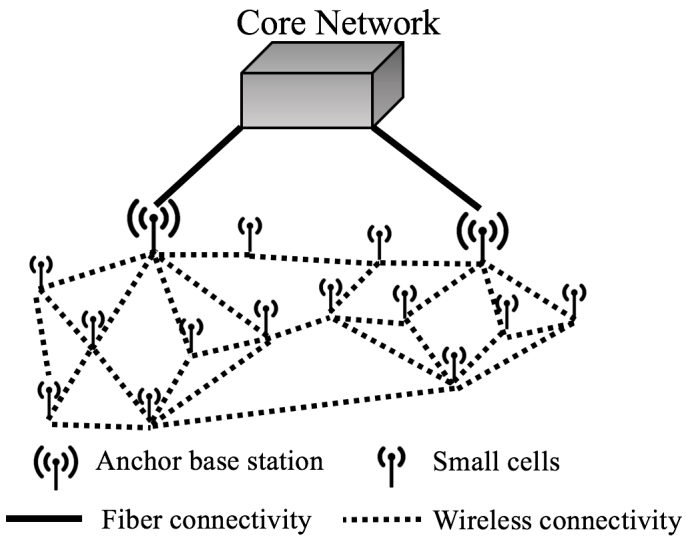

Figure 6.1: Hybrid distributed network architecture

within the mesh network based on the SBS-ABS assignment (see Fig. 6.2 for an example). All traffic is then routed through this virtual tree topology.

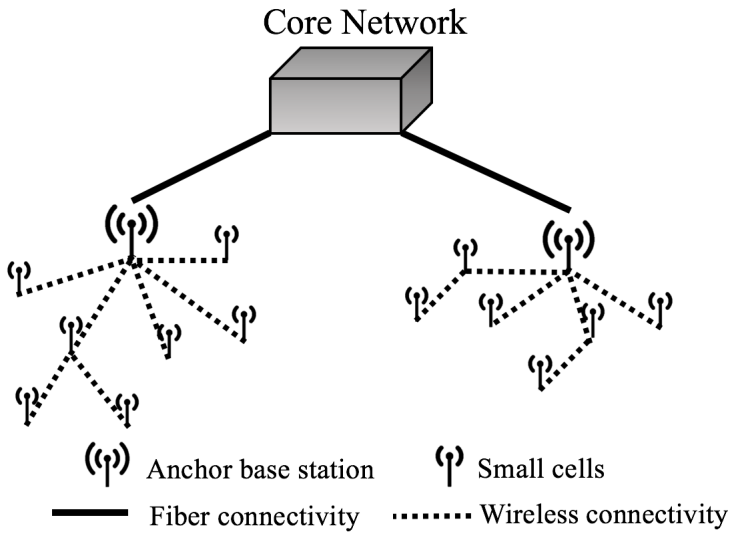

Figure 6.2: Virtual tree topology for routing

As can be seen from Fig. 6.2, each ABS must process the aggregated traffic to/from all of its assigned SBSs through its wireless links. Thus, the wireless capacity of the ABSs becomes the main performance bottleneck in this hybrid architecture and, therefore, it is critical to balance the load as equally as possible among the ABSs. Since traffic demands

are time-varying, the load balancing procedure that produces the virtual tree topology can be periodically re-executed (thereby changing both the SBS-ABS assignment and the routing paths) to maintain a balanced assignment as loads fluctuate.

mmWave backhaul in 3D urban areas: To support the high data rate requirement of mmWave links (around 10 Gbps) in backhaul networks, LoS paths must be utilized. However, LoS paths are susceptible to blocking by physical objects. When considering urban areas specifically, the LoS path between two BSs is often blocked by buildings, walls, trees, and other obstacles. Therefore, we use a 3D model of the environment like our earlier works in chapter 3, 4 and 5, instead of 2D modeling, as it gives us a more practical view of the transmission environment. We used a 3D model of buildings in downtown Atlanta to provide a realistic evaluation environment and use it in the simulations described later. In the simulations, the SBSs are deployed on randomly selected top corners of buildings and ABSs with fiber connection are randomly chosen from these SBSs. Note that the following proposed problems and algorithms are not limited to this specific city model, which is used only for the purpose of producing a realistic environment for simulation.

Interference issues: Mutual interference could exist when multiple physical links transmit and receive simultaneously in close proximity. However, it is commonly assumed that LoS mutual interference is dominant in mmWave networks with high-gain highly-directional antennas and abundant obstacles in the urban environment, and the aggregated non LoS interference is negligible [87]. Therefore, similar to prior works in chapter 3 and 4, we assume that the communications between BSs are interference-free.

6.2.2 Problem formulation

We model the network architecture by a distributed hybrid backhaul topology such as Fig. 6.1. Let the N SBSs in the network be denoted by $B_S = \{B_{S0}, B_{S1}, \ldots B_{S(N-1)}\}$ and the M ABSs be denoted by $B_A = \{B_{A0}, B_{A1}, \ldots B_{A(M-1)}\}$. We denote the set of all base stations by $\mathcal{B} = B_S \cup B_A$. We represent the mesh network as an undirected graph $G(V, L)$, in which $V = \mathcal{B}$ and L is the set of wireless links in the mesh network.

We assume that SBS B_{Si}, $0 \leq i \leq N-1$, has a load TL_i, which represents the traffic load between B_{Si} and the core network. Let B_{Aj}, $0 \leq j \leq M-1$, be any ABS, and let $S_j \subseteq B_S$ be the set of SBSs that are assigned to B_{Aj} through a load-balanced routing procedure. Then, the aggregated traffic load ATL_j of ABS B_{Aj} is

$$\mathrm{ATL}_j = \sum_{i:B_{Si} \in S_j} \mathrm{TL}_i \tag{6.1}$$

A primary metric of a load-balanced routing procedure is the load balance factor (LBF), defined by the following equation:

$$\mathrm{LBF} = \frac{\max_j(\mathrm{ATL}_j) - \min_j(\mathrm{ATL}_j)}{\max_j(\mathrm{ATL}_j)} \tag{6.2}$$

In Eq. 6.2, the maximum and minimum are taken over all ABSs, i.e., over $0 \leq j \leq M-1$. LBF represents the ratio of load difference between the ABS with maximum traffic load and the ABS with minimum traffic load. Note that if all ABSs are assigned identical loads (perfect load balancing), then $\mathrm{LBF} = 0$. Note also that the worst case for load balancing is that some ABS is not assigned any SBSs, i.e., $\min_j(TL_j) = 0$ and, in that case, $\mathrm{LBF} = 1$. Thus, the range of LBF is $[0,1]$ with 0 being the best value (perfect load balancing) and 1 being the worst value (at least one ABS has no load). The problem of optimally balancing the load is, therefore, to assign SBSs to ABSs in order to minimize the value of Eq. 6.2, which amounts to distributing the SBS traffic load as evenly as possible among the ABSs.

6.3 Load-Balanced tree construction

In this section, we describe an algorithm based on a hill climbing procedure that works to minimize the load balance factor (LBF) for a given set of SBSs, ABSs, connected graph representing the mesh network, and SBS traffic loads. Given an initial tree topology, the procedure works by adjusting the topology so as to move toward a smaller LBF based on Eq. 6.2. Since it is well known that one execution of a hill climbing procedure produces a local optimum, we repeat the procedure multiple times from different initial tree topologies

and select the best LBF from among all the resulting local optima. Pseudocode for the algorithm implementing this load balancing optimization procedure is shown in Algorithms 4 and 5 and is described next.

Algorithm 4 **Load-balanced tree construction procedure**

Input: Graph $G(V,L)$, SBS set B_S, ABS set B_A, no. of SBSs N, no. of ABSs M, traffic load vector TL, no. of init. topologies n
Output: tree_paths

```
1:  best_LBF = 1
2:  for i = 1 to n do
3:     paths = Build_Initial_Virtual_Tree_Topology()
4:     curr_LBF = compute LBF using Eq. 6.1, 6.2
5:     ctr = 0
6:     repeat
7:        paths = Adjust_Traffic_Load(paths, curr_LBF)
8:        new_LBF = compute LBF using Eq. 6.1, 6.2
9:        if (new_LBF < curr_LBF) then
10:          curr_LBF = new_LBF
11:          ctr = 0
12:       else
13:          ctr++
14:    until (ctr = 10)
15:    if ((curr_LBF < best_LBF) OR (n == 1)) then
16:       best_LBF = curr_LBF
17:       tree_paths = paths
18: return
19: Build_Initial_Virtual_Tree_Topology()
20: for i = 0 to N − 1 do
21:    assign B_Si to a randomly chosen ABS B_Aj
22:    initial_paths[i] = shortest path between B_Si and B_Aj in G(V,L)
23: return initial_paths
    =0
```

Algorithm 4 shows the main outer loop of the procedure, along with the function that computes different initial trees on which the hill climbing procedure is executed. In addition to the inputs already mentioned, the number of initial trees to use is an input parameter n. The outer loop of the procedure runs n times and executes the hill climbing procedure once in each iteration starting from a different initial topology. Since the mesh network is assumed to be connected, we produce initial tree topologies by simply assigning each SBS to a random ABS and connecting the SBS to its assigned ABS via a shortest path. At the

end of the procedure, the collection of paths that produced the lowest LBF is selected and these paths together form the set of trees used for routing.[1]

The heart of the hill climbing procedure takes place inside the Adjust_Traffic_Load() function, which is shown in Algorithm 5 and is described next. From Eq. 6.2, we can see that to lower the LBF, we can either reduce the maximum aggregated traffic load (ATL) on the ABSs or we can increase their minimum ATL. Adjust_Traffic_Load() searches for a modified SBS assignment that achieves one of these goals or moves in the direction of one of the goals if neither goal can be achieved with a single SBS reassignment. The first loop in Adjust_Traffic_Load() focuses on ABSs that currently have the maximum ATL. For each such ABS, we try reassigning each SBS currently assigned to it to every other ABS in the network. For each such reassignment, we compute the new LBF and, if any of the possible reassignments lowers the LBF from its current value, we select the new assignment that has the lowest LBF among all the reassignments considered. In the second loop, a similar procedure is repeated for the ABSs with minimum ATL, where we try to move an SBS from another ABS *onto* the minimum load ABS. If we are able to lower the LBF with a single SBS reassignment, the collection of paths with the lowest resulting LBF from among all the possibilities over the maximum ATL and the minimum ATL ABSs is returned to the main procedure.

Note, however, that it might not be possible to lower the LBF with a single SBS reassignment. This can occur if there are multiple ABSs all having the maximum ATL and multiple ABSs all having the minimum ATL. In this case, multiple SBS reassignments will be needed to lower the LBF. If there is no single reassignment that lowers the LBF, Adjust_Traffic_Load() will return the first encountered reassignment that maintains the same LBF but reduces the number of maximum load ABSs or the number of minimum load ABSs. By reducing either the number of maximum or minimum load ABSs, the adjust-

[1]Note that, since initially SBSs are assigned to ABSs randomly, some of the initial routing paths might be fairly long. In the algorithm of this section, we focus solely on minimizing LBF. In Sec. 6.5, we modify the algorithm to include a maximum path length constraint so as to avoid long routing paths.

Algorithm 5 **Traffic load adjustment function**

```
1: Adjust_Traffic_Load(paths, curr_LBF)
2: best_LBF = curr_LBF
3: adjusted = FALSE
4: for each B_Ak with max. load, i.e., ATL_k = max_l ATL_l do
5:    for each B_Si assigned to B_Ak do
6:       for each B_Aj ≠ B_Ak do
7:          old_max_ATL = max_l ATL_l
8:          temporarily reassign B_Si to B_Aj
9:          new_LBF = compute LBF using Eq. 6.1, 6.2
10:         if (new_LBF < best_LBF) then
11:            best_LBF = new_LBF
12:            best_SBS = i
13:            best_p = shortest path from B_Si to B_Aj in G(V,L)
14:            adjusted = TRUE
15:         else if ((new_LBF == curr_LBF) AND (NOT adjusted) AND (ATL_j <
           old_max_ATL)) then
16:            best_SBS = i
17:            best_p = shortest path from B_Si to B_Aj in G(V,L)
18:            adjusted = TRUE
19:         cancel B_Si reassignment
20: for each B_Ak with min. load, i.e., ATL_k = min_l ATL_l do
21:    for each B_Aj ≠ B_Ak do
22:       for each B_Si assigned to B_Aj do
23:          old_min_ATL = min_l ATL_l
24:          temporarily reassign B_Si to B_Ak
25:          new_LBF = compute LBF using Eq. 6.1, 6.2
26:          if (new_LBF < best_LBF) then
27:             best_LBF = new_LBF
28:             best_SBS = i
29:             best_p = shortest path from B_Si to B_Ak in G(V,L)
30:             adjusted = TRUE
31:          else if ((new_LBF == curr_LBF) AND (NOT adjusted) AND (ATL_j >
            old_min_ATL)) then
32:             best_SBS = i
33:             best_p = shortest path from B_Si to B_Ak in G(V,L)
34:             adjusted = TRUE
35:          cancel B_Si reassignment
36: if (adjusted) then
37:    paths[best_SBS] = best_p
38: return paths
    =0
```

ment moves in the direction of reducing the LBF even if that cannot be accomplished in a single call to Adjust_Traffic_Load().

The time complexity of the core of our algorithm, namely Adjust_Traffic_Load(), is $O(N^3M)$, where N is the number of SBSs and M is the number of ABSs. Since N and M tend to be fairly small in practical scenarios, we have not tried to lower this complexity and, in fact, all executions of the procedure done to obtain the simulation results in the work terminated very quickly.

6.4 Performance evaluation

Here, we provide results to assess the routing paths that are constructed by the load-balanced routing algorithm presented in the previous section. As mentioned earlier, we use an actual 3D topology of a section of downtown Atlanta to drive the simulations, as was done in chapter 3, 4 and 5.

6.4.1 Simulation setup and example

This 3D topology contains 227 buildings. We use a grid to represent this downtown Atlanta area with each grid element corresponding to a 200m$\times$200m section of the area. We then place one base station within each grid element that has a suitable building located in it. The total area has 63 grid elements, out of which 48 have suitable buildings and are used as base station locations. From these 48 locations, in one execution of our algorithm, a given number of ABSs are randomly picked from these locations and the remaining base station locations are assigned to be SBSs. Since long-distance high-rate links rarely exist in a dense urban environment due to signal attenuation and blockages, we assume each base station has at most four neighbors, which are the base stations in its adjacent 200m$\times$200m areas in the north, south, east, and west directions if they exist.[2] Fig. 6.3 shows an example of this grid topology with the 63 grid elements and the locations of the 48 base stations

[2]If the LoS link between neighboring BSs is blocked by a building, our prior work showed that they can be connected by a high-throughput virtual link using 1–2 relays in almost all cases [85, 90].

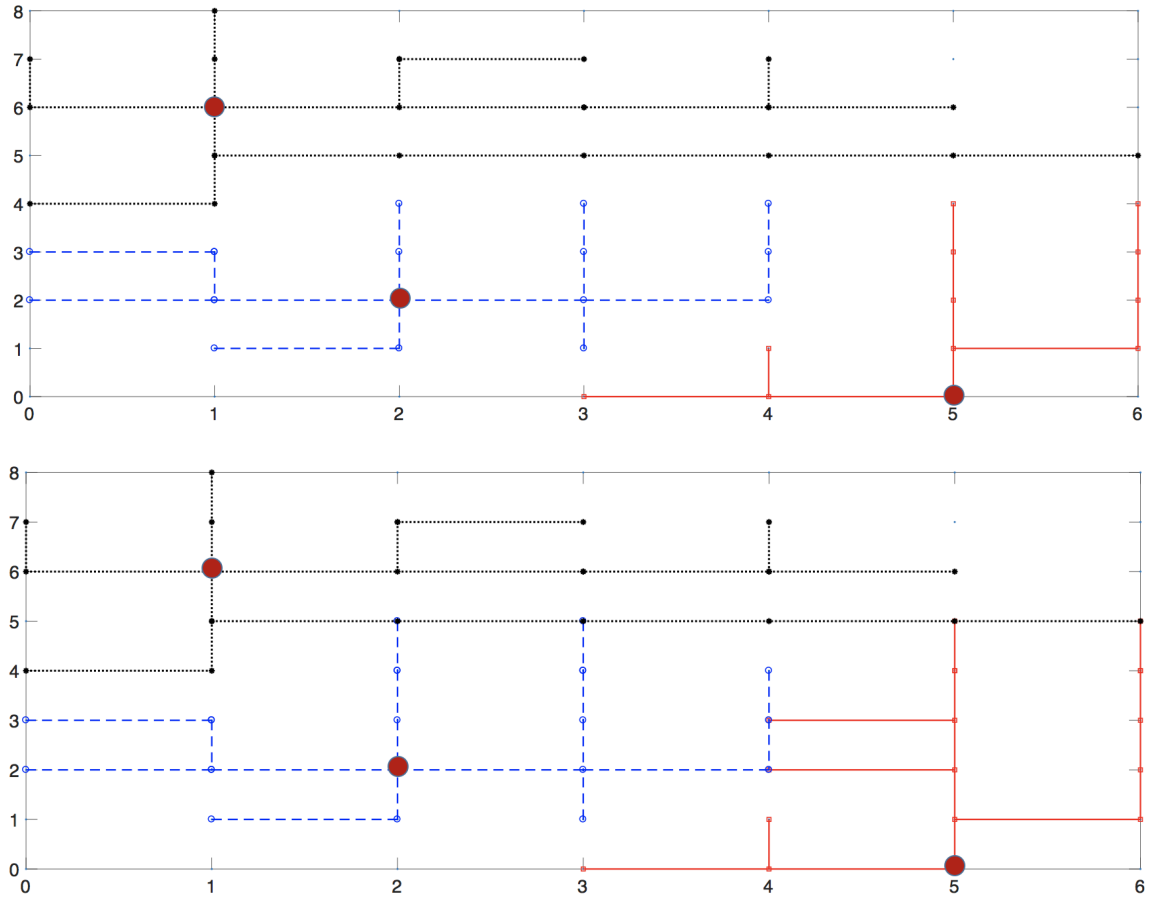

Figure 6.3: (top) Initial virtual tree topology (bottom) Topology modified by the load balancing algorithm

indicated by dots. The larger red dots are the (in this case three) randomly chosen ABSs and the 45 smaller dots represent the SBSs.

Fig. 6.3 (top) shows an initial random tree topology and Fig. 6.3 (bottom) shows the modified virtual tree topology produced by our hill climbing procedure. To simplify the discussion of this example, let us assume that each SBS has one unit of traffic load. Under that assumption, the three ABSs in the initial randomly chosen virtual tree topology have aggregated loads of 19, 15, and 11 units, which results in a load balance factor of $8/19 \approx 0.42$. In the modified virtual tree topology, the aggregated load of each of the three ABSs is 15 units, resulting in a perfect load balance factor of 0.

6.4.2 Simulation results

For each data point in the results of this section, we simulated 100 different random assignments of a given number of ABSs to the 48 possible locations and, for each of the 100 ABS assignments, the remaining locations were assigned to be SBSs. We considered scenarios with 3, 5, and 7 ABSs across the region. Initially, we consider a heterogeneous traffic load scenario, where we assign uniform random traffic loads in a range $[0,2]$ to each SBS, which gives an average traffic load of 1. For each set of ABSs and SBSs with fixed positions, we constructed 100 different random initial topologies and executed our rebalancing procedure on each of them. We then compared the best LBF from the initial topologies (referred to as "initial multiple topologies" in the figures) to the best LBF from all of the rebalancing procedures.

Fig. 6.4 and Fig. 6.5 compare the LBFs and path lengths that are produced by these two different methods. As seen from Fig. 6.4, the LBFs produced by our load balancing procedure are substantially smaller than the best LBF from 100 random topologies. For example, when the number of ABSs is 7, the average LBF of the best initial tree topologies is almost 0.8, while the average LBF of the best rebalanced topologies is less than 0.02, which is nearly perfect load balancing. Thus, using our load-balanced routing algorithm provides a very large improvement in LBF. There are a few exceptions in Fig. 6.4, where the LBF is 1. These are cases where one of the ABSs cannot connect to any SBS, i.e. its only neighbor is another ABS. In that case, no matter how rebalancing is done, the $\min(\mathrm{ATL}_j)$ is always 0 and the LBF is always 1.

We also evaluated the path lengths that are produced by the two methods. Here, we took the best LBF topologies, as discussed in the prior paragraph, and we computed the average of the path lengths from every SBS to their assigned ABS. Fig. 6.5 reports the distribution of these average path lengths across the 100 random BS assignments for each experiment. The figure shows that the topologies modified by the load-balanced routing algorithm have similar average path lengths as the best initial topologies. Together, the results of Fig. 6.4

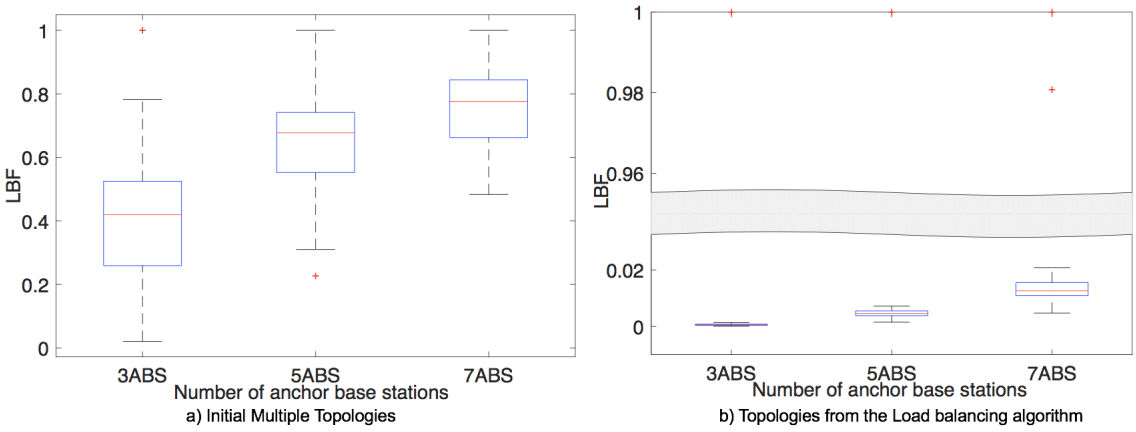

Figure 6.4: LBFs among multiple initial topologies and topologies from the load balancing algorithm: heterogeneous traffic load scenario

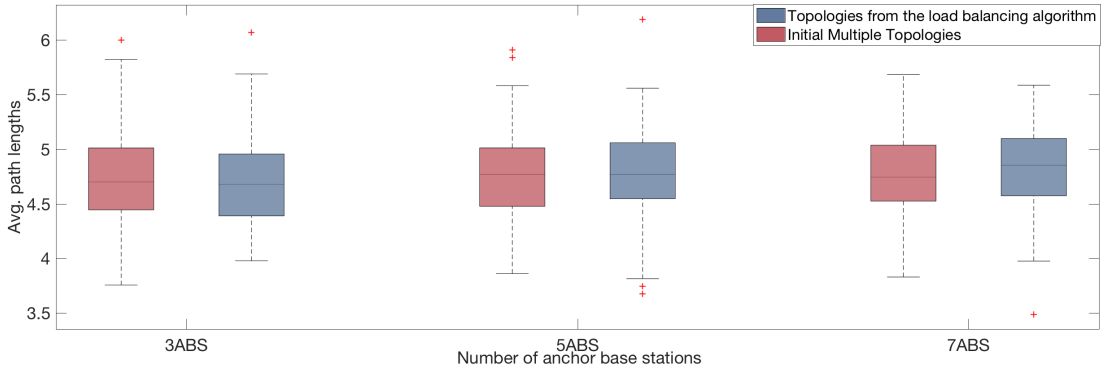

Figure 6.5: Avg. path lengths among multiple initial topologies and topologies from the load balancing algorithm: heterogeneous traffic load scenario

and Fig. 6.5 demonstrate that our load-balanced routing algorithm can achieve very good load balancing with very little impact on path lengths.

In the heterogeneous traffic load scenario, there is no easy way to compare the LBF produced by our algorithm to the best achievable LBF. Therefore, we also evaluated a homogeneous traffic load scenario, where each SBS is assigned one unit of load. In this case, load balancing simply tries to equalize the *number* of SBSs assigned to each ABS and the best possible LBF corresponds to distributing integer numbers of SBSs as equally as possible. Here, the best possible such distribution can be determined easily. Fig. 6.6 and Fig. 6.7 show the LBFs and path lengths under this homogeneous traffic load scenario with all other experimental parameters the same as in the heterogeneous load experiments.

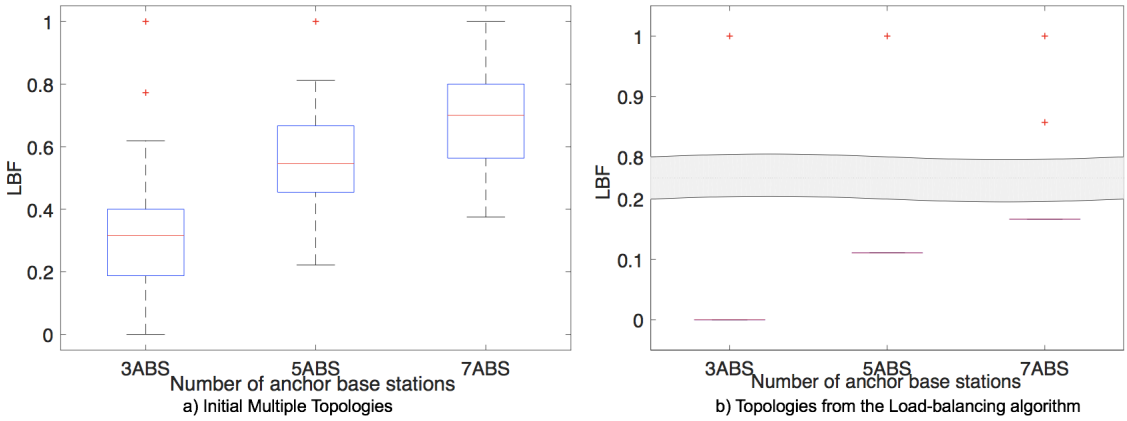

Figure 6.6: LBFs among multiple initial topologies and topologies from the load balancing algorithm: homogeneous traffic load scenario

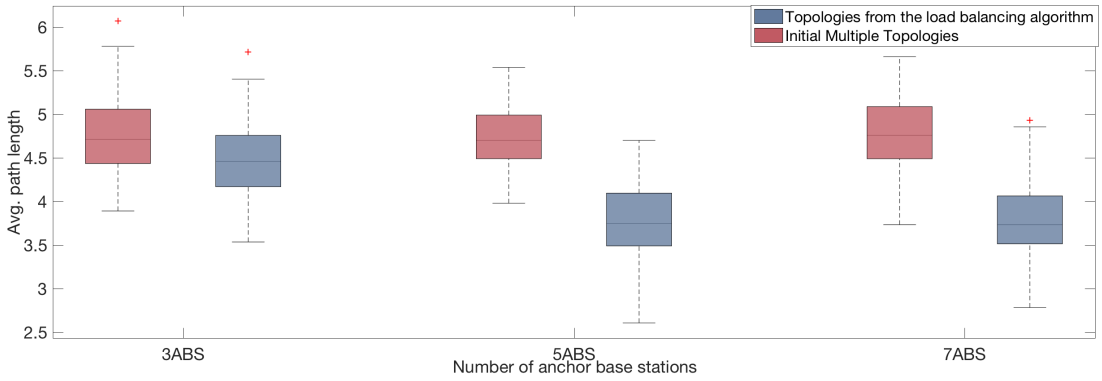

Figure 6.7: Avg. path lengths among multiple initial topologies and topologies from the load balancing algorithm: homogeneous traffic load scenario

With 48 BSs, the optimal values of LBF with homogeneous loads can be easily determined to be 0, 0.125 and 0.1667 for 3ABS, 5ABS and 7ABSs, respectively. Fig. 6.6 shows that most of the LBFs produced by our algorithm are equal to the best possible achievable value. Most of the non-optimal cases are the aforementioned ones where one ABS is isolated from the rest of the network. There is only a single case across all our simulations where a non-optimal LBF was produced without an isolated ABS. Somewhat surprisingly, Fig. 6.7 also shows that the path lengths of our optimized topologies are shorter than from the multiple initial topologies. This indicates that equalizing the numbers of SBSs assigned to ABSs also tends to reduce path lengths compared to more random assignments.

6.5 Load-Balanced tree construction with maximum path length constraint

From. Fig. 6.5 and Fig. 6.7, we see that average path lengths produced by our load-balanced topologies are between 4.5 and 5 for heterogeneous loads and slightly lower for homogeneous loads. Since it has been observed that throughput in wireless multihop paths decreases with path length [101], maintaining relatively short path lengths is another factor to consider in optimizing network performance in addition to the load balance factor, which has been our primary consideration so far. Thus, in this section, we consider adding a maximum path length constraint to our load-balanced routing procedure.

To provide some perspective on the path lengths produced by our basic load balancing procedure, we being by comparing it to shortest path trees, which are the best possible topology in terms of path lengths for a tree-based routing procedure. We also consider a load-balanced modification of the shortest path tree topology (referred to as "load balanced SPT" in the figures), where we run our hill climbing procedure to reduce the LBF starting from a shortest path tree. Fig. 6.8 and Fig. 6.9 compare the topologies produced by these three methods for the same parameters as the prior experiments under the heterogeneous load scenario.

From Fig. 6.8, we see that the average path lengths of the shortest path trees in our simulated scenarios are between 2.5 and 3 with 3 ABSs and slightly more than 2 with 5 and 7 ABSs, which are significantly lower than the average path lengths from our load balancing procedure. We also see that the load balanced modification of the shortest path tree maintains average path lengths in the 2–3 range. In comparing LBFs, Fig. 6.9 shows that the load balanced SPT significantly lowers the LBF compared to the initial shortest path trees, which have a very poor LBF. However, note that the LBF of the load-balanced SPT is still substantially higher than the extremely low LBFs produced by our basic algorithm. These results motivate us to explore the trade-off possible between LBF and path length within the framework of our load balanced routing procedure.

To permit this trade-off study, we modified our load balancing algorithm to include

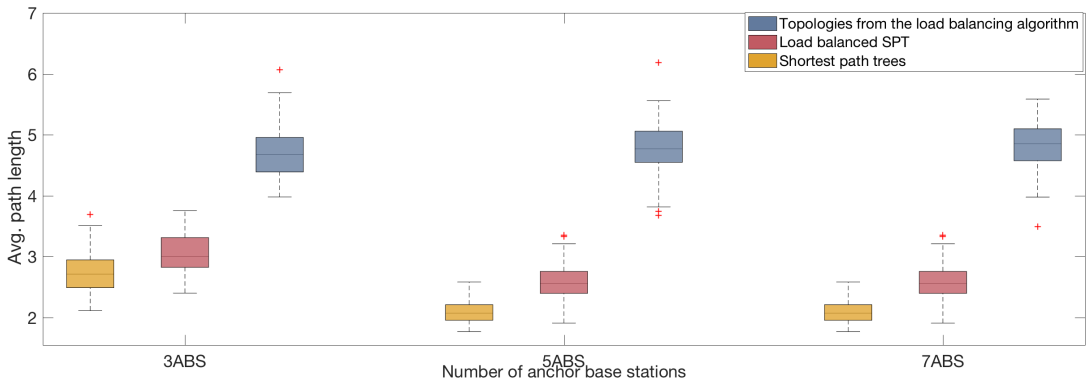

Figure 6.8: Avg. path length comparison of different topologies: heterogeneous traffic load scenario

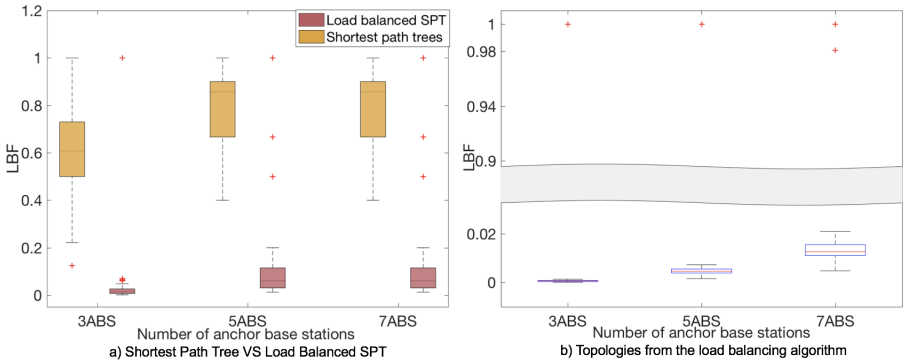

Figure 6.9: LBF comparison of different topologies: heterogeneous traffic load scenario

a maximum path length constraint h. This was included in initial topology construction where the random SBS assignment is done only over ABSs that are within a distance of h or less from the SBS.[3] Also, in the topology adjustment procedure, any adjustments that produce path lengths longer than h are not considered. Fig. 6.10 and Fig. 6.11 show the results of this path length constrained load balancing procedure compared with the load balanced SPT topologies already discussed with different numbers of ABSs.

The figures show that the LBF for the path length constrained algorithm approaches the LBF without any constraint as h increases. Unfortunately, as already discussed, the path length increases with h also. The figures also clearly show how the two metrics can be traded off by simply choosing an appropriate value of h. Smaller h prioritizes shorter path lengths and larger h prioritizes LBF. Intermediate values can produce good values of both.

[3]If no such ABS exists, the SBS is assigned to the closest ABS.

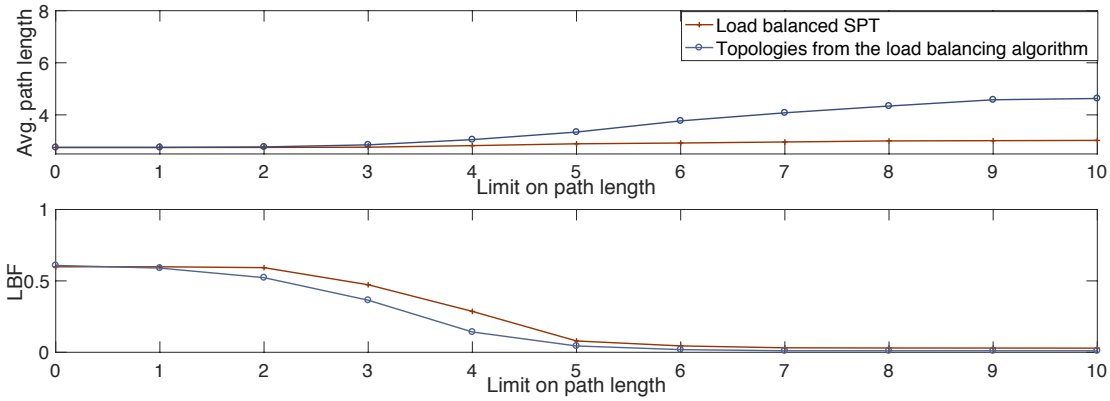

Figure 6.10: Avg. path lengths and LBFs for the load balancing algorithm with path length constraint and load balanced SPT for 3 ABSs

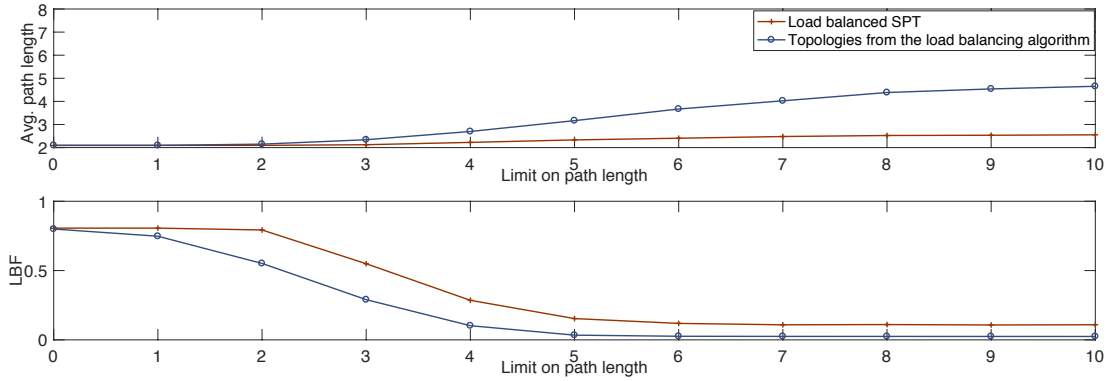

Figure 6.11: Avg. path lengths and LBFs for the load balancing algorithm with path length constraint and load balanced SPT for 5 ABSs

For example, for $h = 4$ in Fig. 6.10, the path lengths of our load balancing algorithm and the load balanced SPT are 3.05 and 2.82 for each, which means a 8% increase. The LBFs of these two algorithms are 0.14 and 0.29, which represents a 50% increase. Similarly, in Fig. 6.11, for $h = 3$, the path lengths of our algorithm and the load balanced SPT are 2.34 and 2.13, respectively, which represents only a 10% increase, while the LBFs of the two methods are 0.29 and 0.55, which represents almost a 50% decrease in LBF from our algorithm.

6.6 Combined relay-assisted path selection with load-balanced routing algorithm

As Section 6.4.1 mentioned, in our load balancing problem with hybrid backhaul networks, we assume each base station has four neighbors from four different directions in our sce-

nario. However, the LoS links between each pair of BSs can be blocked by buildings. If the blockage effect happens between neighboring BSs, our prior works, which select paths between a pair of BSs with relay nodes, can be used here to find communication links. In this section, we consider the use of relays in our routing paths. Once we are doing the routing problem, if neighboring base stations cannot communicate with each other directly because the distance between them is too long to achieve the data rate requirement and/or there are some obstacles between them preventing direct communication, relay nodes are considered as a solution in these situations. Therefore, we combined the relay-assisted path selection algorithm with our load-balanced routing algorithm and compare the path length of routing paths with relays to routing paths without relays in this section.

For the network model in this section, we use the same network backhaul grid topology as aforementioned, the topology contains 227 buildings higher than 5 meters, and for each building with a height between 0 and 200 meters, one of its rooftop corners is randomly picked as a candidate BS position and the diagonal corners of these rooftops are picked as possible relay locations, as was done in Chapters 4 and 5. Then, we have 183 relay positions in total. The relay paths here were selected using the Dijkstra's shortest-path algorithm with AF relays of chapter 3, section 3.6.1. We calculate the lengths of routing paths with relays and evaluate the increase in average path length compared to the lengths without relays.

The figures below show the result of average path length of our load-balancing algorithm with different number of ABSs. The path length of selected routing paths with and without relays are compared in the figures. In our simulations, we were able to find a relay path for all BSs pairs where the LoS path was blocked between them. This shows that adding relays nodes between BS pairs does not prevent the topology from being constructed in practical scenarios.

The results in Fig. 6.12, Fig. 6.13 and Fig. 6.14 show that the path length of routing paths with relays increases rapidly as the path length limit increases, which is similar to the

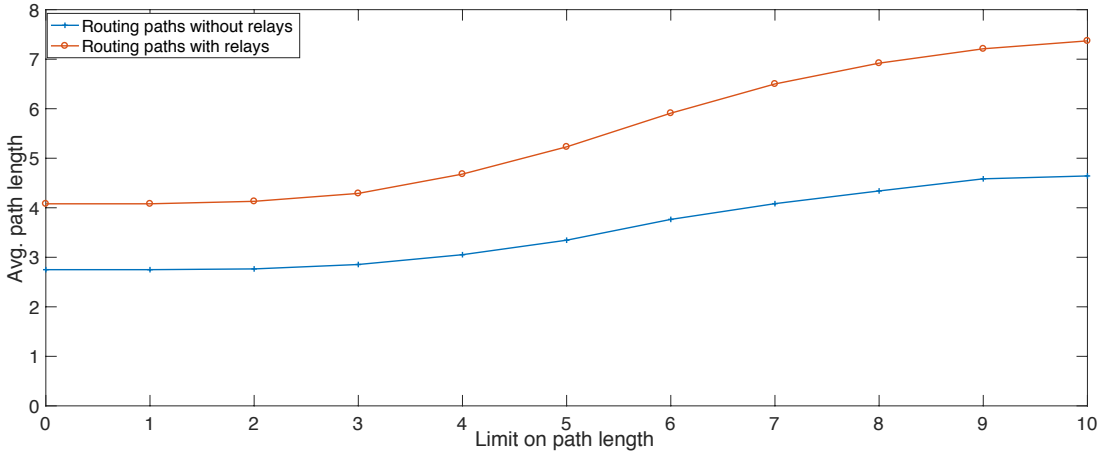

Figure 6.12: Avg. path lengths of load balancing algorithm with path length constraint for 3 ABSs: with and without relays

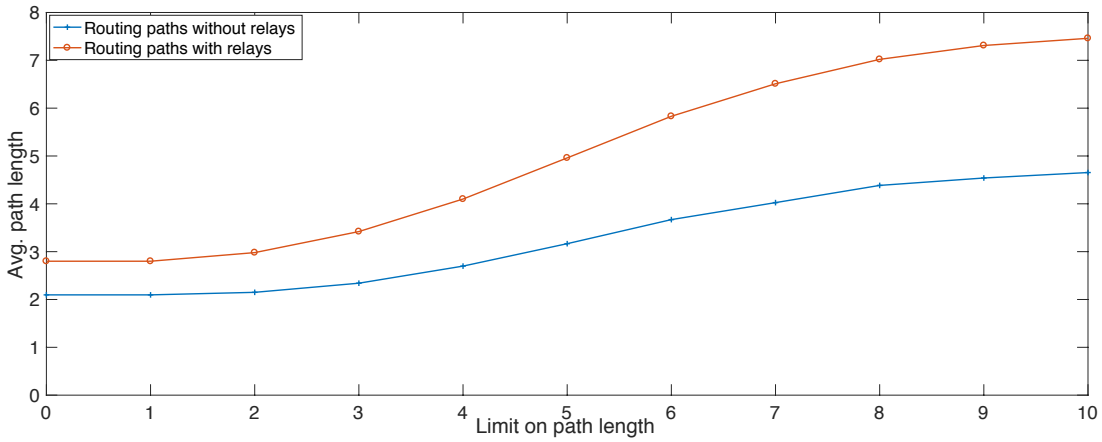

Figure 6.13: Avg. path lengths of load balancing algorithm with path length constraint for 5 ABSs: with and without relays

path length without relays. Therefore, it is always necessary to limit the path length in our routing algorithm. Comparing the average path lengths of routing paths with relays and routing paths without relays, we see that the increase is not too large. For example, with 5 ABSs, the average path length increases by at most 3 even when the path length limit is 10 (almost no constraint on path length). When the path length limit is 4, the average path length only increases by about 1 compared to the no relay cases. As aforementioned, Fig. 6.11 shows that, when the path length limit is 4, we can obtain a close to minimum LBF value while achieving small path lengths. This minor increase in path length will have

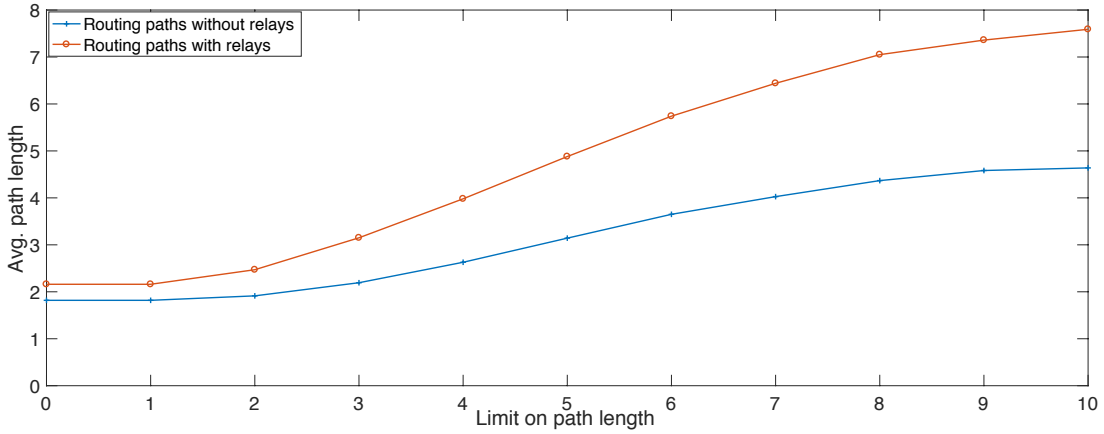

Figure 6.14: Avg. path lengths of load balancing algorithm with path length constraint for 7 ABSs: with and without relays

no meaningful impact on communication latency.

In summary, the results of this section show that to find the routing paths in our hybrid backhaul networks, our previous relay path selection algorithms can be used to effectively construct good routing paths between BSs for the wireless communication links in hybrid backhaul networks.

CHAPTER 7
CONCLUSIONS

7.1 Conclusions

In 5G, the current cellular spectrum is experiencing difficulty in keeping up with the explosive growth of mobile data demand. The use of dense deployment of small cell base stations is considered a compelling technique in 5G communication system to increase the throughput of the system. To densely deploy small cell base stations in the 5G backhaul network, the crucial challenge for mobile backhaul is to provide efficiency and reliable data transmission between different base stations and the core network. The fiber-based wired transmission is an attractive candidate due to its high data rates and low transmission loss. However, most of the small cell BSs have no wired connection and it is costly to deploy wired links for all BSs. Millimeter wave communication becomes another promising solution to this challenge with its enormous amount of spectrum and multi-Gigabit-per-second data rates, but mmWave links have higher propagation loss and severe blockage effect. Therefore, in order to provide high data rate and reliable transmission links for backhaul networks in urban dense area, we propose a relay-assisted hybrid fiber/wireless mmWave backhaul network architecture. Based on the urban dense environment as our scenario, the grid topology is used in our work, since many cities have a grid-based street canyon environment. Different from many related works on 5G backhaul networks, we consider the backhaul links with the help of the relays, which provides more flexibility and reliability for the backhaul links.

In this thesis, we focus on the path selection and routing problem of the relay-assisted hybrid fiber/mmWave backhaul network in the urban dense environment with grid topology. The contribution of each chapter is summarized as follow,

- In chapter 3, we focus on the single path selection problem with AF relay for long-

range ultra-high-speed millimeter wave backhaul links in dense urban area with grid topology. Multiple relays are selected from a set of relay candidates to form a path with maximum throughput value. In this work, we use the end-to-end SNR to evaluate the throughput value and an equation for the SNR of an AF relay path is formulated. Based on this derived SNR equation, this AF relay selection problem is transformed to the path selection problem in graphs. We then proposed and investigated different algorithms to solve this problem with different constraints. Simulation results show that our proposed algorithms work efficiently and can find relay paths with limited number of hops and high throughput.

- In chapter 4, we focus on selecting single path with DF relays for mmWave backhaul communications in urban environments with grid topology. We present three algorithms, based on a novel widest-path formulation of the problem, for selecting DF relay node locations in such paths. The first algorithm guarantees a maximum-throughput relay path when multiple relay nodes can be placed at a single location. The second algorithm finds near-optimal paths when each possible relay location can host only one relay node. Since both algorithms sometimes produce paths with a large number of relays, we also present a third algorithm that finds high-throughput paths using as few relays as possible. We also compare the performance of AF protocol with DF protocol in the same scenario.

- In chapter 5, we focus on the problem of feasibility of multiple path selection with relays for long-range ultra-high-speed millimeter wave backhaul networks in urban environments with grid topology. Multiple interference-free paths will be selected between a pair of base stations. We first formulate the problem as constraint satisfaction problem that have several different constraint functions. Based on the derived equations, we transform the multiple paths selection problem to the Boolean satisfiability problem and use SAT-solver method to solve it. However, the SAT-

solver method is shown to require large number of running time for realistic problem size. Therefore, we propose a heuristic algorithm to find multiple paths using derived max-flow algorithm. The simulation results show that these two algorithms can be combined to find multiple relay paths with a small number of running time and good throughput.

- In chapter 6, we explored load-balanced routing in hybrid fiber-wireless backhaul networks with grid topology. We presented a hill climbing procedure that produces a load-balanced virtual topology for routing, which was shown to provide near-optimal load balancing in simulated settings. We also modified the algorithm to include a maximum path length constraint, which allows trade offs between path length and load balance factor. Moreover, we combined our routing algorithms with our relay-assisted path selection algorithms in previous chapters. The results show that the path length of our routing paths with relays are acceptable values in the backhaul networks.

7.2 Challenges and next steps

We have proposed the path selection and routing algorithms of relay-assisted hybrid backhaul networks in the urban environment. Future works are encouraged in this area. The solutions in this thesis provide a starting point, however, there are still some different cases, adaptations and tests that have been left for the future. Future work concerns deeper analysis of particular algorithms and new proposals to try different methods.

In our works, we used the downtown, Atlanta with grid topologies as our network model. Since there exist many different types of topologies in 5G backhaul network, different topologies and city street canyons need to be generated and used in future works. Moreover, in our network model, we addressed the mutual interference issue and ignored the possible inference signals due to reflections. In future works, it is meaningful to conduct measurements and experiments using real devices in 3D outdoor environments to test the

reflection effect and blockage effect of signals. Moreover, we have a ns-3 related work in [102], which realizing end-to-end simulation of mmWave out-of-band backhaul networks in ns-3. It is useful to add the mmWave backhaul scenario in the ns-3 simulator, more elements and modules need to be developed and added to ns-3 in the near future.

In Chapters 3 and 4, we solved the path selection problem which just consider AF or DF relays in our networks; however, we did not consider the scenario which includes both AF and DF relays in the networks. The throughput evaluation method and path selection algorithm should be different in the scenario which has both AF and DF relay strategies. Therefore, future works need to focus on the path selection problem of relay-assisted networks including both AF and DF relays.

In chapter 4, we reduced the number of locations of DF relays, because the algorithm with novel-weighted graph produces a large number of data sets which badly increase the running time of the algorithm. In future works, new algorithms need to be proposed to deal with this problem with a large set of nodes.

In chapter 5, we used one of the mature SAT-solver method with DPLL algorithm to solve the problem. However, Boolean satisfiability problem is a classic problem in nowadays and there are many different SAT-solver algorithms can be used to solve it. Therefore, different SAT-solver methods need to be evaluated in future works.

In chapter 6, our hill-climbing method can only guarantee the local optimal results instead of global optimal results. Different algorithms can be proposed to find global optimal results in future work. Moreover, future work will consider issues related to dynamic traffic loads, namely how frequently the virtual routing topology should be adjusted and quantifying performance under dynamic conditions, accounting for both the quality of load balancing and the overheads of virtual topology adjustment.

7.3 Publications

As part of the research conducted in this dissertation, we have written several documents that are either published, submitted, or in progress as follows:

- Y. Yan, Q. Hu, and D. Blough, "Load-Balanced Routing for Hybrid Fiber/Wireless Backhaul Networks," Proc. of IEEE Global Communications Conference, 2021.
- Y. Yan, Q. Hu, and D. Blough, "Feasibility of Multipath Construction in mmWave-Backhaul Networks," Proc. of IEEE Int'l Symposium on a World of Wireless, Mobile and Multimedia Networks, pp. 81-90, 2021.
- Y. Yan, Q. Hu, and D. Blough, "Optimal Path Construction with Decode and Forward Relays in mmWave Backhaul Networks," submitted to 2020 International Conference on Computing, Networking and Communications (ICNC).
- Q. Hu, Y. Liu, Y. Yan, and D. Blough, "End-to-end Simulation of mmWave Out-of-band Backhaul Networks in ns-3" Proc. of the Workshop on Next-Generation Wireless with ns-3, 2019.
- Y. Yan, Q. Hu, and D. Blough, "Path Selection with Amplify and Forward Relays in mmWave Backhaul Networks," Proc. of IEEE Int'l Symposium on Personal, Indoor, and Mobile Radio Communications, 2018.

REFERENCES

[1] J. Robson, *Small cells deployment strategies and best practice backhaul. white paper, cambridge broadband networks*, 2012.

[2] O. L. A. Lopez, H. Alves, R. D. Souza, and M. Latva-aho, "Hybrid wired-wireless backhaul solutions for heterogeneous ultra-dense networks," in *2018 IEEE 87th Vehicular Technology Conference (VTC Spring)*, 2018, pp. 1–5.

[3] L. McLaughlin, "In brief: Where wired and wireless networks converge [optical-fiber networks]," *IEEE Distributed Systems Online*, vol. 7, no. 5, pp. 5–, 2006.

[4] P. T. Dat, A. Kanno, K. Inagaki, T. Umezawa, N. Yamamoto, and T. Kawanishi, "Hybrid optical wireless-mmwave: Ultra high-speed indoor communications for beyond 5g," in *IEEE INFOCOM 2019 - IEEE Conference on Computer Communications Workshops (INFOCOM WKSHPS)*, 2019, pp. 1003–1004.

[5] Y. Yan, Q. Hu, and D. M. Blough, "Load-balanced routing for hybrid fiber/wireless backhaul networks," in *2021 IEEE Global Communications Conference (GLOBECOM)*, IEEE, 2021.

[6] M Series, "Imt vision–framework and overall objectives of the future development of imt for 2020 and beyond," *Recommendation ITU*, vol. 2083, p. 0, 2015.

[7] Q. Tech, "Enabling hyper-dense small cell deployment with ultrason," *San Diego: Qualcomm Technologies Inc*, 2014.

[8] M. Agiwal, A. Roy, and N. Saxena, "Next generation 5g wireless networks: A comprehensive survey," *IEEE Communications Surveys & Tutorials*, vol. 18, no. 3, pp. 1617–1655, 2016.

[9] Cisco, "Cisco visual networking index: Forecast and methodology, 2017–2022," *San Jose, CA, USA, CISCO White paper*, Feb, 2019.

[10] T. O. Olwal, K. Djouani, and A. M. Kurien, "A survey of resource management toward 5g radio access networks," *IEEE Communications Surveys & Tutorials*, vol. 18, no. 3, pp. 1656–1686, 2016.

[11] S. Chen and J. Zhao, "The requirements, challenges, and technologies for 5g of terrestrial mobile telecommunication," *IEEE communications magazine*, vol. 52, no. 5, pp. 36–43, 2014.

[12] M. Jaber, M. A. Imran, R. Tafazolli, and A. Tukmanov, "5g backhaul challenges and emerging research directions: A survey," *IEEE access*, vol. 4, pp. 1743–1766, 2016.

[13] N. Bhushan, J. Li, D. Malladi, R. Gilmore, D. Brenner, A. Damnjanovic, R. T. Sukhavasi, C. Patel, and S. Geirhofer, "Network densification: The dominant theme for wireless evolution into 5g," *IEEE Communications Magazine*, vol. 52, no. 2, pp. 82–89, 2014.

[14] M. A. Adedoyin and O. E. Falowo, "Combination of ultra-dense networks and other 5g enabling technologies: A survey," *IEEE Access*, vol. 8, pp. 22 893–22 932, 2020.

[15] Q. Hu, "Design and analysis of millimeter-wave backhaul networks in urban environments," Ph.D. dissertation, Georgia Institute of Technology, 2019.

[16] E. Ternon, P. K. Agyapong, and A. Dekorsy, "Performance evaluation of macro-assisted small cell energy savings schemes," *EURASIP Journal on Wireless Communications and Networking*, vol. 2015, no. 1, pp. 1–23, 2015.

[17] X. Ge, H. Cheng, M. Guizani, and T. Han, "5g wireless backhaul networks: Challenges and research advances," *IEEE network*, vol. 28, no. 6, pp. 6–11, 2014.

[18] R. Taori and A. Sridharan, "Point-to-multipoint in-band mmwave backhaul for 5g networks," *IEEE Communications Magazine*, vol. 53, no. 1, pp. 195–201, 2015.

[19] Z. Gao, L. Dai, D. Mi, Z. Wang, M. A. Imran, and M. Z. Shakir, "Mmwave massive-mimo-based wireless backhaul for the 5g ultra-dense network," *IEEE Wireless communications*, vol. 22, no. 5, pp. 13–21, 2015.

[20] Z. Pi, J. Choi, and R. Heath, "Millimeter-wave gigabit broadband evolution toward 5g: Fixed access and backhaul," *IEEE Communications Magazine*, vol. 54, no. 4, pp. 138–144, 2016.

[21] Y. Zhu, Y. Niu, J. Li, D. O. Wu, Y. Li, and D. Jin, "Qos-aware scheduling for small cell millimeter wave mesh backhaul," in *2016 IEEE International Conference on Communications (ICC)*, IEEE, 2016, pp. 1–6.

[22] A. Ahmed and D. Grace, "A dual-hop backhaul network architecture for 5g ultra-small cells using millimetre-wave," in *2015 IEEE International Conference on Ubiquitous Wireless Broadband (ICUWB)*, IEEE, 2015, pp. 1–6.

[23] F. Idachaba, D. U. Ike, and H Orovwode, "Future trends in fiber optics communication," 2014.

[24] N. Ghazisaidi, M. Maier, and C. M. Assi, "Fiber-wireless (fiwi) access networks: A survey," *IEEE Communications Magazine*, vol. 47, no. 2, pp. 160–167, 2009.

[25] F. Q. Kareem, S. R. Zeebaree, H. I. Dino, M. A. Sadeeq, Z. N. Rashid, D. A. Hasan, and K. H. Sharif, "A survey of optical fiber communications: Challenges and processing time influences," *Asian Journal of Research in Computer Science*, pp. 48–58, 2021.

[26] cartesian, "All-fiber deployment cost study 2019 executive summary," *Fiber Broadband association*, Sep, 2019.

[27] U. Siddique, H. Tabassum, E. Hossain, and D. I. Kim, "Wireless backhauling of 5g small cells: Challenges and solution approaches," *IEEE Wireless Communications*, vol. 22, no. 5, pp. 22–31, 2015.

[28] R.-A. Pitaval, O. Tirkkonen, R. Wichman, K. Pajukoski, E. Lahetkangas, and E. Tiirola, "Full-duplex self-backhauling for small-cell 5g networks," *IEEE Wireless Communications*, vol. 22, no. 5, pp. 83–89, 2015.

[29] D. T. Emerson, "The work of jagadis chandra bose: 100 years of millimeter-wave research," *IEEE transactions on microwave theory and techniques*, vol. 45, no. 12, pp. 2267–2273, 1997.

[30] M. Xiao, S. Mumtaz, Y. Huang, L. Dai, Y. Li, M. Matthaiou, G. K. Karagiannidis, E. Björnson, K. Yang, I Chih-Lin, *et al.*, "Millimeter wave communications for future mobile networks," *IEEE Journal on Selected Areas in Communications*, vol. 35, no. 9, pp. 1909–1935, 2017.

[31] Y. Jian, U. P. Moravapalle, C.-F. Shih, and R. Sivakumar, "Duet: An adaptive algorithm for the coexistence of lte-u and wifi in unlicensed spectrum," in *2017 International Conference on Computing, Networking and Communications (ICNC)*, IEEE, 2017, pp. 19–25.

[32] S.-K. Yong, P. Xia, and A. Valdes-Garcia, *60GHz Technology for Gbps WLAN and WPAN: from Theory to Practice*. John Wiley & Sons, 2011.

[33] A. I. Nasr and Y. Fahmy, "Millimeter-wave wireless backhauling for 5g small cells: Star versus mesh topologies," in *2016 28th International Conference on Microelectronics (ICM)*, IEEE, 2016, pp. 85–88.

[34] Y. Jian, S. Lall, and R. Sivakumar, "Toward a self-positioning access point for wifi networks," in *Proceedings of the 16th ACM International Symposium on Mobility Management and Wireless Access*, 2018, pp. 19–28.

[35] T. S. Rappaport, S. Sun, R. Mayzus, H. Zhao, Y. Azar, K. Wang, G. N. Wong, J. K. Schulz, M. Samimi, and F. Gutierrez, "Millimeter wave mobile communications for 5g cellular: It will work!" *IEEE access*, vol. 1, pp. 335–349, 2013.

[36] G. R. MacCartney Jr, S. Sun, T. S. Rappaport, Y. Xing, H. Yan, J. Koka, R. Wang, and D. Yu, "Millimeter wave wireless communications: New results for rural connectivity," in *Proceedings of the 5th workshop on all things cellular: operations, applications and challenges*, 2016, pp. 31–36.

[37] T. Bogale, X Wang, and L. Le, "Mmwave communication enabling techniques for 5g wireless systems: A link level perspective," in *MmWave Massive MIMO*, Elsevier, 2017, pp. 195–225.

[38] Y. Jian, Y. Liu, S. K. Venkateswaran, D. M. Blough, and R. Sivakumar, "A quantitative exploration of access point mobility for mmwave wifi networks," in *ICC 2020-2020 IEEE International Conference on Communications (ICC)*, IEEE, 2020, pp. 1–7.

[39] S. Nie, G. R. MacCartney, S. Sun, and T. S. Rappaport, "28 ghz and 73 ghz signal outage study for millimeter wave cellular and backhaul communications," in *2014 IEEE International Conference on Communications (ICC)*, IEEE, 2014, pp. 4856–4861.

[40] Y. Zhu, Z. Zhang, Z. Marzi, C. Nelson, U. Madhow, B. Y. Zhao, and H. Zheng, "Demystifying 60ghz outdoor picocells," in *Proceedings of the 20th annual international conference on Mobile computing and networking*, 2014, pp. 5–16.

[41] Y. Niu, Y. Li, D. Jin, L. Su, and A. V. Vasilakos, "A survey of millimeter wave communications (mmwave) for 5g: Opportunities and challenges," *Wireless networks*, vol. 21, no. 8, pp. 2657–2676, 2015.

[42] M. Coldrey, J.-E. Berg, L. Manholm, C. Larsson, and J. Hansryd, "Non-line-of-sight small cell backhauling using microwave technology," *IEEE Communications Magazine*, vol. 51, no. 9, pp. 78–84, 2013.

[43] J. Hansryd, J. Edstam, B.-E. Olsson, and C. Larsson, "Non-line-of-sight microwave backhaul for small cells," *Celebrating 90 years of technology insights*, p. 12, 2014.

[44] G. R. MacCartney and T. S. Rappaport, "73 ghz millimeter wave propagation measurements for outdoor urban mobile and backhaul communications in new york city," in *2014 IEEE International Conference on Communications (ICC)*, IEEE, 2014, pp. 4862–4867.

[45] Y. Liu, Q. Hu, and D. M. Blough, "Joint link-level and network-level reconfiguration for mmwave backhaul survivability in urban environments," in *Proceedings of the 22nd International ACM Conference on Modeling, Analysis and Simulation of Wireless and Mobile Systems*, 2019, pp. 143–151.

[46] Y. Jian, C.-L. Tai, S. K. Venkateswaran, M. Agarwal, Y. Liu, D. M. Blough, and R. Sivakumar, "Algorithms for addressing line-of-sight issues in mmwave wifi networks using access point mobility," *Journal of Parallel and Distributed Computing*, vol. 160, pp. 65–78, 2022.

[47] Y. Liu, Y. Jian, R. Sivakumar, and D. M. Blough, "On the potential benefits of mobile access points in mmwave wireless lans," in *2020 IEEE International Symposium on Local and Metropolitan Area Networks (LANMAN*, IEEE, 2020, pp. 1–6.

[48] Y. Jian, M. Agarwal, S. K. Venkateswaran, Y. Liu, D. M. Blough, and R. Sivakumar, "Wimove: Toward infrastructure mobility in mmwave wifi," in *Proceedings of the*

18th ACM Symposium on Mobility Management and Wireless Access, 2020, pp. 11–20.

[49] Y. Liu, Y. Jian, R. Sivakumar, and D. M. Blough, "Optimal access point placement for multi-ap mmwave wlans," in *Proceedings of the 22nd International ACM Conference on Modeling, Analysis and Simulation of Wireless and Mobile Systems*, 2019, pp. 35–44.

[50] ——, "Maximizing line-of-sight coverage for mmwave wireless lans with multiple access points," *IEEE/ACM Transactions on Networking*, 2021.

[51] E. J. Violette, R. H. Espeland, R. O. DeBolt, and F. Schwering, "Millimeter-wave propagation at street level in an urban environment," *IEEE Transactions on Geoscience and Remote Sensing*, vol. 26, no. 3, pp. 368–380, 1988.

[52] Y. Niu, W. Ding, H. Wu, Y. Li, X. Chen, B. Ai, and Z. Zhong, "Relay-assisted and qos aware scheduling to overcome blockage in mmwave backhaul networks," *IEEE Transactions on Vehicular Technology*, vol. 68, no. 2, pp. 1733–1744, 2019.

[53] H. Utatsu, K. Osawa, J. Mashino, S. Suyama, and H. Otsuka, "Throughput performance of relay backhaul enhancement using 3d beamforming," in *2019 International Conference on Information Networking (ICOIN)*, IEEE, 2019, pp. 120–124.

[54] J. Wannstrom, "Lte-advanced," *Third Generation Partnership Project (3GPP)*, 2013.

[55] A. B. Saleh, S. Redana, B. Raaf, T. Riihonen, J. Hamalainen, and R. Wichman, "Performance of amplify-and-forward and decode-and-forward relays in lte-advanced," in *2009 IEEE 70th Vehicular Technology Conference Fall*, IEEE, 2009, pp. 1–5.

[56] O. Bulakci, S. Redana, B. Raaf, and J. Hämäläinen, "Performance enhancement in lte-advanced relay networks via relay site planning," in *2010 IEEE 71st Vehicular Technology Conference*, IEEE, 2010, pp. 1–5.

[57] Z. Lan, C.-S. Sum, J. Wang, T. Baykas, F. Kojima, H. Nakase, and H. Harada, "Relay with deflection routing for effective throughput improvement in gbps millimeter-wave wpan systems," *IEEE Journal on Selected Areas in Communications*, vol. 27, no. 8, pp. 1453–1465, 2009.

[58] Z. Lan, J. Wang, J. Gao, C.-S. Sum, F. Kojima, T. Baykas, H. Harada, and S. Kato, "Directional relay with spatial time slot scheduling for mmwave wpan systems," in *2010 IEEE 71st Vehicular Technology Conference*, IEEE, 2010, pp. 1–5.

[59] S. Singh, F. Ziliotto, U. Madhow, E. M. Belding, and M. J. Rodwell, "Millimeter wave wpan: Cross-layer modeling and multi-hop architecture," in *IEEE INFOCOM 2007-26th IEEE International Conference on Computer Communications*, IEEE, 2007, pp. 2336–2340.

[60] K. Song, R. Cai, and D. Liu, "A fast relay selection algorithm over 60ghz mm-wave systems," in *2013 15th IEEE International Conference on Communication Technology*, IEEE, 2013, pp. 676–680.

[61] Y. Zhang, M. A. Kishk, and M.-S. Alouini, "A survey on integrated access and backhaul networks," *arXiv preprint arXiv:2101.01286*, 2021.

[62] A. T. Pham, P. V. Trinh, V. V. Mai, N. T. Dang, and C.-T. Truong, "Hybrid free-space optics/millimeter-wave architecture for 5g cellular backhaul networks," in *2015 Opto-Electronics and Communications Conference (OECC)*, IEEE, 2015, pp. 1–3.

[63] J. E. Mitchell, "Integrated wireless backhaul over optical access networks," *Journal of Lightwave Technology*, vol. 32, no. 20, pp. 3373–3382, 2014.

[64] P. T. Dat, A. Kanno, K. Inagaki, and T. Kawanishi, "High-capacity wireless backhaul network using seamless convergence of radio-over-fiber and 90-ghz millimeter-wave," *Journal of Lightwave Technology*, vol. 32, no. 20, pp. 3910–3923, 2014.

[65] O. L. López, H. Alves, R. D. Souza, and M. Latva-aho, "Hybrid wired-wireless backhaul solutions for heterogeneous ultra-dense networks," in *2018 IEEE 87th Vehicular Technology Conference (VTC Spring)*, IEEE, 2018, pp. 1–5.

[66] J. Du, E. Onaran, D. Chizhik, S. Venkatesan, and R. A. Valenzuela, "Gbps user rates using mmwave relayed backhaul with high-gain antennas," *IEEE Journal on Selected Areas in Communications*, vol. 35, no. 6, pp. 1363–1372, 2017.

[67] Q. Hu and D. M. Blough, "Relay selection and scheduling for millimeter wave backhaul in urban environments," in *2017 IEEE 14th International Conference on Mobile Ad Hoc and Sensor Systems (MASS)*, IEEE, 2017, pp. 206–214.

[68] A. Chelli, K. Kansanen, I. Balasingham, and M.-S. Alouini, "Performance analysis and optimization of millimeter wave networks with dual-hop relaying," in *2017 IEEE 85th Vehicular Technology Conference (VTC Spring)*, IEEE, 2017, pp. 1–7.

[69] M Nivedha, S Sukanya, and S Arunmozhi, "Performance analysis of dual-hop relaying networks with nth best-path selection over rayleigh fading channel," *Networking and Communication Engineering*, vol. 7, no. 4, pp. 163–168, 2015.

[70] A. Yılmaz and O. Kucur, "End-to-end performance of transmit antenna selection and generalized selection combining in dual-hop amplify-and-forward relay network in the presence of feedback errors," *Wireless Communications and Mobile Computing*, vol. 14, no. 7, pp. 689–703, 2014.

[71] M. Torabi, W. Ajib, and D. Haccoun, "Performance analysis of amplify-and-forward cooperative networks with relay selection over rayleigh fading channels," in *VTC Spring 2009-IEEE 69th Vehicular Technology Conference*, IEEE, 2009, pp. 1–5.

[72] H. Cui, M. Ma, L. Song, and B. Jiao, "Relay selection for two-way full duplex relay networks with amplify-and-forward protocol," *IEEE Transactions on Wireless Communications*, vol. 13, no. 7, pp. 3768–3777, 2014.

[73] X Rui, J Hou, and L Zhou, "On the performance of full-duplex relaying with relay selection," *Electronics letters*, vol. 46, no. 25, pp. 1674–1676, 2010.

[74] I. Krikidis, H. A. Suraweera, P. J. Smith, and C. Yuen, "Full-duplex relay selection for amplify-and-forward cooperative networks," *IEEE Transactions on Wireless Communications*, vol. 11, no. 12, pp. 4381–4393, 2012.

[75] H. Abbas and K. Hamdi, "Full duplex relay in millimeter wave backhaul links," in *2016 IEEE Wireless Communications and Networking Conference*, IEEE, 2016, pp. 1–6.

[76] A. Ribeiro, X. Cai, and G. B. Giannakis, "Symbol error probabilities for general cooperative links," *IEEE Transactions on wireless communications*, vol. 4, no. 3, pp. 1264–1273, 2005.

[77] V. A. Aalo, G. P. Efthymoglou, T. Soithong, M. Alwakeel, and S. Alwakeel, "Performance analysis of multi-hop amplify-and-forward relaying systems in rayleigh fading channels with a poisson interference field," *IEEE Transactions on wireless communications*, vol. 13, no. 1, pp. 24–35, 2013.

[78] V. N. Q. Bao and H. Y. Kong, "Error probability performance for multi-hop decode-and-forward relaying over rayleigh fading channels," in *2009 11th International Conference on Advanced Communication Technology*, IEEE, vol. 3, 2009, pp. 1512–1516.

[79] E. Morgado, I. Mora-Jimenez, J. J. Vinagre, J. Ramos, and A. J. Caamano, "End-to-end average ber in multihop wireless networks over fading channels," *IEEE transactions on wireless communications*, vol. 9, no. 8, pp. 2478–2487, 2010.

[80] G. Huang, Y. Wang, and J. Coon, "Performance of multihop decode-and-forward and amplify-and-forward relay networks with channel estimation," in *Proceedings of 2011 IEEE Pacific Rim Conference on Communications, Computers and Signal Processing*, IEEE, 2011, pp. 352–357.

[81] W. Muenthetrakoon, K. Khutwiang, and C. Kotchasarn, "Ser of multi-hop decode and forward cooperative communications under rayleigh fading channel," in *2011 Second International Conference on Intelligent Systems, Modelling and Simulation*, IEEE, 2011, pp. 318–323.

[82] K. Dhaka, R. K. Mallik, and R. Schober, "Performance analysis of decode-and-forward multi-hop communication: A difference equation approach," *IEEE transactions on communications*, vol. 60, no. 2, pp. 339–345, 2012.

[83] M. R. Bhatnagar, "Performance analysis of a path selection scheme in multi-hop decode-and-forward protocol," *IEEE Communications Letters*, vol. 16, no. 12, pp. 1980–1983, 2012.

[84] M. R. Bhatnagar, R. K. Mallik, and O. Tirkkonen, "Performance evaluation of best-path selection in a multihop decode-and-forward cooperative system," *IEEE Transactions on Vehicular Technology*, vol. 65, no. 4, pp. 2722–2728, 2015.

[85] Y. Yan, Q. Hu, and D. M. Blough, "Path selection with amplify and forward relays in mmwave backhaul networks," in *2018 IEEE 29th Annual International Symposium on Personal, Indoor and Mobile Radio Communications (PIMRC)*, IEEE, 2018, pp. 1–6.

[86] Z. Wang and J. Crowcroft, "Bandwidth-delay based routing algorithms," in *Proceedings of GLOBECOM'95*, IEEE, vol. 3, 1995, pp. 2129–2133.

[87] Q. Hu and D. M. Blough, "On the feasibility of high throughput mmwave backhaul networks in urban areas," in *2020 International Conference on Computing, Networking and Communications (ICNC)*, IEEE, 2020, pp. 572–578.

[88] Z. Marzi, U. Madhow, and H. Zheng, "Interference analysis for mm-wave picocells," in *2015 IEEE Global Communications Conference (GLOBECOM)*, IEEE, 2015, pp. 1–6.

[89] P. Baumgartner *et al.*, "A first-order logic davis-putnam-logemann-loveland procedure," *AI in the new Millenium, Morgan Kaufmann, Seattle*, 2002.

[90] Y. Yan, Q. Hu, and D. M. Blough, "Optimal path construction with decode and forward relays in mmwave backhaul networks," in *2020 International Conference on Computing, Networking and Communications (ICNC)*, IEEE, 2020, pp. 579–585.

[91] L. Chen and J. Leneutre, "On multipath routing in multihop wireless networks: Security, performance, and their tradeoff," *Eurasip journal on wireless communications and networking*, vol. 2009, pp. 1–13, 2009.

[92] S. Rao. (). "DPLL SAT Solver," (visited on 12/12/2019).

[93] M. Davis, G. Logemann, and D. Loveland, "A machine program for theorem-proving," *Communications of the ACM*, vol. 5, no. 7, pp. 394–397, 1962.

[94] Y. Yan, Q. Hu, and D. M. Blough, "Feasibility of multipath construction in mmwave backhaul," in *2021 IEEE 22nd International Symposium on a World of Wireless, Mobile and Multimedia Networks (WoWMoM)*, IEEE, 2021, pp. 81–90.

[95] S. Singh, M. N. Kulkarni, A. Ghosh, and J. G. Andrews, "Tractable model for rate in self-backhauled millimeter wave cellular networks," *IEEE Journal on Selected Areas in Communications*, vol. 33, no. 10, pp. 2196–2211, 2015.

[96] X. Xu, W. Saad, X. Zhang, X. Xu, and S. Zhou, "Joint deployment of small cells and wireless backhaul links in next-generation networks," *IEEE Communications Letters*, vol. 19, no. 12, pp. 2250–2253, 2015.

[97] R. J. Weiler, M. Peter, W. Keusgen, E. Calvanese-Strinati, A. De Domenico, I. Filippini, A. Capone, I. Siaud, A.-M. Ulmer-Moll, A. Maltsev, *et al.*, "Enabling 5g backhaul and access with millimeter-waves," in *2014 European conference on networks and communications (EuCNC)*, IEEE, 2014, pp. 1–5.

[98] C. Saha and H. S. Dhillon, "Load balancing in 5g hetnets with millimeter wave integrated access and backhaul," *arXiv preprint arXiv:1902.06300*, 2019.

[99] P.-H. Hsiao, A. Hwang, H. Kung, and D. Vlah, "Load-balancing routing for wireless access networks," in *Proceedings IEEE INFOCOM 2001. Conference on computer communications. Twentieth annual joint conference of the IEEE computer and communications society (Cat. No. 01CH37213)*, IEEE, vol. 2, 2001, pp. 986–995.

[100] Y. Yan, L. Ci, R. Zhang, and Z. Wang, "Load balancing routing algorithm among multiple gateways in manet with internet connectivity," in *16th International Conference on Advanced Communication Technology*, IEEE, 2014, pp. 388–392.

[101] J. Li, C. Blake, D. S. De Couto, H. I. Lee, and R. Morris, "Capacity of ad hoc wireless networks," in *Proceedings of the 7th annual international conference on Mobile computing and networking*, 2001, pp. 61–69.

[102] Q. Hu, Y. Liu, Y. Yan, and D. M. Blough, "End-to-end simulation of mmwave out-of-band backhaul networks in ns-3," in *Proceedings of the 2019 Workshop on Next-Generation Wireless with ns-3*, 2019, pp. 1–4.